NASA CR - 159448

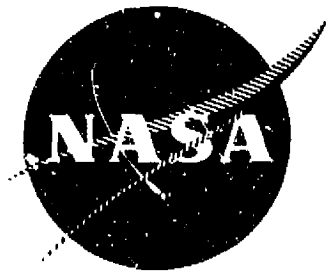

PREDICTION OF PLASMA PROPERTIES IN MERCURY ION THRUSTERS

PREPARED FOR

LEWIS RESEARCH CENTER

NATIONAL AERONAUTICS AND SPACE ADMINISTRATION

Grant NGR-06-002-112

by

Glen Longhurst

Approved by

Paul J. Wilbur
December, 1978
Department of Mechanical Engineering
Colorado State University
Fort Collins, Colorado

TABLE OF CONTENTS

LIST OF FIGURES

LIST OF FIGURES-Continued

LIST OF TABLES

I. INTRODUCTION

Electron bombardment ion thrusters have been operated since 1960 [1] using for the most part mercury as the propellant. Other propellants such as cesium, argon and xenon have been used, but there is much more information available for mercury. Thruster development has been largely experimental due to the relative simplicity of the devices and because the processes obtaining in ion thrusters are complex and have not been well understood. There has been a need for an analytical model which can predict plasma properties from basic design data and controllable operating parameters.

This study deals with the development of such a model. It is derived from considerations of the processes ongoing within the thruster discharge chamber as evidenced by the measurements which have been made of plasma properties and thruster performance data. While the study focuses on mercury thrusters, its methods should be equally applicable to thrusters which use other propellants.

What follows is a somewhat simplified theoretical development which is based on data available in the literature and obtained in the laboratory in support of other objectives. Such data, describing plasma properties in thruster discharge chambers, must be regarded with some reservation because methods of obtaining values for the parameters of interest from raw data have improved substantially over the last few years [2]. For that reason it is to be expected that any theoretical model will give only a first order comparison with much of the data.

Accepting some coarseness in the theoretical model, it is appropriate to make a number of simplifying assumptions regarding the processes and property distributions obtaining. While these may

eliminate some detail and may distort the results somewhat, they will serve to make the problem much more tractable. When such assumptions are made herein, they will be noted and where necessary their reasonability discussed.

After a brief review of the fundamental concepts of ion thruster operation and design, a detailed discussion of the various processes and effects believed to be significant to the operation of the thruster will be presented in which each effect will be quantified in terms of input data or results available from other process descriptions. Then the conservation relations will be applied to the plasma to form the basis of an iterative scheme for obtaining the desired outputs. It is necessary to develop a model for plasma property profiles to satisfactorily account for loss mechanisms at the plasma boundaries. These profiles will be developed for both uniform axial magnetic field and divergent field thruster configurations. Finally, the result of applying the resulting model to several thrusters will be compared with experimental data and various sensitivities of the model to input parameters will be discussed.

II. THRUSTER DESIGN AND OPERATION

Design

There have been a variety of bombardment ion thruster designs investigated since the basic concept was presented [3]. Figure 1 is a schematic drawing of a typical configuration. The body or container is usually a cylindrical vessel closed at the upstream end. The downstream end is bounded by a set of multi-aperture electrode plates called grids. The inner grid is usually held at the same potential as the thruster body and is called the screen grid. The outer grid is biased strongly negatively of the screen grid and is called the accelerator grid. A strong electric field exists between the grids which accelerates the ions to provide thrust. A cathode or electron emitter is located inside the thruster. In mercury thrusters, this is frequently a hollow tube with a small orifice at its downstream end which is located inside a subchamber called the cathode chamber. When a hollow cathode is used, there is usually a small loop anode called a keeper located adjacent to the cathode which draws sufficient electron current to maintain the cathode discharge in the presence of low emission conditions and plasma fluctuations.

The cathode chamber connects to the main discharge chamber via an annular aperture called the baffle aperture. An anode or electron collector is located in the main discharge chamber. This is frequently a cylindrical plate near the chamber's outer edge though other arrangements have been used. Propellant gas is introduced through a manifold which may serve to distribute the gas throughout the discharge chamber. A magnetic field is provided to control electron motion in a manner which will be discussed more fully later.

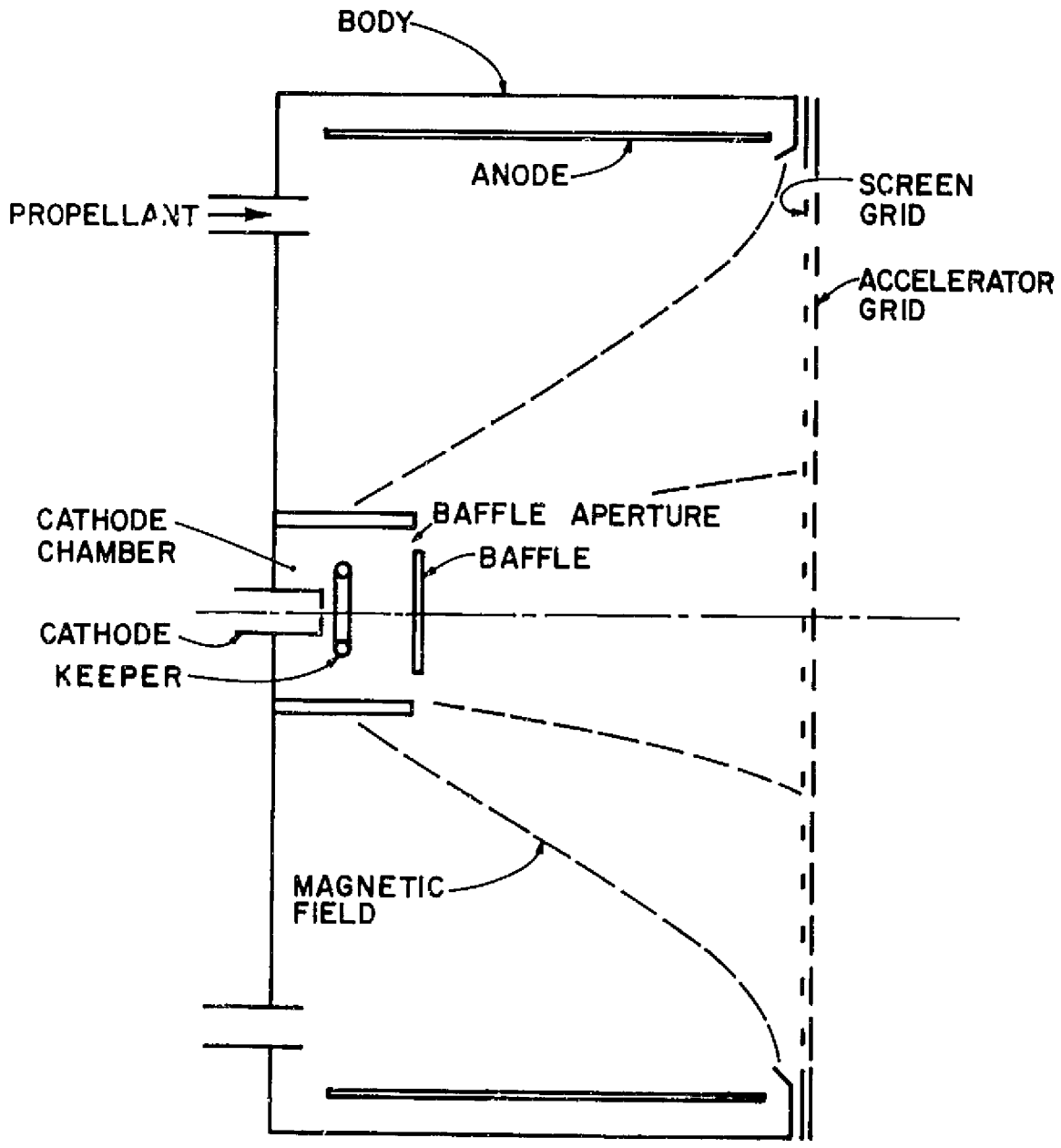

Figure 1. Simplified schematic drawing of a typical ion thruster discharge chamber.

Operation

When the thruster is in operation, the propellant gas flows continuously through the discharge chamber at a regulated rate. The cathode which is heated to incandescence emits a stream of electrons. These electrons are accelerated into the plasma of the main discharge chamber by a potential sheath which exists at the edge of the main discharge plasma. In hollow cathode thrusters the accelerating sheath is near the baffle aperture. Electrons which have been accelerated through this sheath are called primary electrons. They have sufficient energy to ionize the propellant atoms. After having lost their initial energies in collisional processes, they combine with the electrons freed from the propellant atoms in the ionization process to form a population of electrons with a nearly Maxwellian energy distribution. These are collected by the anode. The ions which have been formed disperse throughout the discharge chamber leaving the plasma across the potential sheath which exists at all plasma boundaries. Those which fall on holes in the screen grid are accelerated by the electric field between the grids to become the beam current. Those which fall on solid thruster surfaces recombine with electrons and are varorized back into the discharge chamber as neutral propellant atoms [4].

The cross sections for collisions which involve ionizations are sufficiently low that electrons must travel distances on the order of meters through the discharge chamber at typical thruster plasma densities to have significant probability of experiencing an ionizing collision [4]. Since most ion thrusters have dimensions which are fractions of meters, the electrons must be constrained to stay within the discharge chamber until they have many opportunities for such collisions

if the thruster is to operate with reasonable efficiency. For that reason a magnetic field is provided which inhibits the flow of electrons to the anode. It has been found that the configuration and intensity of this magnetic field are very important to the determination of the plasma properties in the discharge chamber [5]. Because the magnetic field exerts the dominant influence on the plasma electrons in the discharge chamber, it is of major interest in this study.

The performance of ion thrusters is heavily dependent on the densities and energies of the various groups of particles in the discharge chamber. For the electrons this includes the density and Maxwellian temperature of the Maxwellian group and the relative density and energy of the primary electrons. The rate of ion production is directly related to these properties as well as to the density of neutral atoms present. The objective of the present model is the determination of these plasma properties. Ion temperature is of considerably less importance to successful thruster operation.

It is assumed in this model development that any thruster to which the model may be applied is well defined; specifically, it is assumed that the thruster geometry, the configuration and strength of the magnetic field, the potentials of thruster surfaces and the propellant flow rate are all known. It is also assumed that the cathode emission current is a controllable parameter and is known as is the thruster wall temperature. These data will be the inputs to the plasma property model.

SI units will be assumed in this development unless specifically stated otherwise. The SI unit of temperature is the Kelvin degree, and the energy unit is the joule. It is more convenient to express both of

these quantities in electron volts, so that convention will be adopted. Hence, for Maxwellian electrons, the energy quantity kT, where k is Boltzmann's constant and T is temperature, will be replaced by e T_{mx} where e is the electronic charge and T_{mx} is the Maxwellian electron temperature expressed in eV.

III. DYNAMIC PROCESSES

Before a meaningful model of the discharge can be formulated, it is necessary to understand the nature of the various processes and effects that obtain in the discharge chamber. These will now be considered in some detail.

Field Effects

The dominant field in the discharge chamber is the magnetic field which serves to contain the high energy or primary electrons until they can have collisions, some of which will produce ions. Were this field not present, the primary electrons would go very quickly to the anode and be lost from the plasma with an associated high energy loss and very little ion production. Figure 2 shows the magnetic field configurations of several mercury ion thrusters [3]. It may be seen that in each case the magnetic field lies generally parallel to the anode surface and that there is usually some divergence or nonuniformity to the field. This magnetic field turns the trajectories of the electrons preventing them from reaching the anode directly.

Charged particles in the plasma tend to move in helical trajectories around the magnetic field lines. The radius of such motion is called the Larmor radius R_L and is given by

$$R_L = \frac{Mu_\perp}{qB} \tag{1}$$

where M is the mass of the charged particle, q is its charge, $u_\perp$ is the component of the particle velocity which is perpendicular to the local magnetic field, and B is the strength of that field. Typical values of R_L for mercury ion thrusters are a few tenths of meters for ions and a

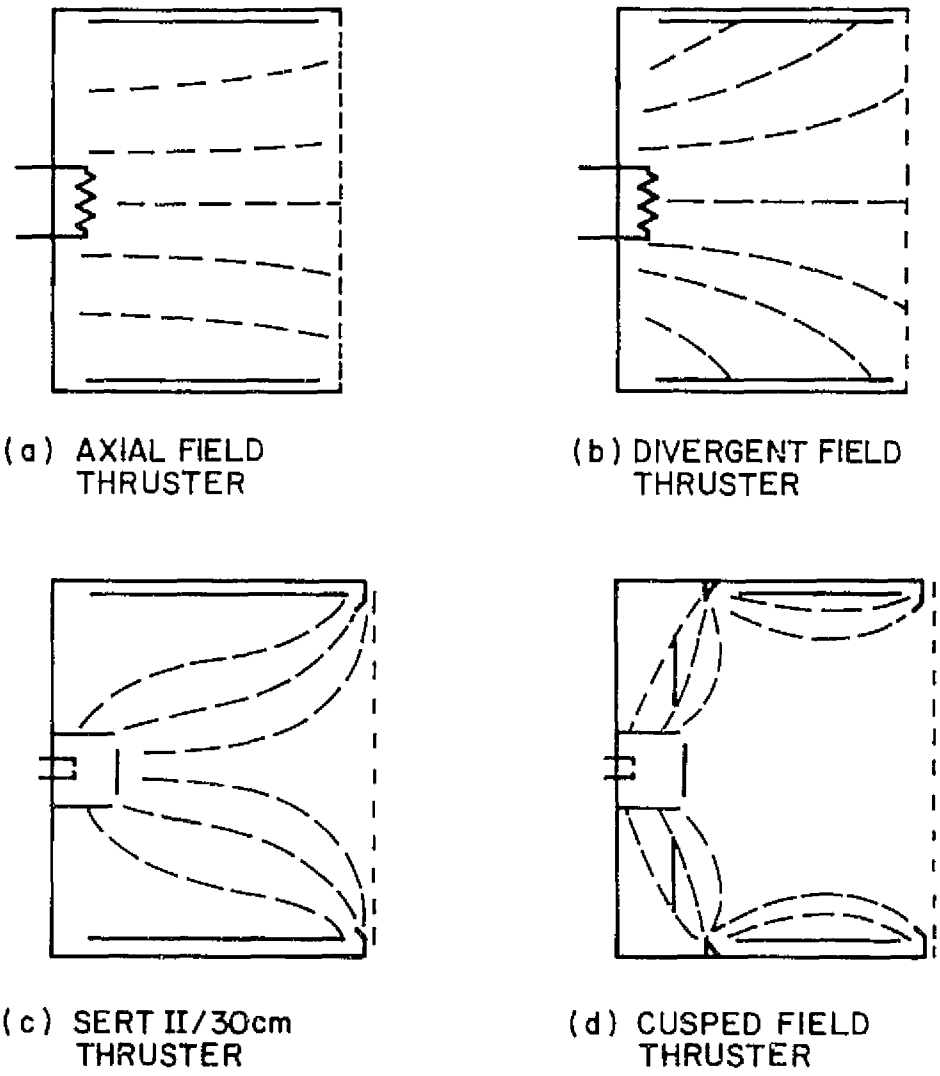

Figure 2. Magnetic field configurations for several mercury ion thrusters.

few millimeters for electrons [4]. Because R_L for ions tends to be of the same order as the diameter of the thruster, effects due to the curvature of ion trajectories are usually ignored. Electron motion, on the other hand, is strongly influenced by the presence of the magnetic field. In the absence of other disturbing influences such as collisions or electric fields, an electron will follow a field line in its helical trajectory until the field line intersects a solid surface or plasma boundary.

At that point the electric field associated with the plasma sheath has a pronounced effect. If the kinetic energy associated with the electron velocity component normal to the sheath is greater than the sheath potential, the electron will cross the sheath and leave the plasma. If not, the electron will be elastically and specularly reflected from the sheath. If the plasma is negative of the potential of the solid surface adjacent to it, the electrons will be accelerated across the sheath, and ions will be reflected. Except for anode potential surfaces, the sheath potential of most thruster plasmas is sufficient to reflect all but the most energetic electrons in the tail of the Maxwellian distribution [4]. At anode potential surfaces, however, there is a significant probability that most electrons will be collected since plasma potential is within a few volts of anode potential [6]. The magnitude of that potential difference will be found in a subsequent section.

The electric fields at the sheaths extend only for a few Debye lengths into the plasma. The Debye length characterizes the greatest distance over which the effects of a single charge may be felt before being masked by the effects of other charges in the vicinity. For ion

thruster plasmas the sheath thickness is usually less than 10^{-4} m [4]. Hence, sheath effects on electron paths may be considered to occur instantaneously and to be strictly confined to a region so thin as to be considered a surface at the plasma boundary.

Weak electric fields may exist over the bulk of the discharge chamber inside of the potential sheaths. Because they are weak, their effects will be negligible in a first order model such as this, so they will be ignored.

Electron Diffusion

Now consider the motion of electrons as they cross the magnetic field. Electron motion may be separated into two parts. One is the helical motion about the magnetic field lines or guiding centers, and the other is the net motion of the guiding centers due to collisions or drifts. The helical motion results in no net travel across the magnetic field, only travel along the field lines. Neglecting that motion for the present, the motion of the electrons across the magnetic field may be assumed to be just the guiding center motion.

Classical theory [7,8] predicts that for a plasma immersed in a magnetic field where electric fields are unimportant the motion of the electrons should be describable by the diffusion equation

$$\Gamma_e = -D \cdot \nabla n_e \qquad (2)$$

where Γ_e is a vector particle flux and D is a tensor describing the diffusivity of the electrons which have number density n_e. This diffusion results from the electrons suffering collisions and having their guiding centers changed, as well as from their motion between collisions. For situations where the collision frequency is much less than the

cyclotron frequency, which describes the angular rate of their helical motion, electron motion along field lines ought to be much faster than electron diffusion across the field which results from the random walk of their guiding centers across the magnetic field due to collisions and a density gradient [9].

To examine this process, consider the sketch in Figure 3. A typical ion thruster magnetic field has been shown with important field lines labelled. The inner and outer critical field lines are those field lines whose surfaces of revolution define the region which is directly accessible to the primary electrons which have come from the cathode through the baffle aperture. The virtual anode field line is the innermost field line that intersects the anode. It is so named because electrons which become bound to it or to one exterior to it have a significant probability of being collected by the anode when they move along the field line to its intersection with the anode. Electrons bound to field lines interior to the virtual anode field line will for the most part be reflected back into the plasma by the potential sheaths which exist at cathode potential plasma boundaries. Electrons with sufficient energy to ionize the propellant atoms will only be found in significant numbers inside the region bounded by the virtual anode surface [10]. Accordingly, the region of the discharge chamber interior to the virtual anode surface is defined as the ion production region.

Because it is within the ion production region that all of the interesting and important processes related to thruster performance occur, it is the only region of the discharge chamber of real concern in this analysis. Processes outside the ion production region will only be considered when they have direct bearing on plasma properties inside that region.

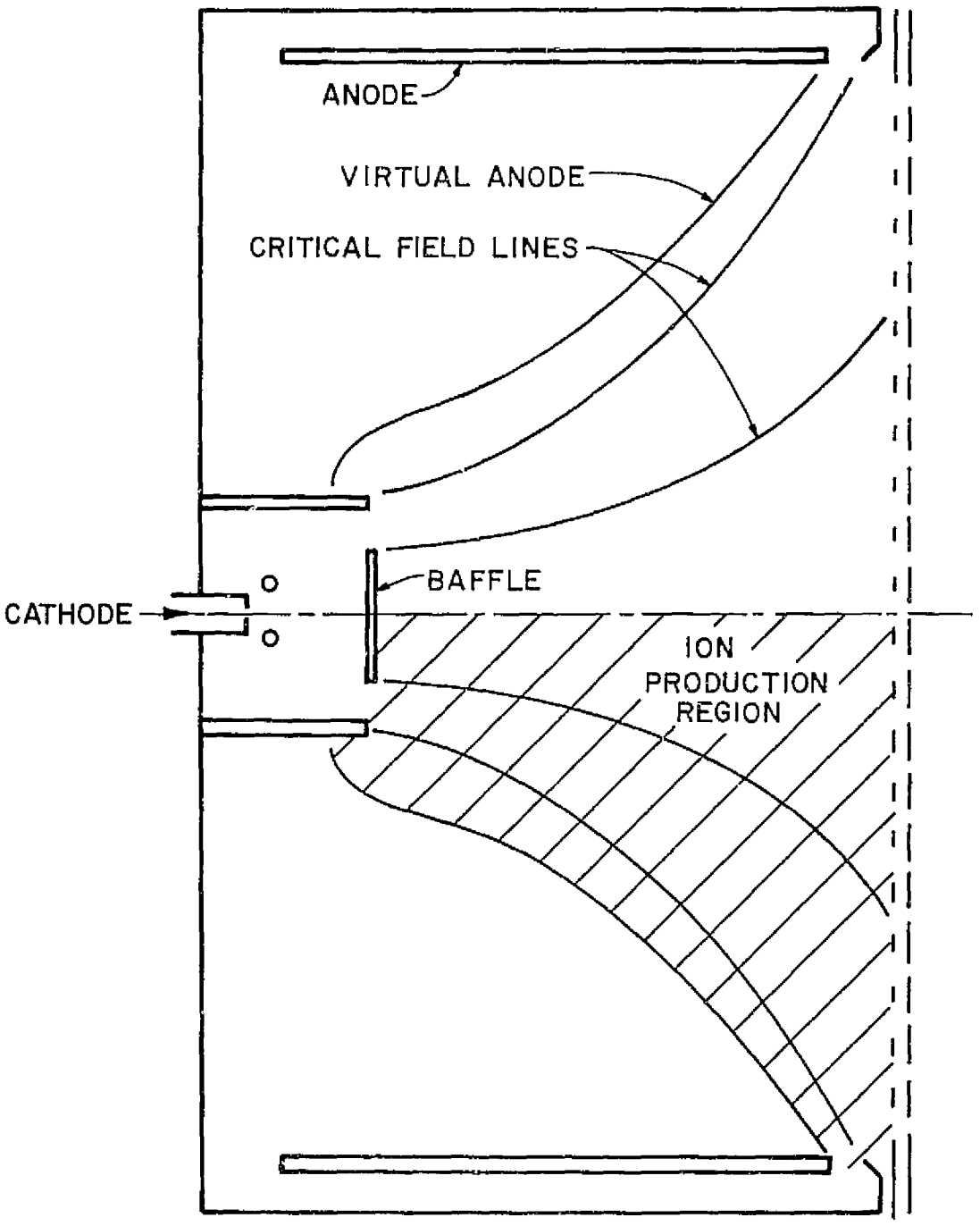

Figure 3. Important magnetic field lines in a typical ion thruster configuration using a hollow cathode.

It may be seen that while there is a flow of primary electrons into the ion production region from the baffle aperture, the only place electrons can leave it in significant numbers is at the virtual anode surface. Hence, it is concluded that there is only negligible net flux of Maxwellian electrons along the magnetic field lines in the ion production region. Since aximuthal motion is of no immediate interest, the diffusion of Maxwellian electrons through the ion production region may be approximately modelled one dimensionally, i.e., in the direction orthogonal to the magnetic field. Equation (2) then becomes a one dimensional equation

$$\Gamma_{mx} = -D_{\perp} \nabla_{\perp} n_{mx} \tag{3}$$

where now the subscript mx refers to Maxwellian electrons. The pertinent density gradient is now orthogonal to the magnetic field and the diffusivity is now a scalar. Further consideration of this one-dimensionality will be given in a later chapter.

If motion of the Maxwellian electrons along the magnetic field lines is much more rapid than their motion across the field, it should be observed that the Maxwellian electron temperature T_{mx} (in eV) is nearly constant along the field lines. Figure 4 is a plot of lines of constant Maxwellian electron temperature for three different thruster configurations [9] superimposed on the magnetic field configuration. These isotherms were obtained by simple linear interpolation of unsmoothed data for the axial field and SERT-II thrusters studied by Knauer [6] and for Beattie's cusped field thruster [11]. It may be seen that considering errors in probe location and data reduction which may exist, there is fair alignment of the lines of constant temperature

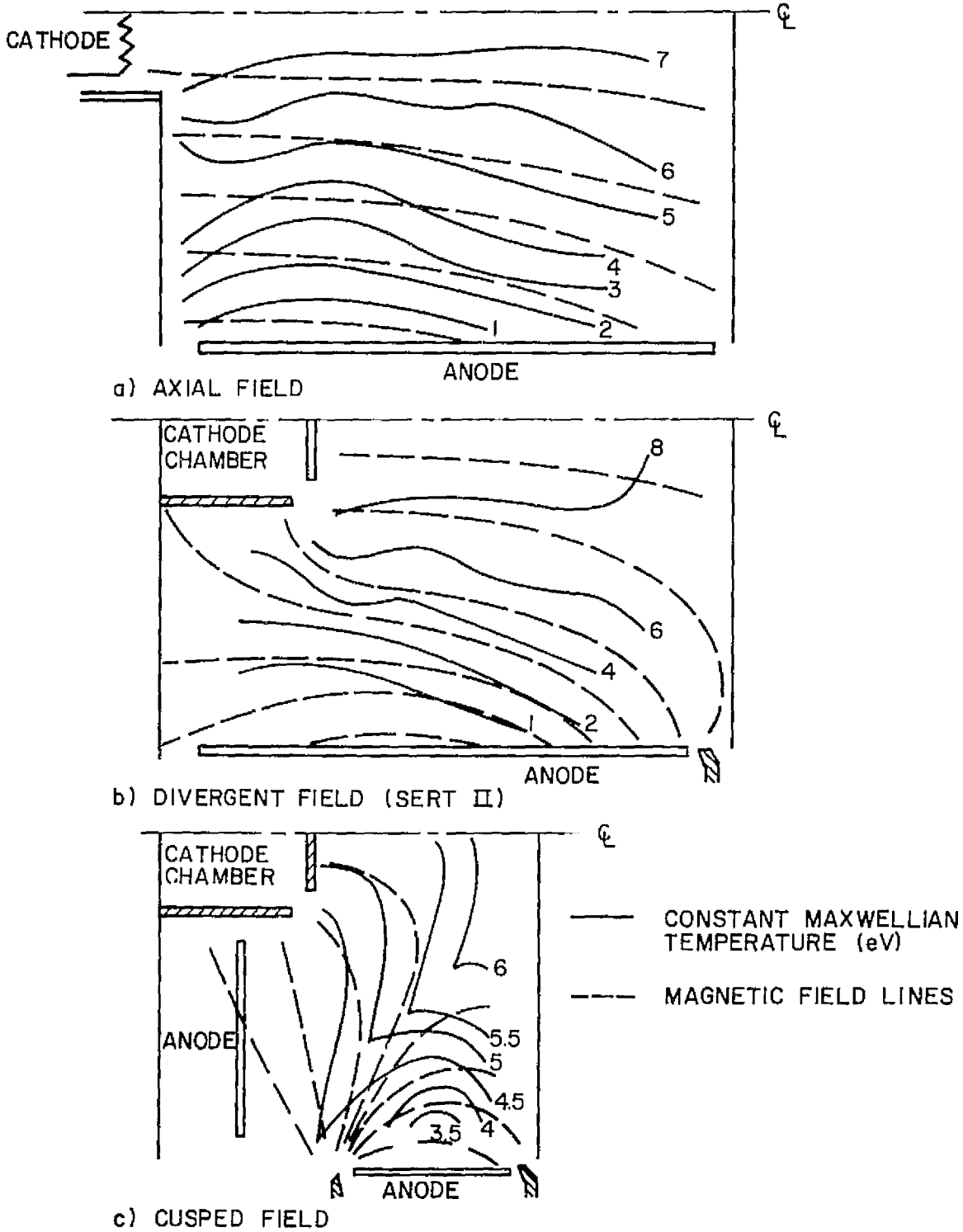

Figure 4. Correlation of Maxwellian electron temperature contours with magnetic field lines-of-force.

with the magnetic field lines in each of the cases. This indicates that the Maxwellian electrons do in fact move freely along the magnetic field lines compared with their motion across the field. It will be assumed, therefore, that electron temperature is constant along magnetic field lines. It has also been tacitly assumed that the single parameter T_{mx} is sufficient to describe the energies of the Maxwellian electrons when in fact $T_{mx\,\parallel}$ and $T_{mx\perp}$ ($\parallel$ and $\perp$ meaning with respect to the direction of the magnetic field lines) need not be identical.

For Maxwellian electrons the diffusivity of Equation (3) is given by classical theory [8] as

$$D_{\perp} = \frac{T_{mx}\, M_e \nu}{e\, B^2} \tag{4}$$

where M_e is the electron mass, ν is the electron momentum exchange collision frequency and other quantities are as previously used. If the collision frequency used is that given by accepted cross sections and known plasma densities, it is found [12,13,14] that the value of $D_{\perp}$ as given by Equation (4) is far too low to agree with much of the experimental data. A much better expression, uncertain to a factor of 2 or 3, and given by Bohm [15] is

$$D_B = \frac{T_{mx}}{16\, B}. \tag{5}$$

This expression is an empirical result, but it has been found to give reasonable agreement with data from a variety of experiments.

The reason for the departure from the classical theory to what has been termed "anomalous" diffusion is not completely clear. It has been theorized [12] that the process relates to plasma instabilities. One candidate is the Landau instability [16]. This instability arises

when there is a region in the particle energy distribution function which has a positive slope at an energy above the average energy for the distribution. Electric perturbations with phase velocities in the interval over which the positive slope exists tend to grow, drawing energy from particles slightly faster than the waves and giving energy to particles slightly slower than the waves, until the positive slope is eliminated from the distribution function or until some other limitation is encountered. Figure 5 is an electron energy distribution such as is expected in ion thruster plasmas. Depending on the energy spread and relative density of the primary electrons it may have a region of positive slope near the primary electron energy which could support the Landau instability. Hence, it is possible that the Landau instability is the major one responsible for the enhanced diffusivity observed.

Other instabilities are also possible and have been studied [17,18]. Regardless of what the instability mode may be, it appears that the effective collision frequency for classical diffusion in Equation (4) is altered by the interaction of electrons with electric waves as well as with other particles. It is noted in passing that if the collision frequency ν in Equation (4) is made equal to one sixteenth the cyclotron frequency of the electrons, then Equations (4) and (5) become identical. Since Bohm diffusivity has been found to give fair results in ion thruster analyses [9,13], it will be assumed that it is sufficiently accurate to model the transport of the Maxwellian electrons across the magnetic field of the ion production region.

Consider now the primary electron motion. If primary electrons undergo a random walk across the magnetic field as a result of

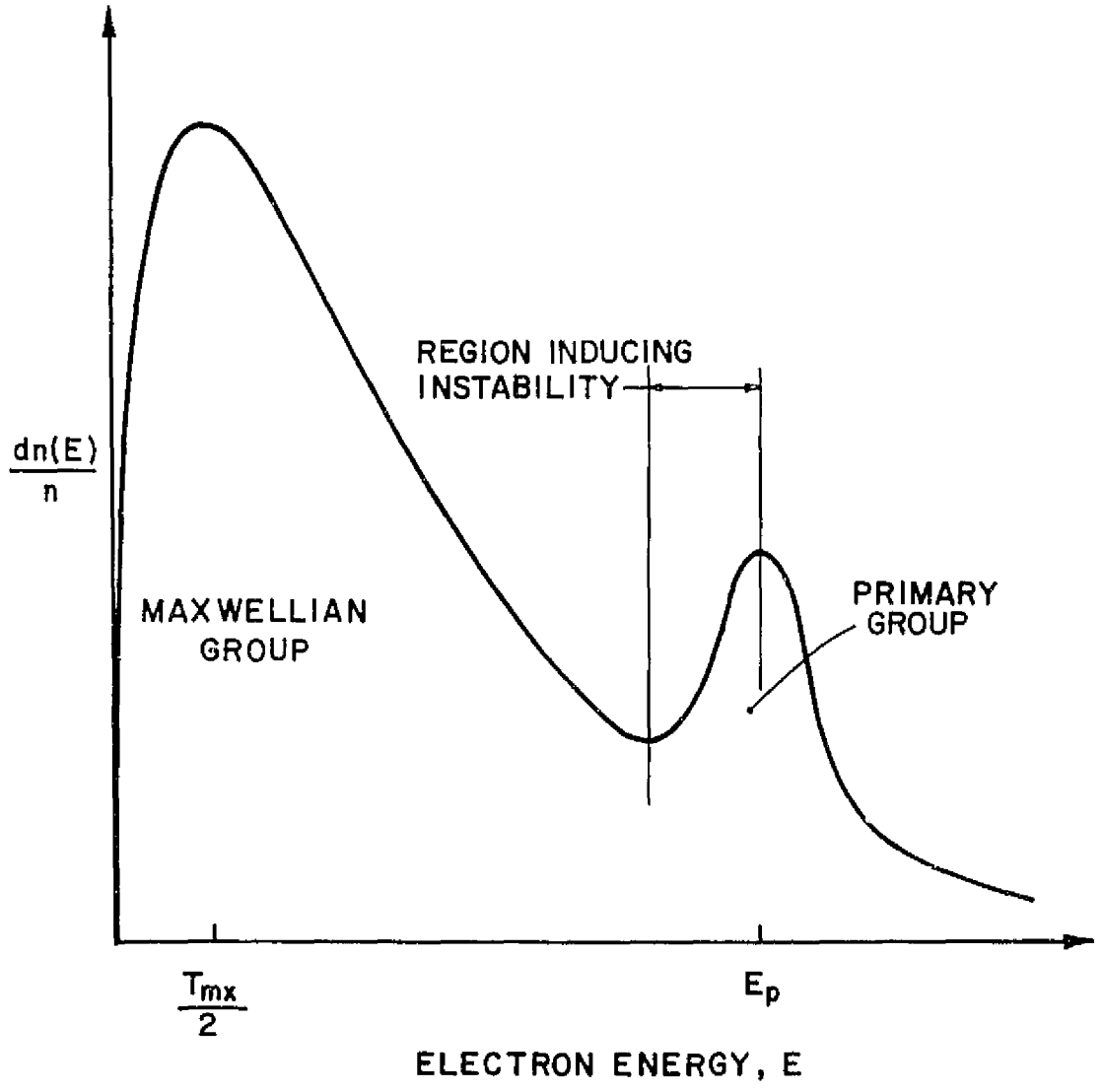

Figure 5. Two group electron energy distribution showing the region of the distribution function subject to Landau instability.

momentum altering collisions with other particles, it may be expected that they would lose energy in the process. Recalling from Figure 3 that there is a relatively small region of the discharge chamber to which primary electrons have direct access without benefit of such collisions, it would be expected that a decrease in primary electron energy and/or density would be observed as one looked inward from the inner critical field line toward the center line. The energy loss would result from collisions, and the density depletion would result from the increasingly rapid thermalization or slowing down of the primary electrons as they lose energy to the point where they lose their identities as primary electrons and become part of the Maxwellian electron population. This decrease toward the center line is not observed in the data.

Figure 6 is a mapping of both primary and Maxwellian electron properties from SERT-II [19]. It is seen that there is no significant decline in either primary electron density or energy away from the inner critical field line toward the center line. Indeed, primary electron energy appears to be constant over the entire ion production region to a first approximation, and primary electron density appears to have its maximum along the thruster axis. Similar primary electron property distributions appear in data for other thrusters [4,11]. The fact that the primary electron property variations described previously are not observed suggests that primary electrons, too, are subject to some form of electric turbulence. The constancy of primary electron energy over the ion production region as compared with the variation of Maxwellian electron temperature evidenced in Figure 6 suggests that primary electrons are more severely influenced by that turbulence than are the

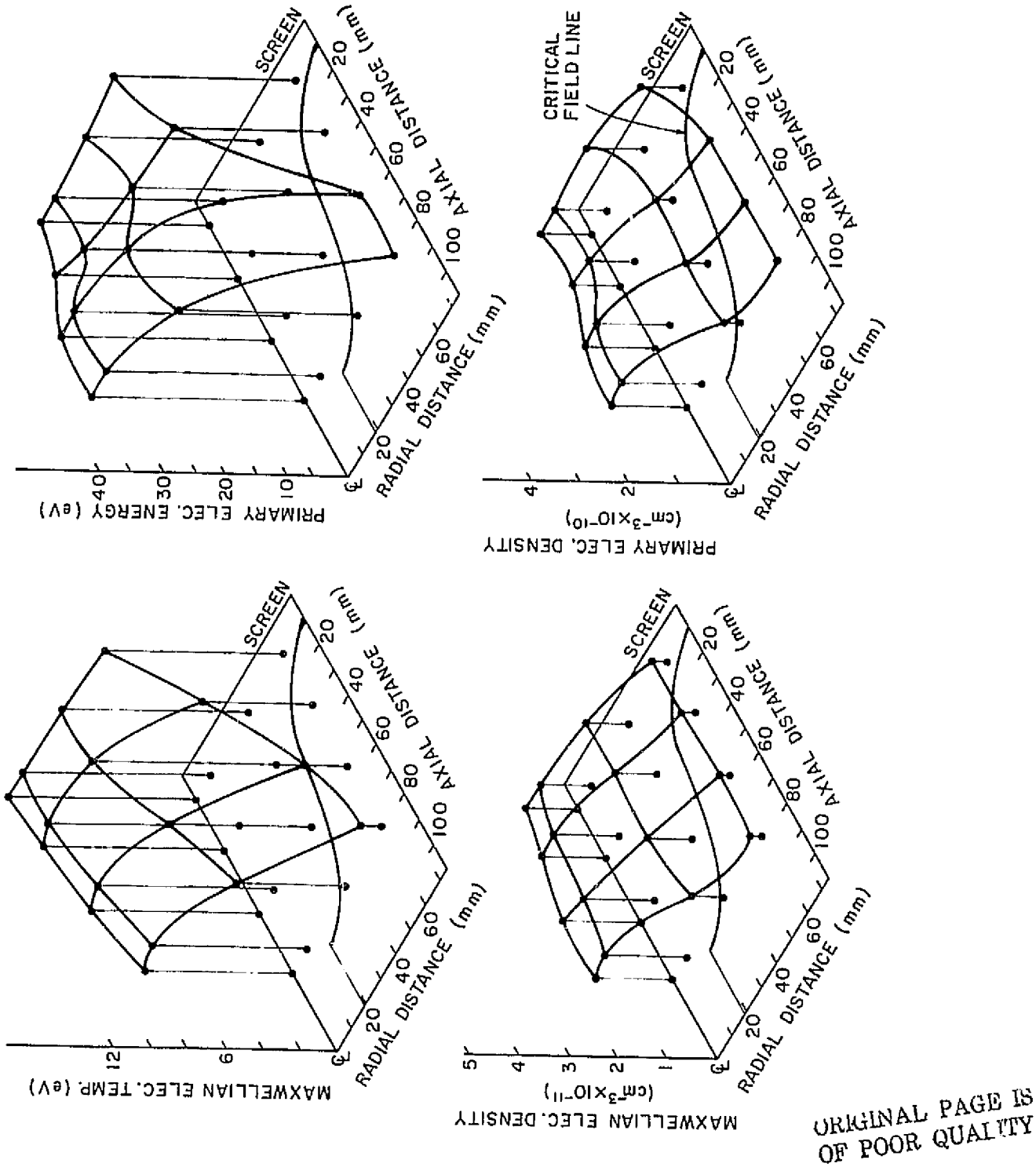

ORIGINAL PAGE IS
OF POOR QUALITY

Figure 6. Plasma property profiles for the SERT-II Thruster.

Maxwellian electrons, consistent with considering the Landau instability as a possible mechanism.

With the motion of the primary and Maxwellian electrons as discussed, it should be found that most electron collection is done by that part of the anode near its intersection with the virtual anode surface. That conclusion is supported by two independent results. Reader [20] investigated a 10 cm diameter mercury ion thruster having the general configuration of Figure 1 to which both a divergent and a nearly axial magnetic field were applied. The axial length of the cylindrical anode was varied from 15 cm to 1 cm while keeping its downstream end essentially fixed in the discharge chamber. Reader found that there was virtually no change in the discharge chamber performance with anode length in either configuration, though there was a difference between the performances of the two magnetic field configurations. In other studies at Colorado State University of Beattie's cusped field thruster [11] it was observed from anode melting patterns and from measurements of current to different anode segments that by far the greatest anode current density appeared at the intersection of the anode with the virtual anode surface.

Ion Motion

As indicated previously, the response of ions to magnetic fields is usually neglected in ion thruster analyses. The major influence on ion motion is the presence of electric fields. A principal effect is the acceleration of the ions to their sonic or Bohm velocity before they leave the plasma. The phenomenon is analagous to gas particles being accelerated across an expansion wave except it is the electric force on the ions which causes the acceleration. The Bohm velocity is

directed normal to the plasma boundary. It is predicted by the Bohm stable sheath criterion [4,21] and is given by

$$V_B = \left[\frac{q\, T_{mx}}{M_i} \left(1 + \frac{n_{pr}}{n_{mx}}\right) \right]^{\frac{1}{2}} \qquad (6)$$

where q is the charge of the ion, M_i is the ion mass, and n_{pr}/n_{mx} is the ratio of primary to Maxwellian electron densities. T_{mx} is the local Maxwellian electron temperature in eV. It has been shown [10] that the Bohm velocity should be achieved by ions by the time they reach the edge of the ion production region in ion thrusters.

The motion of ions within the ion production region in response to other electric fields is of little consequence at present in determining plasma properties.

IV. ENERGETIC PROCESSES

To understand the nature of the various processes undergone by the electrons in the discharge chamber which involve exchange or transport of energy, these processes will be reviewed in the general sequence that they would be experienced by an electron which has been emitted from the cathode. It will be assumed that a hollow cathode configuration is used although similar processes hold for oxide cathode thrusters.

Acceleration

Electrons which have been emitted from the cathode are accelerated into the main discharge plasma across the potential sheath which exists at their point of entry. For hollow cathodes, this sheath is found often near the baffle aperture, whereas for oxide cathodes which emit directly into the main discharge plasma, the sheath exists near the cathode surface [6]. The energy gained through this acceleration depends on the potential difference across the sheath. Fo the present purpose, it will be assumed that the potential of the plasma in the cathode chamber is near keeper potential V_k. Then for plasma potential V_p in the main discharge chamber, the energy gain ΔE will be

$$\Delta E = e(V_p - V_k) \tag{7}$$

where e is again the electron charge. V_k is zero for oxide cathode thrusters provided cathode potential is taken as the reference. V_p will be near anode potential V_a being separated from it by the anode sheath potential V_{s_a}. A corresponding sheath potential V_{s_k} will separate the potential of the plasma in the cathode chamber from keeper potential because that potential difference is thought to be small and being

difficult to calculate, it will be neglected. An equation which may be used to estimate the anode sheath potential V_{s_a} and which could be used in estimating V_{s_k} will be derived later.

It should be noted here that before being accelerated into the main discharge chamber, the primary electrons have a thermal energy of a few eV. Electron temperatures of 1 to 3 eV are frequently seen in the cathode chamber [22]. The total primary electron energy will thus be greater than ΔE of Equation (7) by the initial thermal energy. The spread of primary electron energies is believed to be sufficiently narrow for most thrusters that it is sufficiently accurate to assume that all the primary electrons have the single energy E_p.

Thermalization

Two things happen to the primary electrons to slow them down and take from them their primary electron energies. Many of them undergo inelastic collisions which will be discussed in a subsequent section. All of them are subject to multiple small angle, elastic collisions with the slower Maxwellian electrons and with the cold ions which are in the discharge chamber plasma. Because of the mass difference between the primary electrons and the ions, there is not much exchange of electron kinetic energy with the ions as compared with electron-electron interactions. These collisions, while usually not substantially deflecting the primary electron velocity direction, do act as a drag force which causes the faster electrons to give up their energies to the Maxwellian electron population [16]. There is also a spreading of the primary electron energies associated with this drag force. Ultimately, the thermalization process stops, and the primary electrons lose lose their identities and become part of the Maxwellian group.

The quantity of energy given up by primary electrons to the Maxwellian population will on the average be just the difference between their average initial or primary electron energy E_p and the average energy of the Maxwellian electrons. From this must be subtracted the average kinetic energy given up by primary electrons to inelastic processes before they become thermalized. Thermalization occurs at an increasing rate with decreasing electron energy [16]. It is appropriate, therefore, to neglect primary electrons in the latter stages of thermalization and assume that all the primary electrons have their initial primary energy.

Inelastic Collisions

Electrons which have energies above the threshold energy for exciting the atoms present may have inelastic collisions. A variety of excitations is possible which result in photon emission or ionization [23,24]. In each of these there is a loss of kinetic energy from the incident electron. That energy is subsequently carried from the ion production region by the excited atoms which migrate to the walls or by photons which are released when the atoms de-excite to lower energy levels. Primary electrons and many of the Maxwellian electrons have sufficient energies to undergo such collisions. For each particular excitation there is a cross section or probability of its occurrence which is a function of the incident electron energy. There is also a characteristic energy associated with each excitation which is given up by the incident electron when the excitation takes place.

Most excitations are to resonance states where de-excitation takes place almost immediately. Some excitations are to metastable states which have lifetimes long enough to allow them to undergo superelastic collisions with electrons [25]. In these superelastic collisions the

metastable atoms give back their excitation energies to other electrons with which collisions occur. Thus, in these collisions, there is a return of kinetic energy to the Maxwellian electron population. The net effect of the superelastic process in a steady state discharge is a lowering of the effective excitation cross sections. These reduced cross sections have been published for mercury [26] where the formation and destruction of the metastable states 6^3P_0 and 6^3P_2, the resonance states 6^3P_1 and 6^1P_1 and a collection of more highly excited states called the lumped or combined state were considered. Cross sections for single ions were also given.

It is assumed in this study that all states except ions and metastable states immediately de-excite by photon emission to reach, utlimately, the ground state. Actually, some transitions from higher excited states to metastable states have been observed in mercury ion thrusters [23], and transitions from metastable states to resonance states have been seen [27]. These processes are believed to be unimportant in first order analyses such as the present one [28], so they will be neglected. The two metastable states 6^3P_0, and 6^3P_2 will be populated only by excitation from 6^1S_0 neutral ground state atoms and to be destroyed by excitation to higher states as characterized by the combined state cross sections [26] and ionization cross sections [19] or by loss to the walls. Single ions will be assumed formed from ground state and metastable state atoms and lost to double ionizations and to the walls. Doubly charged ions will be assumed formed exclusively from singly charged ions [19] and lost only to the walls. While this rather arbitrary assumption is only approximately correct, it is believed to be sufficiently accurate for the present purpose.

The rate per unit target atom density and per electron at which electron kinetic energy is deposited in the excitation of state "a" atoms by monoenergetic electrons having energy E is characterized by the monoenergetic energy rate factor

$$p_a(E) = \sum_j \sigma_a^j(E)\ v_e(E)\ \Delta E_a^j \tag{8}$$

where the summation indicated is over the important inelastic processes involving the excitation of state "a" atoms to state j and where σ_a^j is the cross section for that excitation and ΔE_a^j is the characteristic energy of the reaction. $v_e(E)$ is the incident electron velocity. The terms $\sigma_a^j(E)\ v_e(E)$ are frequently combined into a monoenergetic reaction rate factor

$$P_a^j(E) = \sigma_a^j(E)\ v_e(E). \tag{9}$$

A corresponding reaction rate factor for Maxwellian electrons is obtained from

$$Q_a^j(T_{mx}) = \int_0^\infty P_a^j(E)\ g(E,T_{mx})\ dE \tag{10}$$

where $g(E,T_{mx})$ is the Maxwellian energy distribution function. Reaction rate factors for the important reactions in the present problem are given in Appendix A. An energy rate factor for Maxwellian electrons can be obtained by integrating the monoenergetic energy rate factor of Equation (8) over the Maxwellian energy distribution function:

$$q_a(T_{mx}) = \int_0^\infty P_a(E)\ g(E,T_{mx})\ dE. \tag{11}$$

Energy rate factors as given by Equation (8) for primary electrons and by Equation (11) for Maxwellian electrons are also given in Appendix A for the four states considered important in the present problem. All

double ions are assumed to be lost from the discharge chamber before they can be involved in inelastic processes.

Energy Transport

Consider now the way in which electron kinetic energy is transported across the magnetic field of the ion production region. While the Maxwellian electrons are undergoing their random walk process toward the anode, their energies are altered through the numerous collisions they experience such that they tend to be in thermal equilibrium with the other Maxwellian electrons in their immediate vicinity. It was shown in Figure 4 that there is a gradient of Maxwellian electron temperature in the direction perpendicular to the magnetic field. The value of thermal conductivity which characterizes the rate of kinetic energy transport across the magnetic field is usually accepted to be [29]

$$K_{\perp} = 4.7 \frac{n_{mx} e T_{mx}}{M_e \omega_{ce}^2 \tau_e} \qquad (12)$$

where τ_e is the electron effective collision period, ω_{ce} is the electron cyclotron frequency, and other quantities are as previously used. This conductivity is used with a temperature gradient measured in energy units per unit length to give the power transport per unit area. From the relation between classical and Bohm diffusivity, it is apparent that the effective period for electron collisions is $16/\omega_{ce}$ if the conductivity of Equation (12) is to bear the proper relationship to the diffusivity which is assumed to be the Bohm diffusivity. Making that substitution and using Equation (5) for Bohm diffusivity results in

$$K_{\perp} = 4.7\, n_{mx}\, D_B \,. \qquad (13)$$

Boundary Losses

Electron kinetic energy which is conveyed to the boundaries of the ion production region is carried across the boundaries by the electrons which escape from the plasma there. Most electrons which have come through the processes described previously leave the plasma of the ion production region by diffusing across the virtual anode surface and being quickly collected by the anode. A few of the electrons leave at cathode potential boundaries. Because the sheath potential at all cathode potential surfaces is strong compared with the average energy of the electrons, only the most energetic electrons in the tail of the Maxwellian energy distribution function escape to those surfaces. While the flux of electrons to cathode potential surfaces is small compared with the flux to the anode, it is not negligible for energy balance purposes because the energy of the electrons which do escape is so high.

For any plasma sheath the average energy of the electrons escaping across the sheath will depend on the electron temperature adjacent to the sheath and on the potential drop across the sheath. Assuming that the plasma is positive of the boundary surface potential (as it usually is in ion thrusters) by a potential difference V_s, then the minimum velocity u_{min} normal to the sheath required for an electron to be collected by the surface is

$$u_{min} = \left(\frac{2\ e\ V_s}{M_e} \right)^{\frac{1}{2}} . \qquad (14)$$

For the velocity distribution functions f(u), f(v) and f(w) where v and w are velocities in the two orthogonal directions perpendicular to u, the average energy of electrons leaving the plasma is found from

$$\langle E_c \rangle = \frac{\int_{u_{min}}^{\infty} u \int_{-\infty}^{\infty} \int_{-\infty}^{\infty} \frac{M_e}{2} (u^2+v^2+w^2)\, f(u)\, f(v)\, f(w)\, dw\, dv\, du}{\int_{u_{min}}^{\infty} u \int_{-\infty}^{\infty} \int_{-\infty}^{\infty} f(u)\, f(v)\, f(w)\, dw\, dv\, du} \tag{15}$$

If the simplifying assumption is made that the velocity distribution functions are isotropic and Maxwellian, Equation (15) may be solved to give

$$\langle E_c \rangle = 2\, T_{mx} + V_s \tag{16}$$

Now consider the simplified sketch of the plasma boundary for the ion production region in Figure 7. The control volume is assumed to be everywhere at plasma potential and bounded by the plasma sheath except at the virtual anode surface. The electron flux density to any surface can be found from

$$\Gamma_{mx} = n_{mx} \int_{u^*}^{\infty} u \int_{-\infty}^{\infty} \int_{-\infty}^{\infty} f(u)\, f(v)\, f(w)\, dw\, dv\, du \tag{17}$$

Again invoking the isotropic Maxwellian assumption on the velocity distribution functions, Equation (17) reduces to

$$\Gamma_{mx} = \left(\frac{e\, T_{mx}}{2\pi M_e}\right)^{\frac{1}{2}} \exp\left(\frac{-V_s}{T_{mx}}\right) n_{mx} \tag{18}$$

It is seen that if the electron density is very low, as it is in the thruster outside the ion production region (see Figure 6), or if the sheath potential V_s is much greater than the electron temperature T_{mx} as it is near the grids where the screen area is small and the effect of accelerator potential is manifest, then the electron flux to the surface is very small, and boundary losses of kinetic energy to those regions can be safely neglected. For typical thrusters this

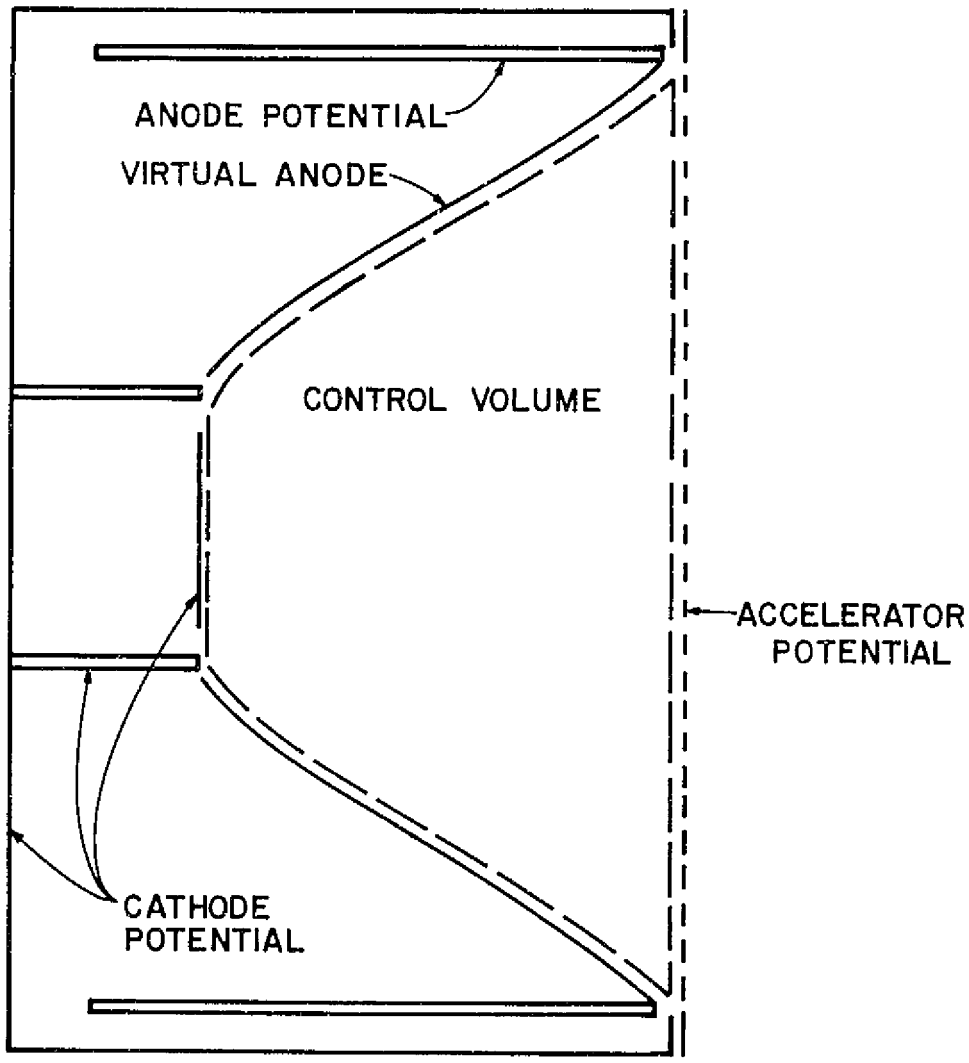

Figure 7. Control volume for boundary energy losses.

leaves the area at the upstream end of the ion production region including the baffle aperture as a cathode potential boundary where Maxwellian electron kinetic energy loss must be considered. The kinetic energy loss rate to that surface will be approximately

$$\dot{E}_b = n_{mx_u}\left(\frac{e\,T_{mx_u}}{2\pi M_e}\right)^{\frac{1}{2}} \exp\left(\frac{-V_p}{T_{mx_u}}\right)(2\,T_{mx_u} + V_p)\,A_u \qquad (19)$$

where the area averaged density and temperature at the upstream end replace local values, and where it is assumed that the sheath potential is the plasma potential V_p where

$$V_p = V_a + V_{s_a}\,, \qquad (20)$$

V_a being anode potential and V_{s_a} being the sheath potential at the anode. A_u in Equation (19) is the area of the upstream end of the ion production region.

The kinetic energy carried by the Maxwellian electrons to the anode may be found in a similar fashion except that the area of collection A_c and the anode sheath potential V_{s_a} are not readily available. If it is assumed that the total Maxwellian electron current collected along the virtual anode field line surface is given by

$$I_{mx} = I_c + I_b \qquad (21)$$

where I_c is the cathode emission current and where I_b is the magnitude of the beam current. Then, using Equations (16) and (21), the Maxwellian electron kinetic energy loss at the virtual anode will be given by

$$\dot{E}_a = \frac{1}{e} (I_c + I_b) \quad (2\, T_{mx_a} + V_{s_a}) \,. \tag{22}$$

The electron temperature and sheath potential which must be used are those at the intersection of the anode with the virtual anode surface. It has been assumed that there is enough collection of ambient electrons at low temperatures along the majority of the anode length to balance the ion current to the anode surface.

Before the magnitudes of $\dot{E}_a$ and $\dot{E}_b$ can be accurately specified, sheath potential V_{s_a} at the anode must be found. If the Maxwellian electron flux density as given by Equation (18) is multiplied by the area over which the Maxweillian electrons are effectively collected A_c, the result should be the Maxwellian electron current as given by Equation (21) divided by the electronic charge:

$$\Gamma_{mx} A_c = \frac{I_{mx}}{e} \,. \tag{23}$$

Substituting the appropriate expressions from Equations (18) and (21) into Equation (23) and solving the result explicitly for V_{s_a} gives

$$V_{s_a} = T_{mx_a} \ln \left[\frac{A_c\, e\, n_{mx_a}}{I_c + I_b} \left(\frac{e\, T_{mx_a}}{2\pi M_e} \right)^{\frac{1}{2}} \right] \tag{24}$$

Assuming that the electron collection location values of Maxwellian electron density n_{mx_a} and temperature T_{mx_a} can be found, the important quantity in Equation (24) is the effective electron collection area A_c. As suggested by Figure 8, which shows schematically the electron collection region geometry, this area, which is $2\pi R_a w$, where R_a is the anode radius, could be found if the thickness d of the electron collection layer was known. The width w of the electron collection area on

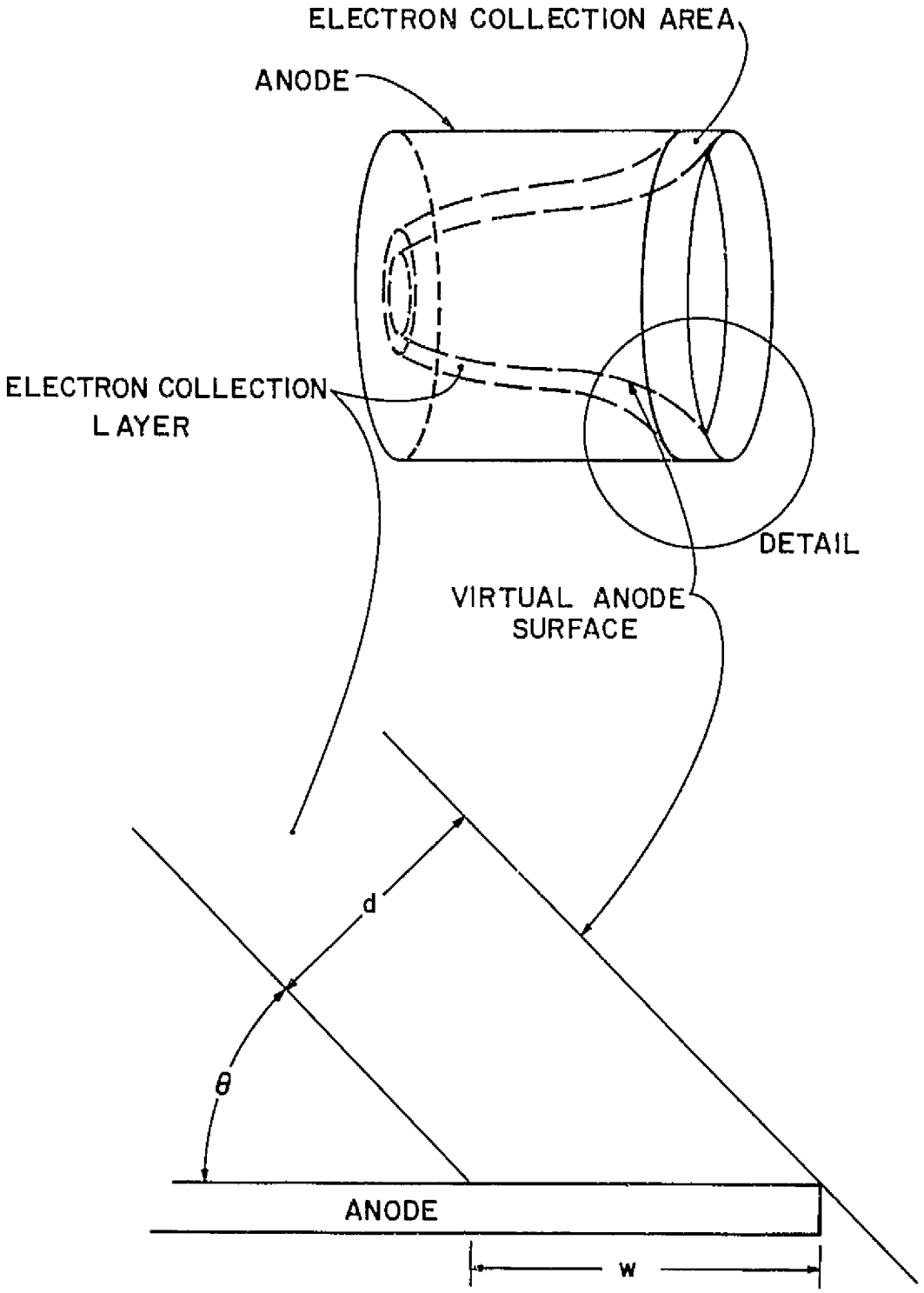

Figure 8. Schematic of electron collection region geometry.

the anode is related to the collection layer thickness d through the magnetic field incidence angle θ.

To estimate the thickness d consider a plane perpendicular to the magnetic field in the vicinity of the virtual anode as shown in Figure 9. Recalling that electrons tend to travel in helical paths about the magnetic field lines, the electron paths project as circles in the plane referred to. The center of the circle is the electron's guiding center in the plane. When an electron has a collision, its guiding center changes location in the plane abruptly and randomly to a place where it is again its Larmor radius distant from the location of its collision. Since the average location of its last collision is its previous guiding center, it is seen that the average step length of the random walk of the guiding centers across the magnetic field is the average Larmor radius.

The average Larmor radius can be obtained from Equation (1) using $u = \langle u_\perp \rangle$ the average electron velocity perpendicular to the magnetic field. The average electron velocity in any direction for isotropic Maxwellian velocity distribution functions is known to be

$$\langle u_\perp \rangle = \left(\frac{8\, e\, T_{mx}}{\pi M_e} \right)^{1/2} . \qquad (25)$$

Thus choosing the direction as one perpendicular to the magnetic field, the average Larmor radius becomes

$$\langle R_L \rangle = \frac{M_e}{eB} \left(\frac{8\, e\, T_{mx}}{\pi M_e} \right)^{1/2} \qquad (26)$$

This value becomes in effect the mean free path for electrons diffusing by collisions across the magnetic field near the virtual anode.

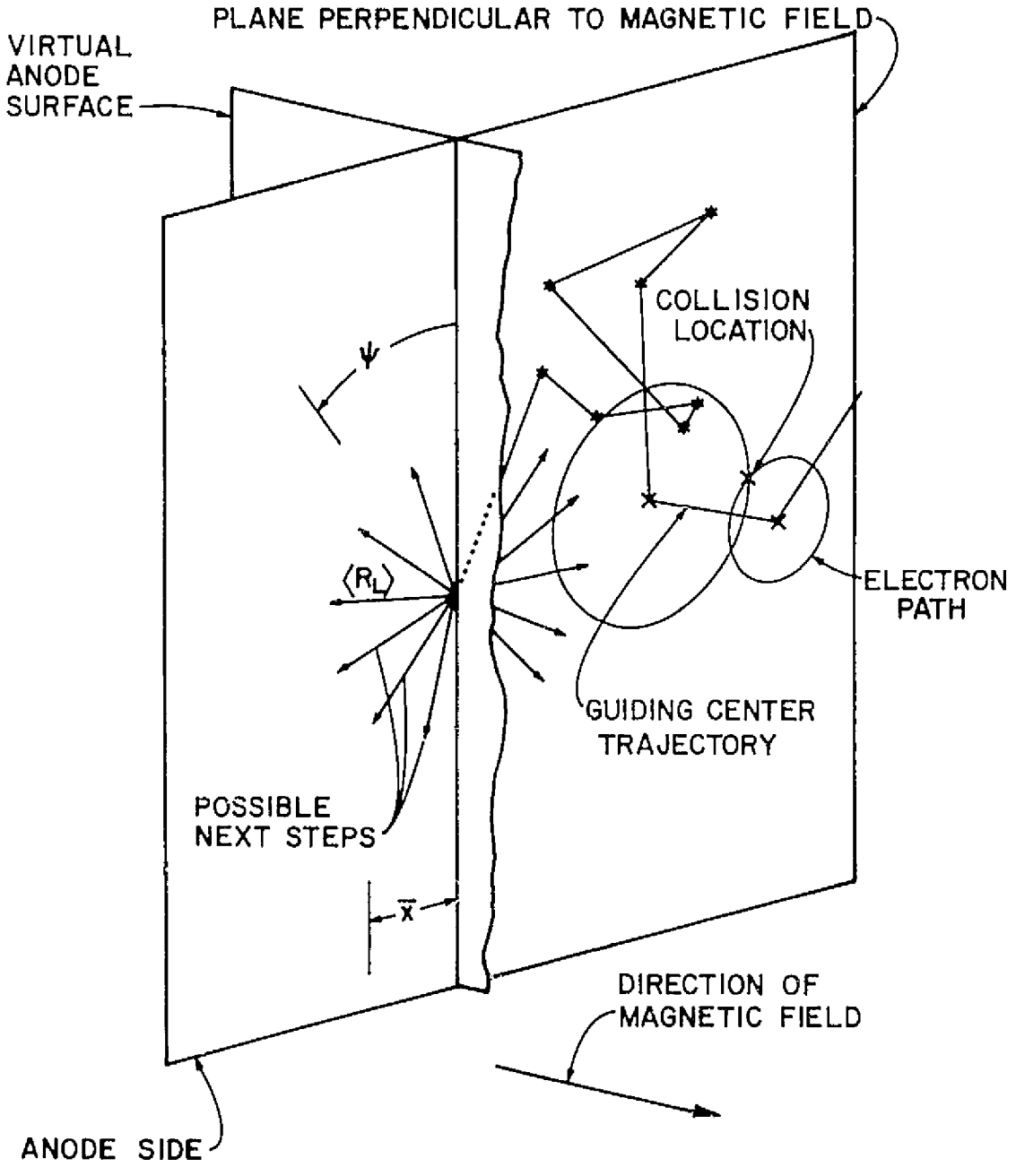

Figure 9. Visualization of electron guiding center drift across virtual anode surface in random walk.

The average distance from the virtual anode of guiding centers which effectively diffuse across that surface will be the average mean step length in a direction perpendicular to the virtual anode. To find that consider a line in the plane perpendicular to the magnetic field as shown in Figure 9 which represents the intersection of that plane with the virtual anode surface. The angle ψ which the next guiding center trajectory step makes with the intersection of the planes, assuming the last guiding center to be on the line, is a random variable. Therefore, the average distance $\bar{x}$ from the virtual anode to an electron's next guiding center, provided it is on the anode side of the virtual anode surface, may be calculated from

$$\bar{x} = 2 \int_0^{\pi/2} \langle R_L \rangle \sin\psi d\psi = \frac{2}{\pi} \langle R_L \rangle . \qquad (27)$$

With the guiding centers of the electrons scattered into the electron collection layer a distance $\bar{x}$ from the virtual anode surface on the average, it is observed that the average location of the electrons themselves will be their new guiding centers after scattering. Thus, $\bar{x}$ becomes equivalent to d where

$$d = \bar{x} = \frac{2}{\pi} \langle R_L \rangle . \qquad (28)$$

Using this value for d with the appropriate anode radius, magnetic field strength and angle θ for three different thrusters, the value of V_{s_a} was solved for. That value is compared with observed values (taken as the approximate average plasma potential less anode potential) in Table 1. Also shown in Table 1 are the parameter values used in calculating V_{s_a}. Data for the axial field thruster and SERT-II thrusters are taken

Table 1. Comparison of calculated plasma potential at the anode with observed difference between average plasma potential and anode potential with critical parameters required for computation also listed.

Thruster	Axial Field	SERT-II	SIT-8
T_{mx_a} (eV)	4.6	5	11.6
B (Tesla)	.0019	.0015	.0044
θ (deg)	26	75	55
R_a (m)	.075	.075	.044
$I_c + I_b$ (A)	1.03	1.7	0.72
n_{mx_a} (m^{-3}) x 10^{-16}	0.8	2.0	2.0
V_{s_a} (V)	1.69	1.30	6.33
$V_p - V_a$ (V)	1.5	1.5	7

from Knauer [6], and the SIT-8 data was taken at Colorado State University [30]. Considering the uncertainties associated with estimating the values of the parameters at the electron collection point and the approximation of the average plasma potential, the agreement between theory and experiment is surprisingly good.

V. CONSERVATION RELATIONS

Having developed descriptions for the processes which govern the discharge plasma of the ion production region, it remains to apply the conservation relations of mass, electronic charge and energy to complete the system of equations which may be used to obtain the plasma properties being sought in this investigation. The fundamental relation for each quantity is that the rate of supply to the ion production region must for steady state be balanced by an equal rate of loss. These supply and loss rates can be given in terms of geometry variables and plasma preoperties.

Mass Conservation

The conservation of electron mass will be discussed in connection with charge conservation. That leaves conservation of the mass of the propellant atoms to be discussed since it is assumed that all other components of the thruster are fixed and durable.

The rate at which propellant atoms are supplied to the thruster discharge chamber is usually given as an equivalent propellant current I_p where the atom flow rate is multiplied by the electronic charge e. Once in the discharge chamber, it is assumed that the propellant atoms distribute themselves uniformly over the discharge chamber volume and that they are in thermal equilibrium with the chamber walls. For the control volume of the ion production region as shown in Figure 7 it is assumed that the density of each excited neutral state is spatially uniform. Ions respond to electromagnetic forces and will be distributed differently. For virtually all thrusters the only way for atoms to leave the thruster is through the grids via the ion production region.

It is, therefore, appropriate to assume that the total propellant flow goes into the ion production region. I_p will be known from thruster operating data.

Atom mass flow from the grids has two parts. Charged particles are assumed to leave the plasma at the Bohm velocity given by Equation (6). From statistical thermodynamics [31] it is found that the neutral atom flux density to any surface will be given by

$$\Gamma_o = \frac{n_o}{4}\left(\frac{8\ k\ T_o}{\pi M_o}\right)^{\frac{1}{2}} \tag{29}$$

where n_o is the local neutral atom density, k is Boltzmann's constant, M_o is the neutral atom mass, and T_o is the neutral atom temperature (in degrees Kelvin) which is assumed to be equal to the thruster wall temperature. Thus for optics with screen area A_s, screen open area fraction ϕ_s and accelerator open area fraction ϕ_a (less than ϕ_s) the conservation relation for atoms is

$$\frac{I_p}{e} = A_s\left[\phi_a \frac{n_o}{4}\left(\frac{8\ k\ T_o}{\pi M_o}\right)^{\frac{1}{2}} + \phi_s \langle n_i\ V_B \rangle_s\right] \quad . \tag{30}$$

Because ion density n_i and Bohm velocity (which relies on local Maxwellian electron temperature) are not constant over the grid area, area-averaged values of these quantities must be used in Equation (30). These can be related to volume averaged values by using a plasma uniformity factor similar to the one used by Peters [19]. This factor is defined by

$$F_s = \frac{\int n_i\ T_{mx}\ dA_s}{\text{Screen Area}\ A_s\ n_i^*\ T_{mx}^*} \tag{31}$$

where the asterisks denote volume averaged quantities in the ion production region. Then recalling from quasineutrality that $n_i \approx n_e$,

$$\langle n_i \, v_B \rangle_s = F_s \, n^*_{mx} \left(1 + \frac{n_{pr}}{n_{mx}}\right) v^*_B \qquad (32)$$

where v^*_B is the Bohm velocity calculated using volume averaged temperature T^*_{mx}. In order to calculate F_s it is necessary to know both density and temperature profiles. These will be developed in a later chapter. To use Equations (30) and (32) it is also necessary to know the primary to Maxwellian electron density ratio. That will be discussed in the next section. The chief value of Equation (30) is to relate atom density n_o to electron density and temperature.

Another application of the atom mass conservation principle is in the determination of the relative densities of the various excited states of propellant atoms in the ion production region. Figure 10 shows in schematic the various production and loss mechanisms (indicated by the arrows) which are considered important in the ion production region of a mercury thruster. The important atomic states are indicated by the circles. Using the reactions indicated in Figure 10 and the appropriate reaction rate factors given in Appendix A, together with the atom fluxes to the boundaries as previously discussed, a set of equations describing the production and loss of each of the states considered may be written. A typical equation is the following for the production and loss of the 6^3P_0 metastable state atoms:

$$n^*_{mx} \Psi \left[\frac{n_{pr}}{n_{mx}} P^m_o(E_p) + Q^m_o(T_{mx})\right] n_o - \left\{ A_p \left(\frac{k\,T_o}{2\pi M_o}\right)^{\frac{1}{2}} + n^*_{mx} \Psi \left[\frac{n_{pr}}{n_{mx}} P^+_m(E_p) + Q^+_m(T_{mx})\right] \right\} n_m = 0 \; . \qquad (33)$$

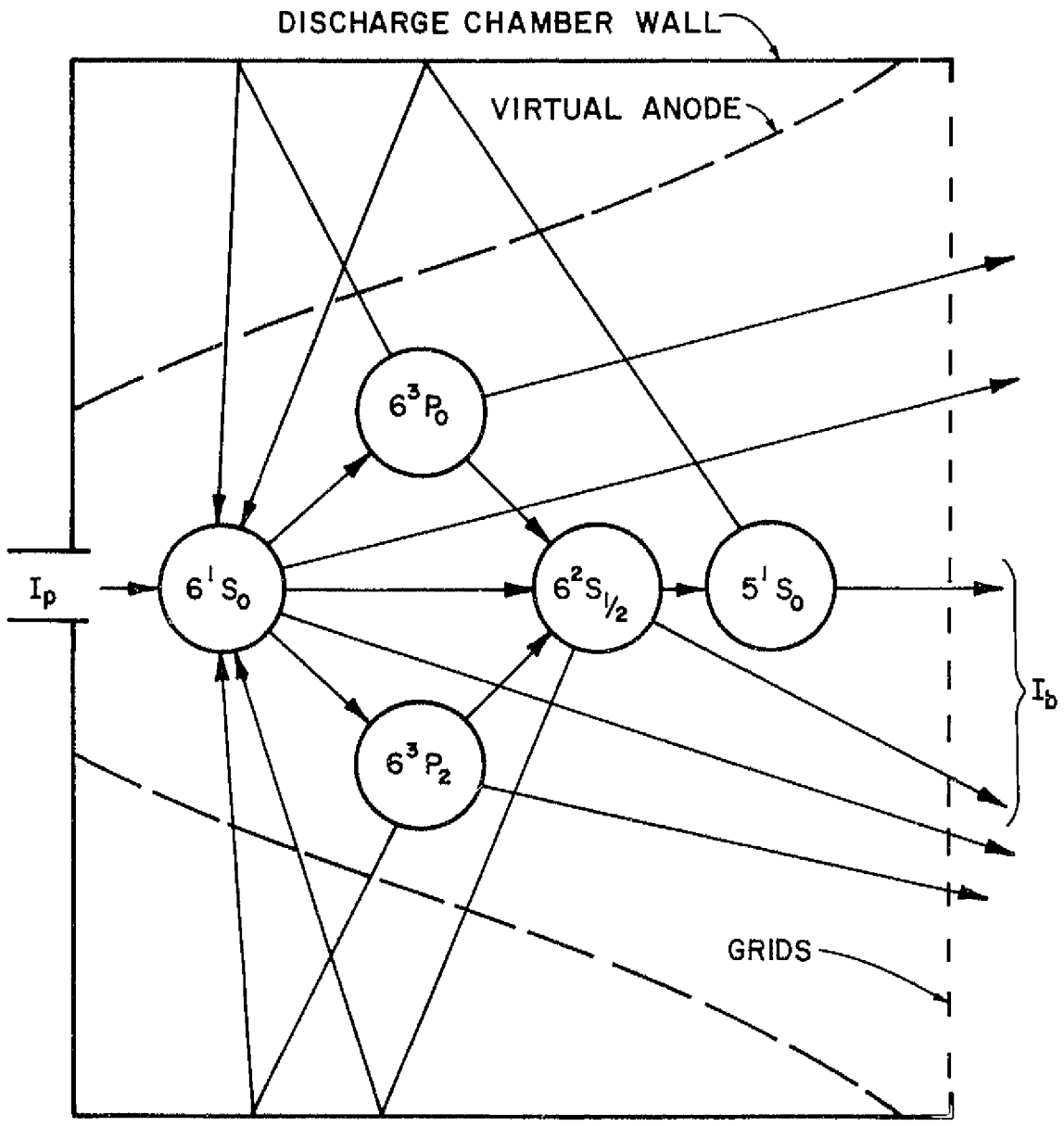

Figure 10. Schematic of important mass flows and transitions in mercury ion thrusters.

The first term accounts for the creation of metastable atoms from the neutral ground state by both primary and Maxwellian electron impingement. The first part of the second term is the rate at which these metastable atoms having temperature T_o escape across the ion production region boundary area A_p to reach the walls to de-excite or be lost from the discharge chamber. The second part of the second term is the rate at which single ions are created from the metastable atoms by electron impact. A similar equation may be written for each of the states considered important. Since each of the equations is linear in the atomic state densities n_a, the set may be easily solved to give those densities in terms of the plasma properties, propellant characteristics, and design data.

Having thus determined the densities of the various atomic states in the ion production region and related plasma properties to those densities, the conservation of electrons will now be discussed.

Charge Conservation

Because all of the positive charge is assumed to be carried by the atomic nuclei, charge conservation in the present problem reduces to the accounting for all of the electrons. Maxwellian electrons will be considered first, then some observations will be made concerning primary electrons.

It was shown in a previous section that virtually all Maxwellian electrons leave the ion production region by diffusing to the virtual anode surface where they are quickly collected by the anode. It was also indicated that the current to the anode consisted of the cathode emission current I_c plus a current component equivalent in magnitude to the beam current I_b. Macroscopically, this statement satisfies the

charge conservation law for the Maxwellian electrons in the ion production region. Obviously, all the electrons which enter the ion production region from the cathode must be removed in steady state. This is done mainly at the anode. It is assumed that all the primary electrons become thermalized and leave as Maxwellian electrons. In addition to those electrons, it is necessary to remove from the ion production region all of the electrons which are freed from the propellant atoms in the ionization process to avoid the rapid buildup of negative space charge by the escapting positive ions. Assuming that the electron flux to the thruster walls to counter the ion current is small compared with other electron currents, the electrons freed from the ions which make up the beam current will nearly all be collected along the virtual anode.

The density of the Maxwellian electrons in the ion production region will be governed mainly by the density of the ions present. A fundamental assumption of plasmas is that the densities of ions and electrons must be nearly the same to prevent excessively large electric fields. This is the quasineutrality assumption. Because the ions are so massive compared with the electrons, it is the electrons which do most of the adjusting to satisfy the quasineutrality condition. When there are restrictions to electron flow, as there are in ion thrusters due to the magnetic field, then electric fields are set up which modify ion density. Macroscopically, the average electron density will be the same as the average ion density. Recalling that primary electrons are also present this relation becomes

$$n^*_{mx} = \frac{n^*_i}{(1 + \frac{n_{pr}}{n_{mx}})} \quad . \tag{34}$$

Concerning the conservation and density of primary electrons in the ion production region, it is observed from plasma property maps [6,13,19] that to a first approximation the ratio of primary to Maxwellian electron densities is constant inside the ion production region. It is also very convenient for computational purposes to assume that the ratio is constant. A method of obtaining the volume averaged primary electron density n^*_{pr} is therefore sought.

The conservation relation requires that all the primary electrons which enter the ion production region be eventually collected by the anode. If it is assumed that all the primary electrons become thermalized after just one collision, which ought to be an upper bound on the thermalization rate if particle collisions are the mechanism of thermalization, then the balance between supply and loss rate of primary electrons in the ion production region will be described by

$$I_c = n^*_{pr} \forall\, e\, \nu_t \tag{35}$$

where ν_t is the thermalizing collision frequency per primary electron which is given approximately by

$$\nu_t = \left(\frac{2\,E_p}{M_e}\right)^{\frac{1}{2}} (n_a\, \sigma_i + 2\, n_e\, \sigma_e)\ . \tag{36}$$

In Equation (36) n_a is the number density of the atomic particles present including ions which can undergo inelastic collisions with cross section σ_i, and twice the electron density n_e represents reasonably well the density of charged particles which undergo elastic momentum exchange collisions with cross section σ_e.

Using accepted cross sections and atom densities as given by the production and loss rate equations, described previously, in

Equations (35) and (36), the cathode emission current I_c, as given by the difference between anode current and beam current, was calculated for three different thrusters. The comparison between calculated and measured values is given in Table 2. Data for the SERT-II, SIT-8 and cusped field thrusters are presented which come respectively, from References [19], [30] and [11]. It will be seen that the agreement between calculated and observed values is fairly poor. This suggests that either there is some other mechanism for thermalizing the primary electrons or that many of them go directly to the anode without being thermalized.

Because a detailed investigation of primary electron thermalization phenomena is outside the scope of this treatise, it will suffice here to use values of primary electron density in the ion production region which are obtained by correlation of empirical data from 8 cm, 15 cm and 30 cm diameter divergent field thrusters. This correlation is shown in Figure 11. The corresponding equation for calculating that density is

$$n^*_{pr} = 2.75 \times 10^{15} \left(I_a^{0.15} V_a^{0.75} - 12\right) \qquad (37)$$

where I_a is the total anode current and V_a is the anode potential. After calculating the anode current as the sum of the controllable cathode current I_c and the beam current, the value of n^*_{pr} from equation (37) can be found and divided by n^*_{mx} to get the primary to Maxwellian electron density ratio. While this will not be totally accurate, it will do for most thrusters where that ratio is small and errors in it will not have a pronounced effect on other plasma properties. Discussion now turns to the conservation of energy. Because electron potential

Table 2. Comparison of calculated primary electron currents to the ion production regions of three thrusters with the observed primary electron current to the anode

Thruster	SERT-II	SIT-8	Cusped Field
n_a (m^{-3}) x 10^{-17}	7.6	8.7	8
n_{mx} (m^{-3}) x 10^{-16}	8.3	7.5	30.2
n_{pr} (m^{-3}) x 10^{-16}	.75	1.75	1.7
$\forall$ (m^3) x 10^4	7.9	2.0	11.2
E_p (eV)	29.6	29.4	27.9
σ_i (m^2) x 10^{19}	1.4	1.4	1.4
σ_e (m^2) x 10^{19}	.95	.95	1.05
ν_t (sec^{-1}) x 10^{-5}	4.0	4.5	4.6
I_c calc (A)	.38	.25	1.4
$I_a - I_b$ (A)	1.46	.644	3.67

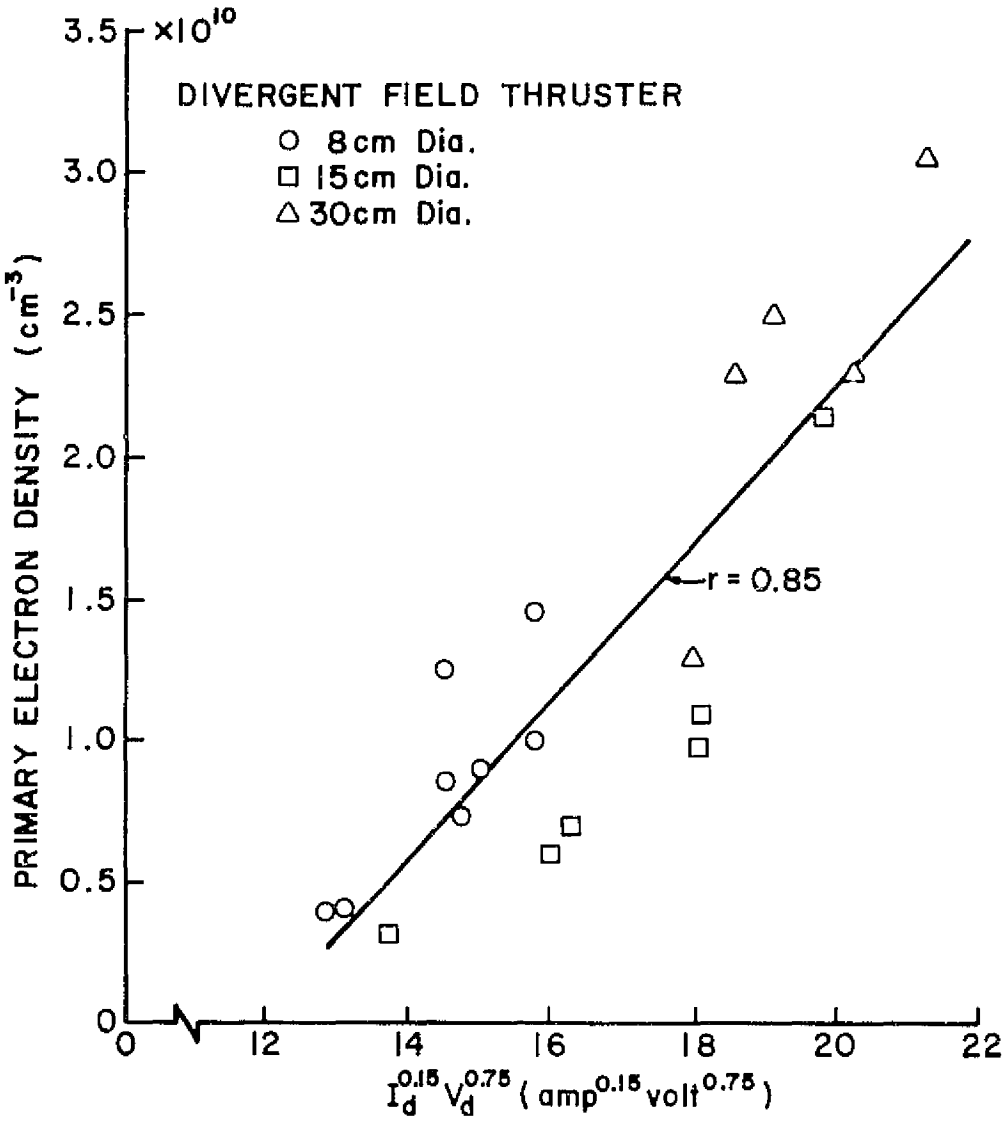

Figure 11. Average primary electron density correlation.

energies have been neglected in the ion production region, the kinetic energy of the electrons will be of chief concern.

Energy Conservation

If the Maxwellian electrons in the ion production region are considered as a system, the conservation of energy requires that any energy they receive from primary electrons must be lost to inelastic processes within the ion production region or be lost at the boundaries of the region. The rate per Maxwellian electron at which primary electron energy is transferred to the Maxwellian population is given by

$$\dot{E}_{mx_{in}} = \frac{I_c E_p}{e \Psi n^*_{mx}} - \frac{n_{pr}}{n_{mx}} \sum_j n_j p_j(E_p) \tag{38}$$

where the first term on the right is the rate of primary electron energy supplied to the ion production region, and the second is the rate at which the primary electrons lose energy to inelastic processes with $p_j(E_p)$ being the primary electron energy rate factor given by Equation (8). The summation implied is over the various atomic states present in the ion production region.

The rate per Maxwellian electron at which the Maxwellian electrons lose energy to inelastic processes within the ion production region is

$$\dot{E}_{mx_{\Psi}} = \sum_j n_j q_j(T^*_{mx}) \tag{39}$$

where $q_j(T^*_{mx})$ is the Maxwellian energy rate factor given by Equation (11). The rate per Maxwellian electron at which energy is lost to the boundaries of the ion production region is

$$\dot{E}_{mx_b} = \frac{\dot{E}_a + \dot{E}_b}{n^*_{mx} \Psi} \tag{40}$$

where $\dot{E}_a$ and $\dot{E}_b$ are the boundary loss rates to the anode and upstream end given respectively by Equations (22) and (19). Note that both $\dot{E}_a$ and $\dot{E}_b$ depend on boundary values of plasma properties rather than the volume averaged values. Again the need for property profiles is evident. The conservation of energy requires that

$$\dot{E}_{mx_{in}} = \dot{E}_{mx_{\Psi}} + \dot{E}_{mx_b} \quad . \tag{41}$$

This is the fundamental relation which governs the Maxwellian electron temperature in ion thrusters.

The relations derived thus far are difficult to solve for average plasma property values given the input data without a fairly lengthly iteration process. This is most easily done by a computer. The inverse problem of obtaining input data given plasma properties is much simpler. An example of how that can be done from the macroscopic point of view is presented in Appendix B for the SER-II thruster. There the current required from the cathode to support a given plasma state is obtained.

A complication to a plasma property predictor model which has not yet been dealt with is to obtain the plasma property profiles. The macroscopic balance equations obtained previously can be used to get volume averaged properties, but they rely on property profiles as has been stated to give good results. The following two chapters deal with that problem.

First, these profiles will be obtained for the case of a uniform axial field thruster, then those concepts will be applied to divergent field thrusters.

VI. PLASMA PROPERTY PROFILES FOR A UNIFORM AXIAL MAGNETIC FIELD

It was found earlier that to satisfactorily account for boundary fluxes it is necessary to know something about the spatial distribution of the plasma properties in the ion production region. These profiles can be approximated from a consideration of the processes ongoing in the ion production region and the local application of the conservation laws. This is most easily accomplished in the ion production region of a thruster which has a uniform axial magnetic field.

Density Profiles

It was shown previously that virtually all Maxwellian electrons leave the ion production region by diffusing to the virtual anode surface where they are quickly collected by the anode. In the case of a thruster with a uniform axial magnetic field, the virtual anode and the actual anode coincide over the anode length. Also, the only diffusion across the magnetic field is in the radial direction, so that Equation (3) may be written as

$$n_{mx} v = - D \frac{\partial n_{mx}}{\partial r} \tag{42}$$

where it is noted that even though axial density gradients may exist, there is no net flux in the axial direction.

The steady state continuity equation may be written for Maxwellian electrons in the ion production region which is now cylindrical as

$$\nabla_r \cdot (n_{mx} \bar{v}) = n_{mx} (\nu_i + \tau) \tag{43}$$

where ν_i is the Maxwellian electron production rate per Maxwellian electron due to ionization, and τ is the Maxwellian electron production rate per Maxwellian electron due to the thermalization of primary electrons. The first of these ν_i is given by

$$\nu_i = \sum_j n_j \left[\frac{n_{pr}}{n_{mx}} P_j^i(E_p) + Q_j^i(T_{mx}) \right] \tag{44}$$

where the summation implied is over all the states which can be ionized, and the superscript i denotes ionization reactions. Reactions from singly to doubly ionized states are included in the above. The density of each state is indicated by n_j, and it is assumed that the atomic densities are uniform over the ion production region volume. Because the pressure in thruster discharge chambers is so low, this ought to approximate reality.

τ in Equation (43) is the rate per Maxwellian electron at which the primary electrons become thermalized and enter the Maxwellian electron population. It may be found from

$$\tau = \frac{I_c}{e\, n_{mx}^* \Psi} \tag{45}$$

where I_c is the emission current coming from the cathode, and Ψ is the volume of the ion production region. Both ν_i and τ have units of inverse time.

Differentiating Equation (42) with respect to r and substituting the result into Equation (43) gives

$$\frac{\partial^2 n_{mx}}{\partial r^2} + \frac{1}{r} \frac{\partial n_{mx}}{\partial r} + n_{mx} \left(\frac{\nu_i + \tau}{D} \right) = 0 \tag{46}$$

By using the Bohm diffusivity based on the volume averaged temperature T_{mx}^*, the coefficient of n_{mx} in Equation (46) becomes a spatial constant

for a given operating condition. Equation (46) thus becomes a zero order Bessel equation having as its solution for n_{mx} bounded at $r = 0$

$$n_{mx} = n_{mx_o} J_o\left(\sqrt{\frac{\nu_i + \tau}{D_B}}\, r\right) \tag{47}$$

where n_{mx_o} is the value of n_{mx} along the thruster axis. Since electric fields and ion motion have been ignored, it is appropriate to assume that n_{mx_o} is a constant independent of z. This center line density is related to the volume averaged density n^*_{mx} through the relation

$$n_{mx_o} = \frac{n^*_{mx}\, X}{2\, J_1(X)} \tag{48}$$

where X is the argument of the Bessel function in Equation (47) evaluated at $r = R$, the radius of the ion production region. The magnitudes of these densities must be such as will satisfy the requirement for quasineutrality with the ions.

Temperature Profiles

An expression is now sought which will give the spatial distribution of Maxwellian electron temperature in the ion production region. It was seen earlier that Maxwellian electron kinetic energy is transported across the magnetic field of the ion production region by conduction at a rate characterized by the conductivity $K_\perp$ which was given by Equation (13). Hence, the conduction equation, which is the result of applying energy conservation locally, becomes for radial conduction

$$\frac{1}{r}\frac{d}{dr}\left(r\, K_\perp \frac{dT_{mx}}{dr}\right) = -\, U\, n_{mx}. \tag{49}$$

$U\, n_{mx}$ in this equation is the net volumetric energy addition rate. It will be recalled that energy is added to the Maxwellian electron population by the thermalization of primary electrons and taken away by the various inelastic processes undergone by the electrons. Both these processes occur at rates which are proportional to the Maxwellian electron density. Because the thermal conductivity along the magnetic field lines is so much greater than that across the field, it may be taken as effectively infinite, and the loss of energy to the upstream boundary of the ion production region, which is also density dependent, may be included in the local net energy addition U. Hence, U is given by

$$U = (\dot{E}_{mx_{in}} - \dot{E}_{mx_{\Psi}} - \dot{E}_{mx_{b}}) \tag{50}$$

where the energy rates in parentheses are given by Equations (38) to (40). These three rates are assumed to be spatially invariant because they are calculated from averaged properties and, $K_{\perp}$, given by Equation (13), is assumed to be spatially invariant except for its Bessel function dependence through the density n_{mx}. Equation (47) may be used with Equation (13) to cause Equation (49) to become

$$\frac{1}{r}\frac{d}{dr}\left[r\, J_o(Yr)\, \frac{dT_{mx}}{dr}\right] = -\frac{U\, J_o(Yr)}{4.7\, D_B} \tag{51}$$

where

$$Y = \sqrt{\frac{\nu_i + \tau}{D_B}} \tag{52}$$

Performing the indicated differentiation, this becomes

$$\frac{d^2T_{mx}}{dr^2} + \frac{dT_{mx}}{dr}\left[\frac{1}{r} - \frac{Y\, J_1(Yr)}{J_o(Yr)}\right] + \frac{U}{4.7\, D_B} = 0 \ . \tag{53}$$

While this equation is not amenable to analytical solution, it is easily solved using numerical techniques. The result is a curve $T_{mx}(r)$ which is very similar to the parabola

$$T_{mx}'(r) = T_{mx_o} - \frac{1}{4}\left(\frac{U}{4.7\ D_B}\right) r^2 \qquad (54)$$

but is slightly steeper. T_{mx_o} is the value of the Maxwellian electron temperature along the thruster axis. It will be that value which satisfies the energy conservation requirement that the energy carried to the boundaries plus that lost to the inelastic processes must equal that brought in by the primary electrons as described in Equation (41).

T_{mx_o} can be related to the volume averaged value T_{mx}^* by integrating $T_{mx}(r)$ over the volume of the ion production region. Because the temperature is assumed not to vary in the z direction, this is equivalent to averaging over the thruster cross sectional area:

$$T_{mx}^* = \frac{2}{R^2} \int_0^R r\, T_{mx}(r)\, dr\ . \qquad (55)$$

Again this is not convenient using analytical techniques but is easily done numerically. R in the above equation is the radius of the ion production region.

Data for a thruster having a truly uniform axial magnetic field are not readily available, however, the axial field thruster of Knauer [6] has the most nearly uniform field of the thrusters for which data is available. Figure 12 shows the variation of Maxwellian electron density and temperature in the ion production region of that thruster. It may be seen that density has somewhat the appearance of a Bessel function over the inner part of the region, however, because

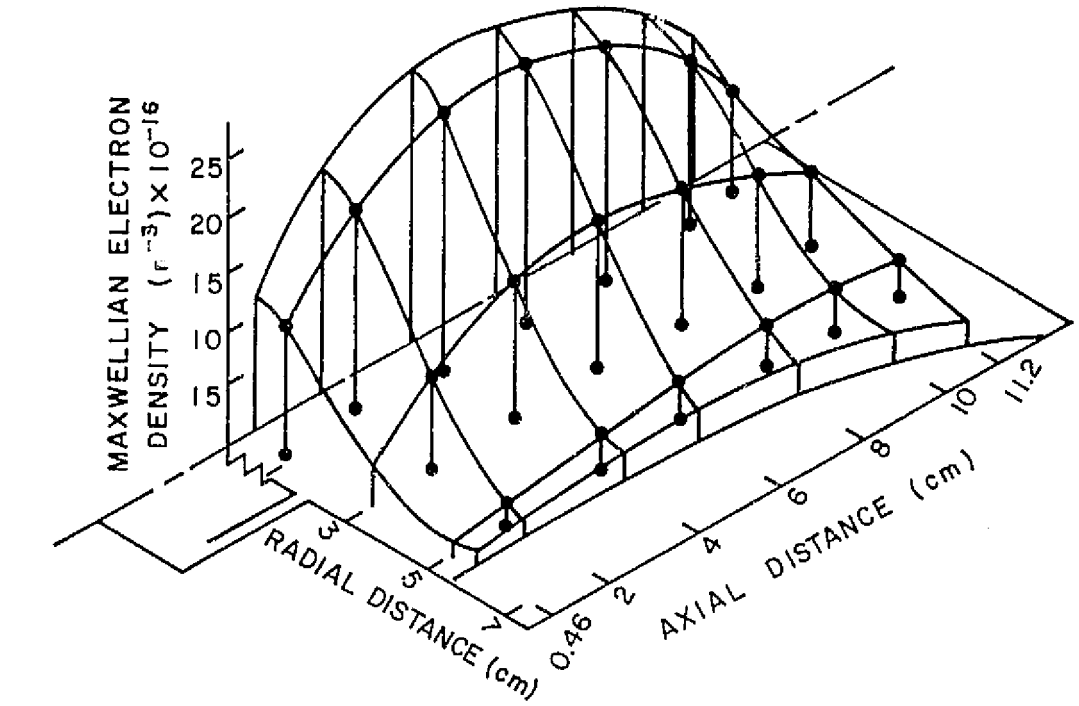

(a)

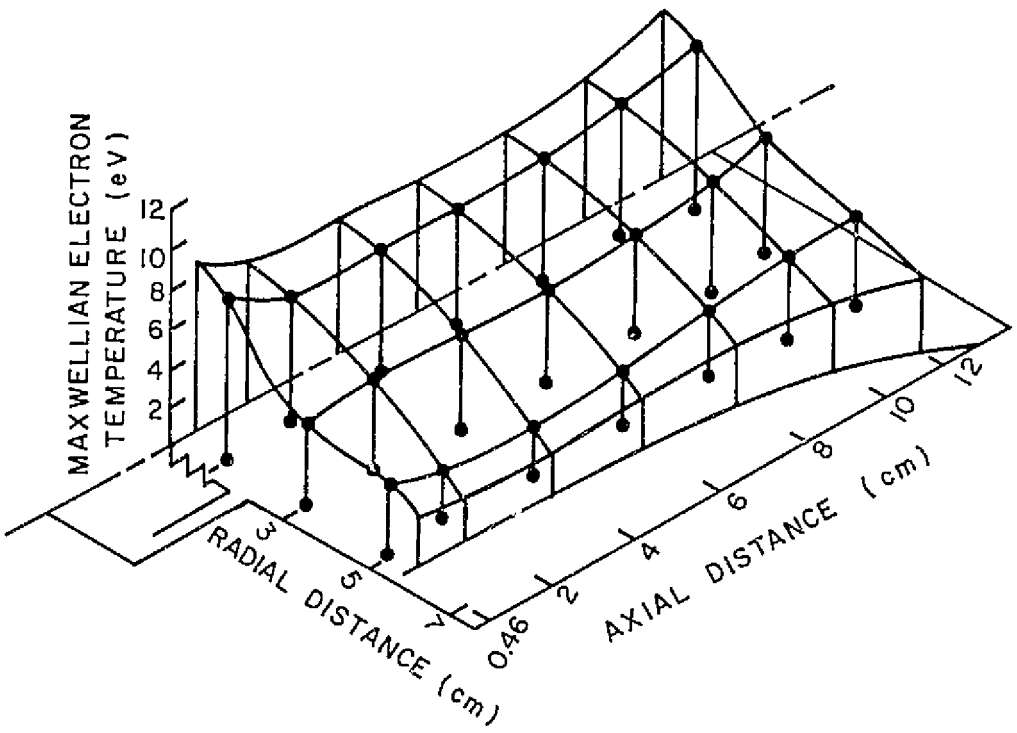

(b)

Figure 12. Measured Maxwellian electron (a) density and (b) temperature in the axial field thruster.

of the acknowledged non-constancy of n_{pr}/n_{mx} in that thruster, there is more ion production near the center line and less toward the outer edge giving rise to the general curve shape observed. Temperature profiles do appear parabolic, however, there is also some axial variation of both density and temperature for which the present model does not account. This is believed due to the influence of ion mass and electric fields near the region boundaries which have been neglected.

VII. PLASMA PROPERTY PROFILES FOR A DIVERGENT MAGENTIC FIELD

In the case of a uniform, axial magnetic field the calculation of plasma property profiles was accomplished with one-dimensional equations. It would simplify the analysis of divergent field thrusters greatly if a scheme could be devised whereby energy and electron transport in these thrusters could be described with similar, one-dimensional equations. A heuristic argument for such a simplification is discussed in the following sections.

Temperature Profiles

Figure 13 shows the magnetic field configuration of a typical divergent field thruster. Magnetic field lines extend from the upstream pole piece, which bounds the cathode chamber, to the downstream pole piece. Lines have been drawn orthogonal to the magnetic field lines in the ion production region. The z' direction is by definition the direction of the magnetic field lines while the r' direction is along the orthogonal lines. It has been observed experimentally that lines of constant Maxwellian electron temperature approach congruence with the magnetic field lines (Figure 4) making T_{mx} effectively independent of location in z'. This suggests that Maxwellian electrons move freely along field lines until they reach cathode potential boundaries where they are reflected back into the plasma. Hence, within the ion production region they experience no net motion in the z' direction.

It is postulated that Maxwellian electrons diffuse outward in the r' direction under a density gradient. This process is described mathematically by a one-dimensional equation of the form of Equation (46)

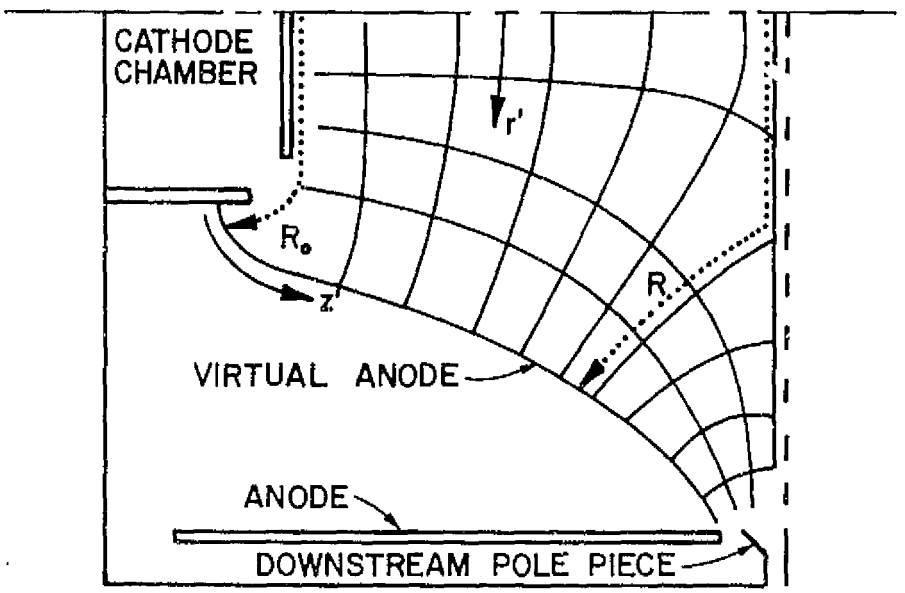

Figure 13. Curvilinear geometry of a divergent magnetic field.

if the density gradient, and hence the direction of net flow, is not appreciably different from the radial direction. It is noted a new non-dimensional variable in the r' direction could be selected such that its value would be constant along field lines. Such a variable would be

$$\rho = \frac{r'}{R} \tag{56}$$

where R is the distance in the r' direction from the thruster axis to the virtual anode. ρ then varies from zero to unity as one moves from the center-line to the virtual anode along any orthogonal to the magnetic field lines. When field lines intersect the screen grid it is argued that the r' and R paths could be determined reasonably as suggested by the dotted trajectory labelled R in Figure 13. If one argues next that the functional nature of the temperature variations in r' for the divergent field geometry will be similar to those in r for the cylindrical chamber, then the differential equation describing the radial energy diffusion for the cylindrical case can be assumed approximately correct in the divergent field case. In non-dimensional form, Equation (53) may be rewritten as

$$\frac{d^2\theta}{d\rho^2} + \frac{d\theta}{d\rho}\left[\frac{1}{\rho} - X\,\frac{J_1(X\rho)}{J_0(X\rho)}\right] + \frac{1}{4.7} = 0 \tag{57}$$

where

$$\theta = \frac{T_{mx}\, D_B}{UR^2} \tag{58}$$

is the non-dimensionalized temperature and

$$X = \sqrt{\frac{\nu_i + \tau}{D_B}}\; R \quad . \tag{59}$$

If ρ is assumed constant along field lines, the argument ($X\rho$) of the Bessel functions in Equation (57) will also be constant along field lines. Solutions to Equation (57) will thus satisfy the experimental observation that Maxwellian electron temperature is constant along magnetic field lines. The description of temperature variation in divergent field thrusters is thus much simplified.

Density Profiles

The transverse variation of Maxwellian electron density across the magnetic field of the ion production region can be found in the same way as the temperature variation was found. The dimensionless variables ρ and X of Equations (56) and (59) can be substituted into Equation (46), making assumptions and approximations similar to those that were made for the temperature profiles, to give a dimensionless diffusion equation with

$$\frac{n_{mx}}{n_{mx_o}} = J_o\ (X\rho) \tag{60}$$

as its solution. Again assuming that ρ is constant along magnetic field lines, this says that the ratio of Maxwellian electron density at any point to the density at the location on the thruster axis where the orthogonal to the magnetic field line through the given point crosses the thruster axis will be constant. It does not necessarily imply that density will be constant along magnetic field lines in divergent field geometries. Indeed, density is observed to vary along magnetic field lines [9].

Before examining this variation in density along z', a field divergence parameter "a" is defined by

$$a = \frac{R_o}{R} \tag{61}$$

where R_o is the distance from the thruster axis to the virtual anode at the upstream end of the ion production region as shown in Figure 13. Again assuming that the field is not strongly divergent, it will be approximately true that

$$\frac{a^2}{B} = \text{const.} \tag{62}$$

The approximation is best for the least field divergence.

Figure 14 now shows the variation in Maxwellian electron density along the axes of four different thrusters. The circular symbols are measured densities which have been normalized with respect to the density midway between the upstream and downstream ends on the thruster axis. The solid lines which are shown are the values of the square of the divergence parameter "a" which have also been normalized with respect to the value of a^2 midway along the thruster axis. Except for a characteristic reduction in density at the upstream end, which is to the left in Figure 14, the agreement between these curves and the measured data is reasonably good. The SERT-II and axial field data are from Knauer [6], the 30 cm thruster data are from Hughes Research Laboratories [32], and the 8 cm thruster data were taken at Colorado State University [30].

While the physical explanation for the a^2 dependence cannot be stated with certainty, one possibility is that, except near the ends

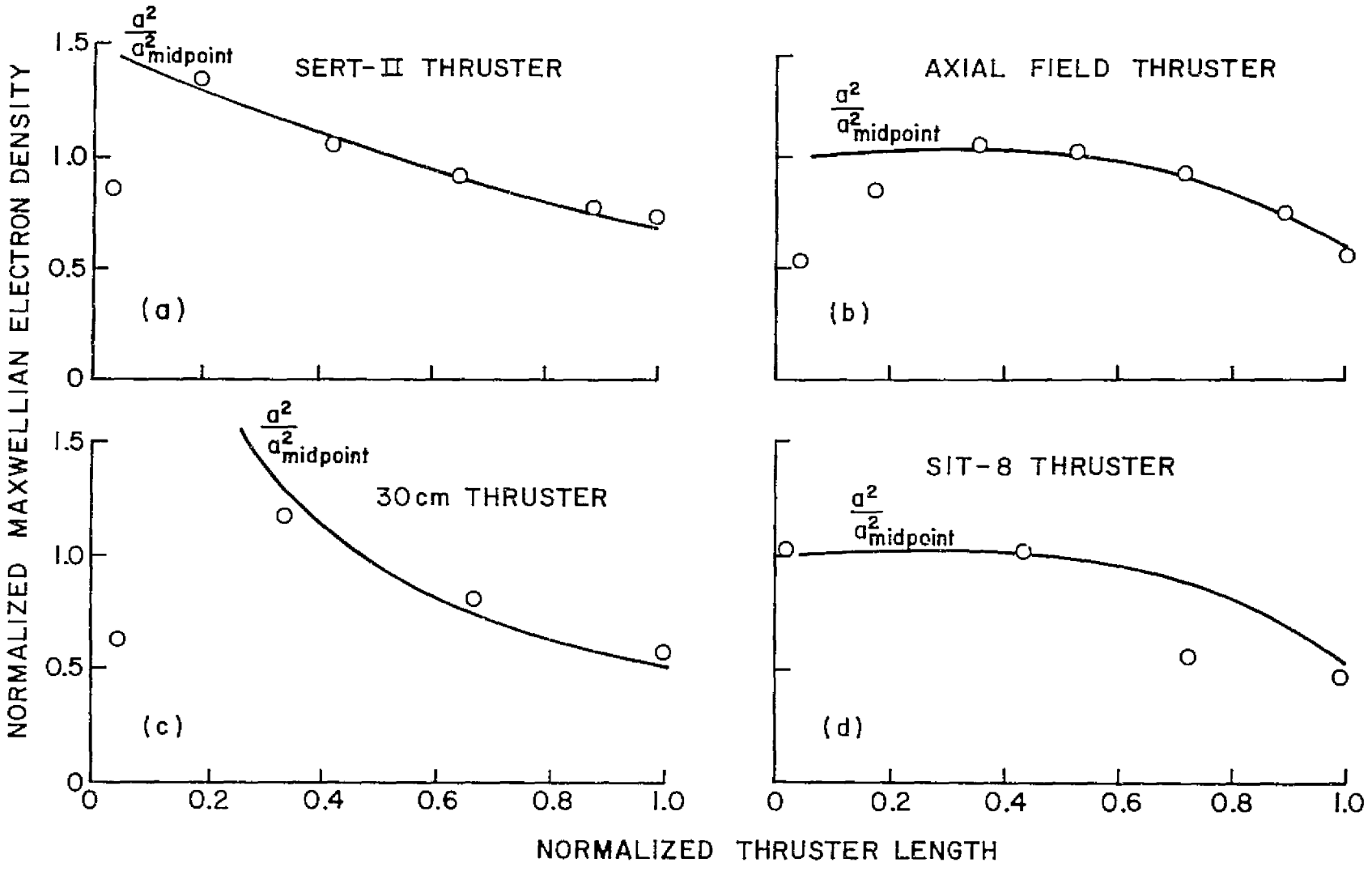

Figure 14. Comparison of density normalized with respect to its midpoint value with the square of the normalized magnetic field divergence parameter "a".

of the discharge chamber, the various forces which might tend to effect the axial density distribution, such as drift forces and those due to electric fields, are relatively unimportant compared with phenomena tending to keep the electrons in local equilibrium. Continuity requires that for a control volume bounded by magnetic field lines along which electrons move with velocity $u_{\parallel}$, i.e.

$$n_1 u_{\parallel 1} A_1 = n_2 u_{\parallel 2} A_2 \quad . \tag{63}$$

The subscripts 1 and 2 refer to any two arbitrary locations along the control volume and it is assumed that the perpendicular area A may vary along the magnetic field lines. Normally one thinks of $u_{\parallel}$ as changing along field lines of a diverging magnetic field, however, if it is assumed that $u_{\parallel}$ is constant,

$$\frac{n_1}{n_2} = \frac{A_2}{A_1} \quad . \tag{64}$$

Again assuming that the field is not strongly divergent, it will be approximately true that

$$\frac{A_2}{A_1} = \left[\frac{R_2}{R_1}\right]^2 = \left[\frac{a_1}{a_2}\right]^2 \tag{65}$$

which gives density the a^2 dependence indicated by Figure 14.

One condition that would cause $u_{\parallel}$ tend to be constant along the magnetic field lines would be that collisions which alter electron momentum may be sufficiently frequent that equilibrium is approached in a length short compared with thruster length. If that were true, the energy associated with $u_{\parallel}$ would tend to be a constant fraction of the total kinetic energy of the particle which is characterized by

T_{mx}. Since T_{mx} is apparently constant along magnetic field lines, u_n would then also be nearly constant.

In support of the concept of frequent collisions, it was observed previously that if the effective collision frequency for electrons were one sixteenth the cyclotron frequency, then the diffusivity given by the classical expression and the Bohm diffusivity become identical. Because the Larmor radius for most electrons is only a small fraction of the thruster length, it is possible that the effective mean free path of electrons along the magnetic field is sufficiently short to approximate local equilibrium while still preserving total energy along the magnetic field for constant temperature.

With the results of Equations (64) and (65) which characterize the observations of Figure 14, and denoting by N the value of the center line density at the location on the thruster axis where a = 1, a two-dimensional density distribution equation for the Maxwellian electrons can be obtained. From Equation (60) it is given in terms of the dimensionless variables X and ρ as

$$n_{mx} = N a^2 J_o(X\rho) \quad . \tag{66}$$

This can be related to a spatial distribution when it is recalled that "a" is a function of the curvilinear coordinate z', and depends on both r' and z' (note that R is a function of z').

With the approximations and the equations developed thus far, the analysis of ion thruster discharge chambers may be carried out. The following chapters indicate how that may be done and give some

results of that analysis for several thruster configurations for which the data is available for comparison.

VIII. COMPUTATIONAL TECHNIQUE

Algorithm

The equations which have been developed to describe the various processes and conditions which appear to goven the discharge of ion thrusters are many, and they are extensively coupled. They do, however, form a complete set which may be used to estimate to first order the properties of the Maxwellian electrons in the ion production region of a mercury ion thruster, which is what was sought at the outset. Because of the complexity of the system of equations, the only practical way to solve for Maxwellian electron properties is by combining the equations into a computer program which can be iteratively solved to arrive at plasma properties. A computer program has been written which performs that task. The basic algorithm is to first solve for a Maxwellian electron spatial density distribution, based on an assumed Maxwellian electron temperature and the other inputs referred to previously which characterize the ion production region in terms of design and control variables. The equations for the density distribution in the ion production region are much less sensitive to temperature errors than are the temperature equations to density errors. Having iteratively converged on a density profile for the Maxwellian electrons which is self consistent with all the pertinent equations relating to density determination for the assumed Maxwellian temperature, the equations related to the energy balance on the Maxwellian electrons in the ion production region are solved. This leads to a temperature error associated with the energy balance which is characterized by Equation (41). If the net energy addition rate per unit Maxwellian electron density U as given by Equation (50) is negative, then the assumed temperature was too high

because more energy is going into inelastic processes and to the boundaries than is being brought in by the primary electrons, a condition which is not physically realizable. If the energy rate to the anode is less than UΨ, then the assumed temperature is too low, and a higher temperature will result in more volumetric energy loss (lower UΨ) and a higher anode loss, and vice-versa. After correcting the guess on temperature, the density equations are solved again, and a better estimate of temperature is obtained. When the error value in both density and temperature loops is within acceptable limits (two per cent has been used successfully), the iteration stops and the important parameters are listed on the output.

Example

To see how the input values are obtained from basic thruster data, an example will be presented. SERT-II will be used as an example because it is better known than some others. Figure 15 is a representation of the SERT-II thruster magnetic field inside the virtual anode field line surface. Magnetic field lines shown were made from tracing iron filings maps. Lines have been drawn orthogonal to the magnetic field, and the divergence parameter "a" has been listed for each orthogonal line. Other geometric and magnetic field parameters needed to describe the ion production region have also been listed in Figure 15. L is the length of the virtual anode, measured along the magnetic field line, a_s is the value of the divergence parameter averaged over the screen grid area, B_o is the average value of the magnetic field strength at the upstream end of the ion production region, ϕ_a and ϕ_s are the open area fractions of the accelerator and screen grids, respectively, and R_o is

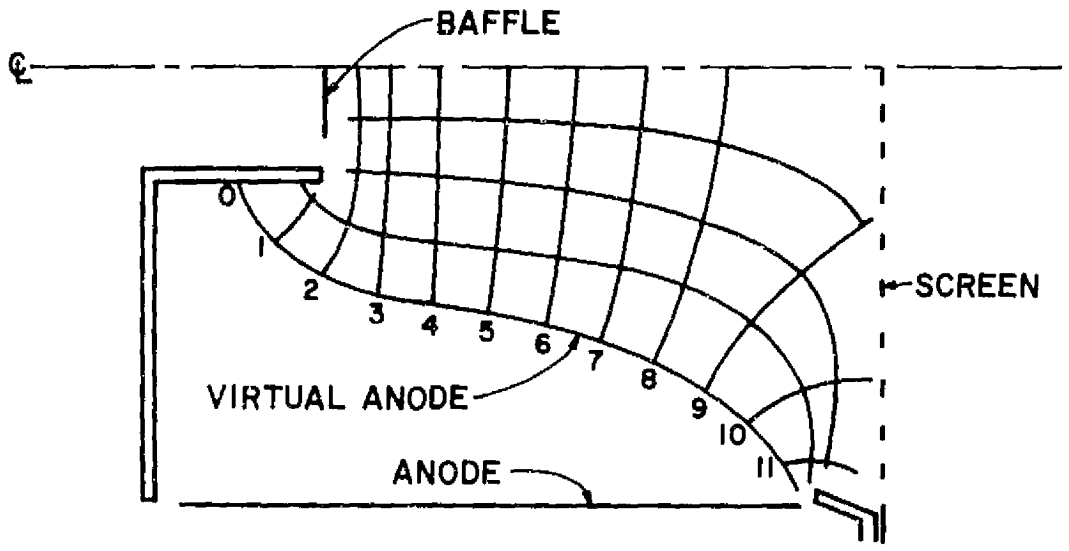

SERT-II MAGNETIC FIELD CONFIGURATION

PHYSICAL CONSTANTS

Ion Production Region Volume = 8.4×10^{-4} m^3

Ion Production Region Area = .05 m^2

Upstream Area = .003 m^2

Screen Area = .0154 m^2

Virtual Anode Area = .03 m^2

Anode Radius = .075 m

B at Electron Collection Point = .0015 Tesla
θ = 75 deg

MAGNETIC FIELD DIVERGENCE PARAMETERS

z'(m)	a	z'(m)	a	z'(m)	a
0.00	1.00	0.04	.816	0.08	.643
0.01	1.00	0.05	.778	0.09	.510
0.02	.862	0.06	.743	0.10	.448
0.03	.847	0.07	.700	0.11	.380

R' = .03 m

L = .11 m

$\emptyset_s$ = .72

$\emptyset_a$ = .50

a_s = .45

B' = .004 Tesla

Figure 15. Input data for SERT-II ion thruster.

the distance from the thruster axis to the virtual anode at the upstream end measured along a path perpendicular to the magnetic field.

The operating conditions chosen are a propellant mass flow of .307 A_{eq}, a cathode emission current I_c of 1.44 A (based on anode current of 1.7 A and beam current of .258 A), an anode potential V_a of 37.2 V, and a thruster wall temperature of 600°K. When these data are put into the computer model, the Maxwellian electron density and temperature profiles for the ion production region shown in Figures 16 and 17 are obtained. Measured values for the same thruster at the same operating conditions are also shown in those figures. The data for the measured values are from Peters [19]. The plasma was calculated to have a primary to Maxwellian electron density ratio of .11 as compared with Peters' value of .08. It was calculated that 5.4 per cent of the atoms were single ions, 0.1 per cent were double ions, and 13.8 per cent were in the metastable states of which 93 per cent were in the 6^3P_2 state. The calculated anode sheath potential was 3 V, compared with 1.6 V observed.

Other Results

To get a feel for the validity of the model in predicting plasma properties for thrusters in general, it was exercised for several other configurations for which data are available. Figures 18 and 19 show the comparison between calculated and measured Maxwellian electron density and temperature for the axial field thruster studied by Knauer [6], and Figures 20 and 21 show the same comparison for the Hughes 30 cm divergent field thruster [32]. There is moderate agreement between calculated and measured values in all cases except for Maxwellian electron density in the 30 cm thruster where the average density is approximately four times the measured value (note the difference in scale between the

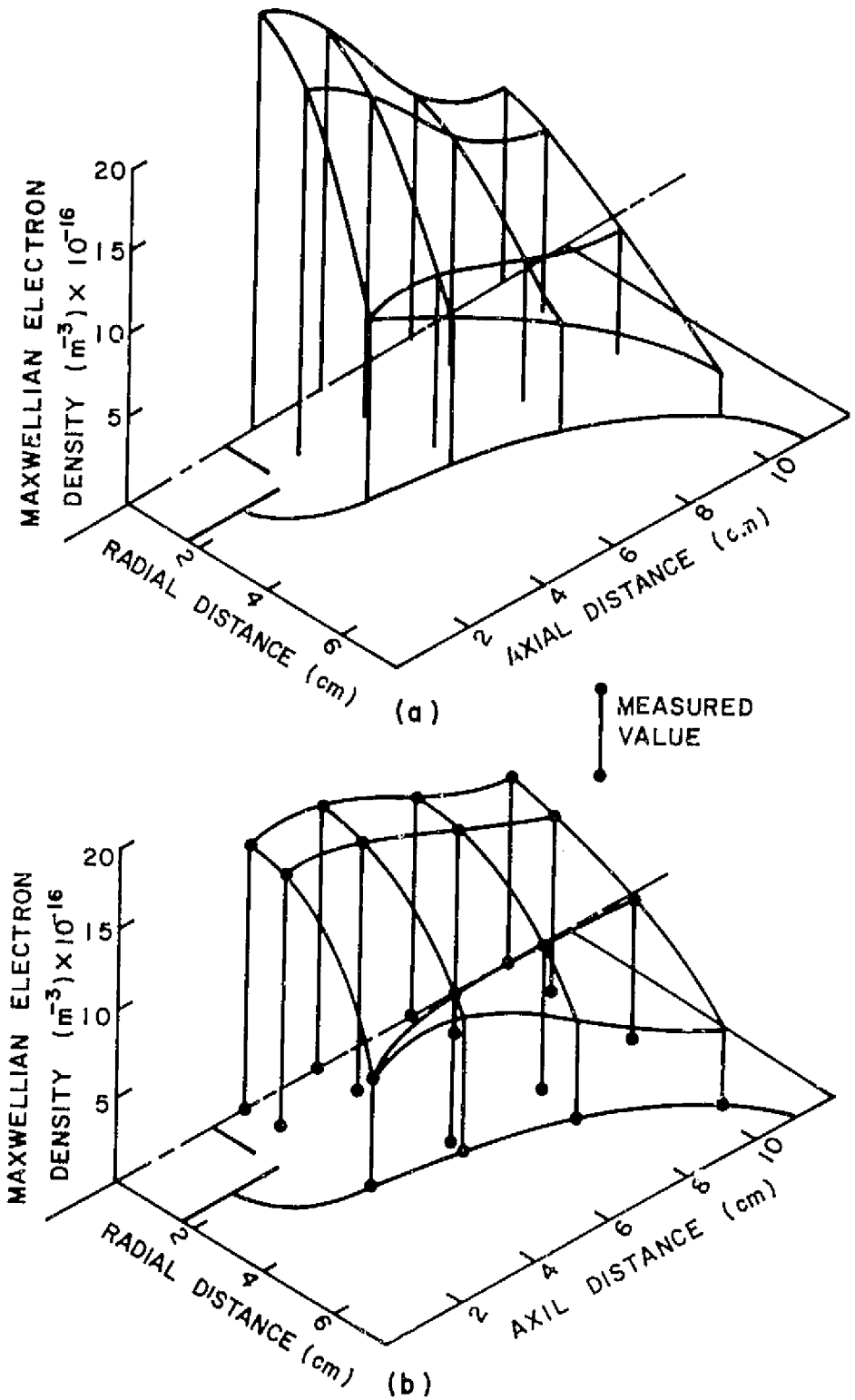

Figure 16. Comparison of (a) calculated with (b) measured Maxwellian electron density for the SERT-II thruster operating at 1.7 A, 37.2 V and .307 Aeq propellant mass flow rate.

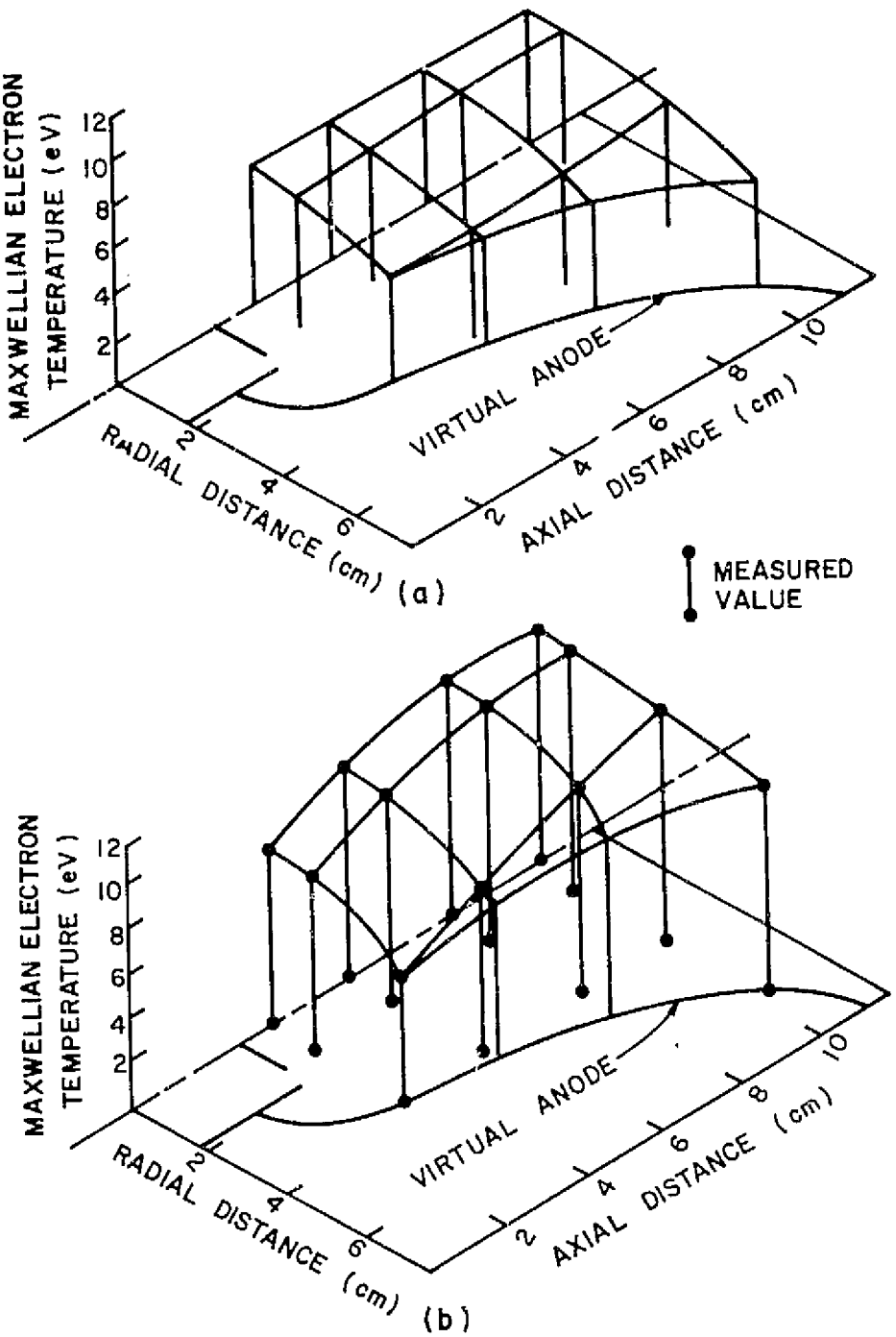

Figure 17. Comparison of (a) calculated with (b) measured Maxwellian electron temperature for the SERT-II thruster operating at 1.7 A, 32.7 V and .307 Aeq propellant mass flow rate.

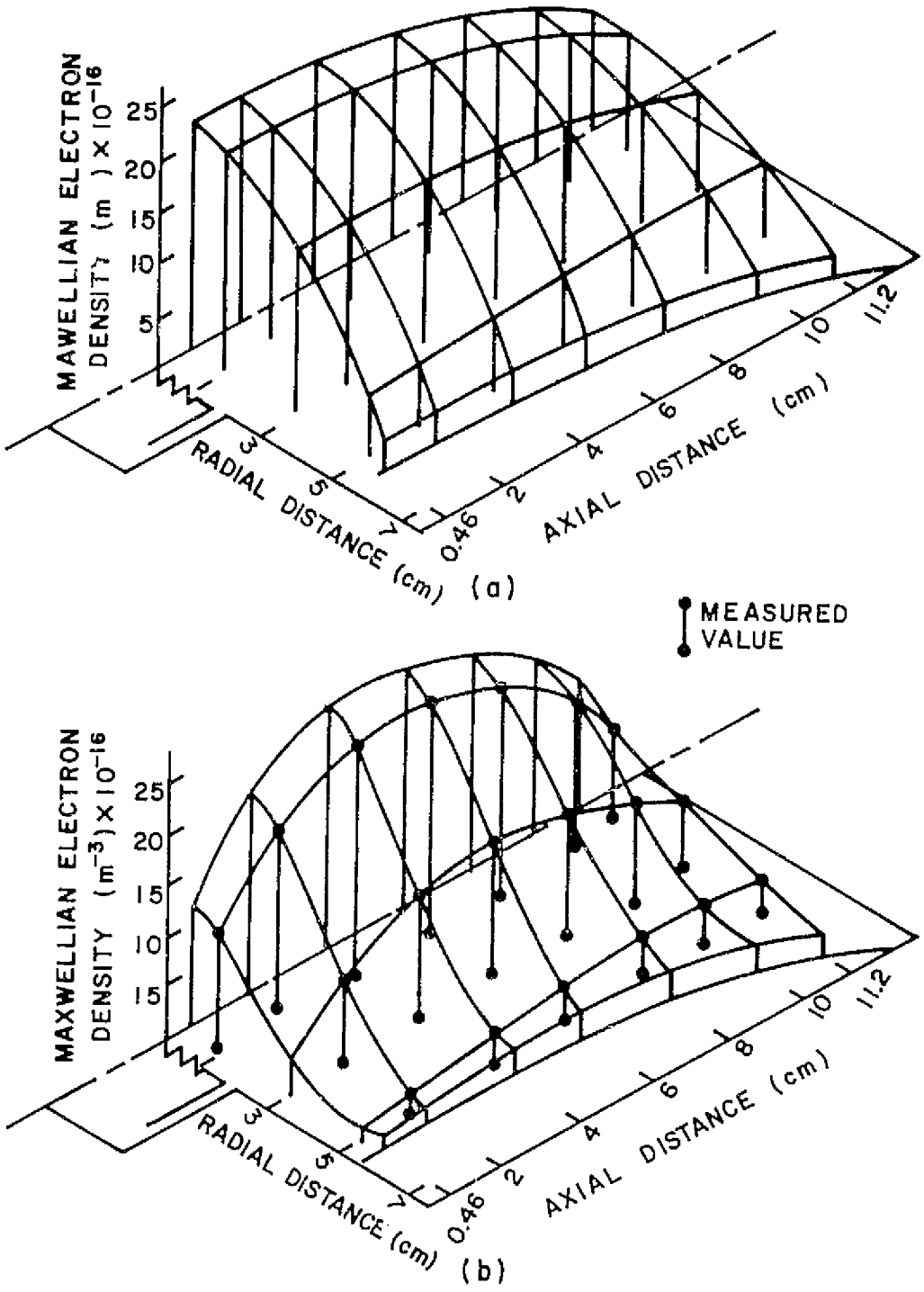

Figure 18. Comparison of (a) calculated with (b) measured Maxwellian electron density for the axial field thruster operating at 1.03 A, 40.4 V and .330 Aeq propellant mass flow rate.

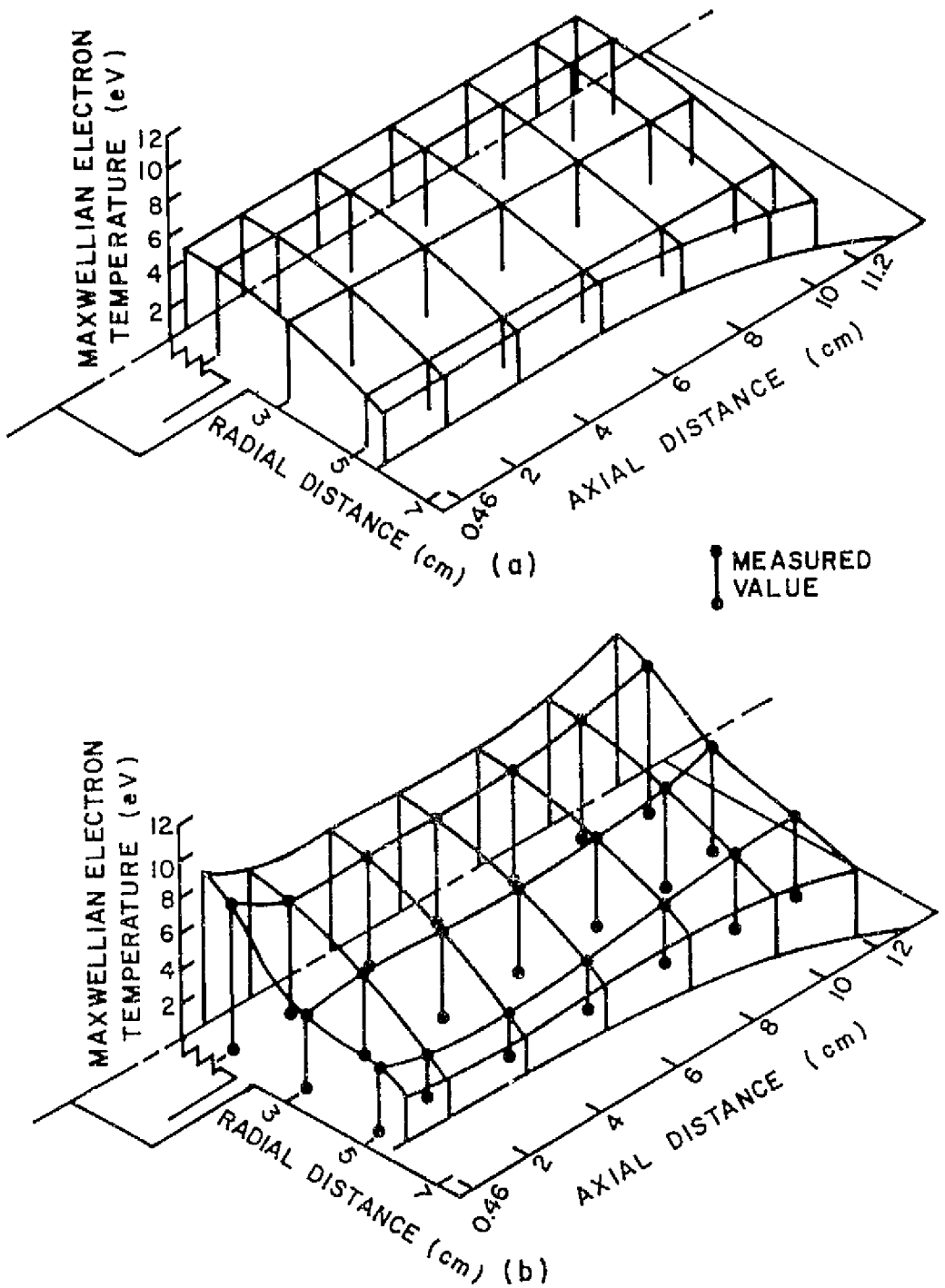

Figure 19. Comparison of (a) calculated with (b) measured Maxwellian electron temperature for the axial field thruster operating at 1.03 A, 40.4 V and .330 Aeq propellant mass flow rate.

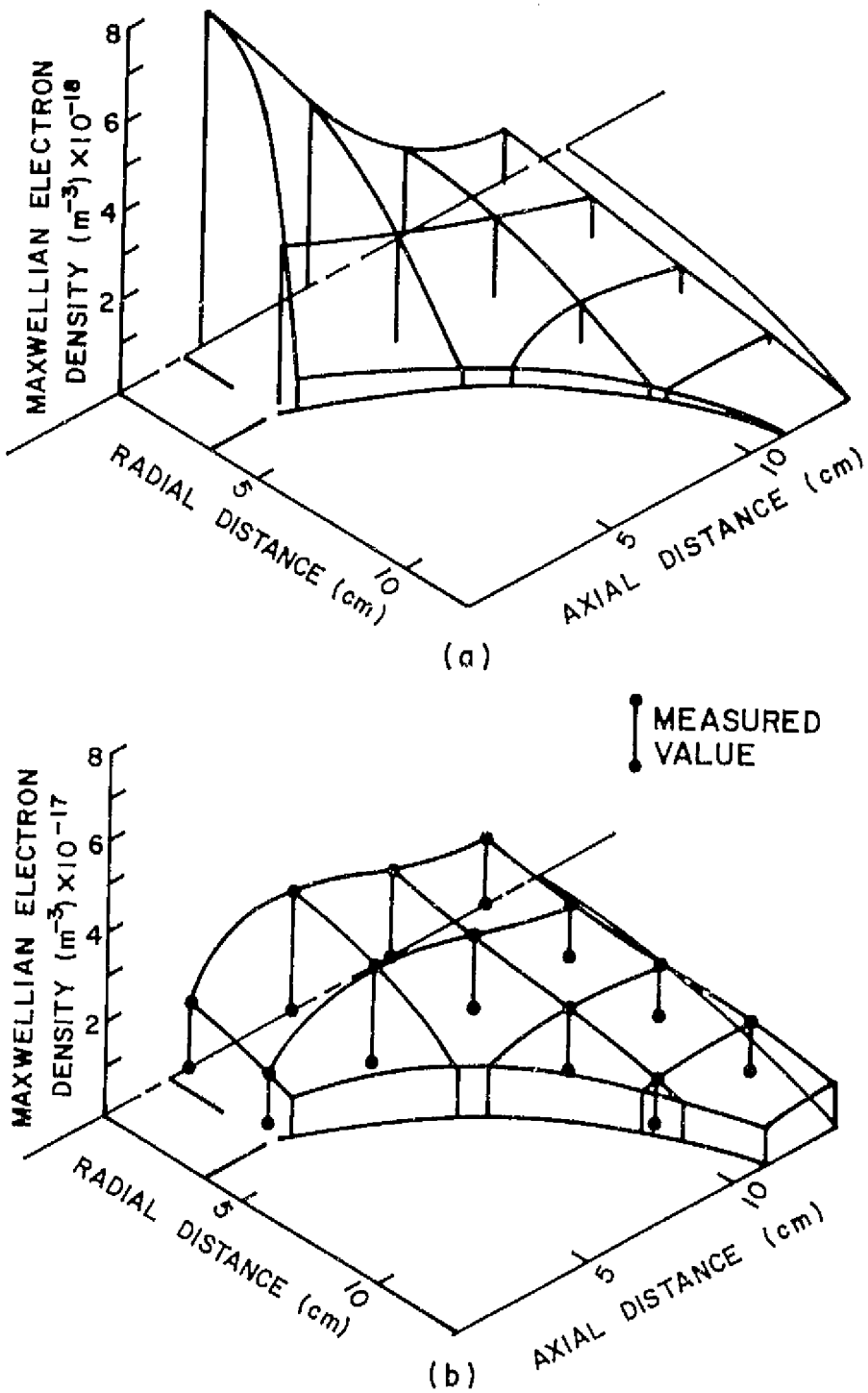

Figure 20. Comparison of (a) calculated with (b) measured Maxwellian electron density (note difference in density scales) for the 30 cm thruster operating at 11.7 A, 30 V and 2.30 Aeq propellant mass flow rate.

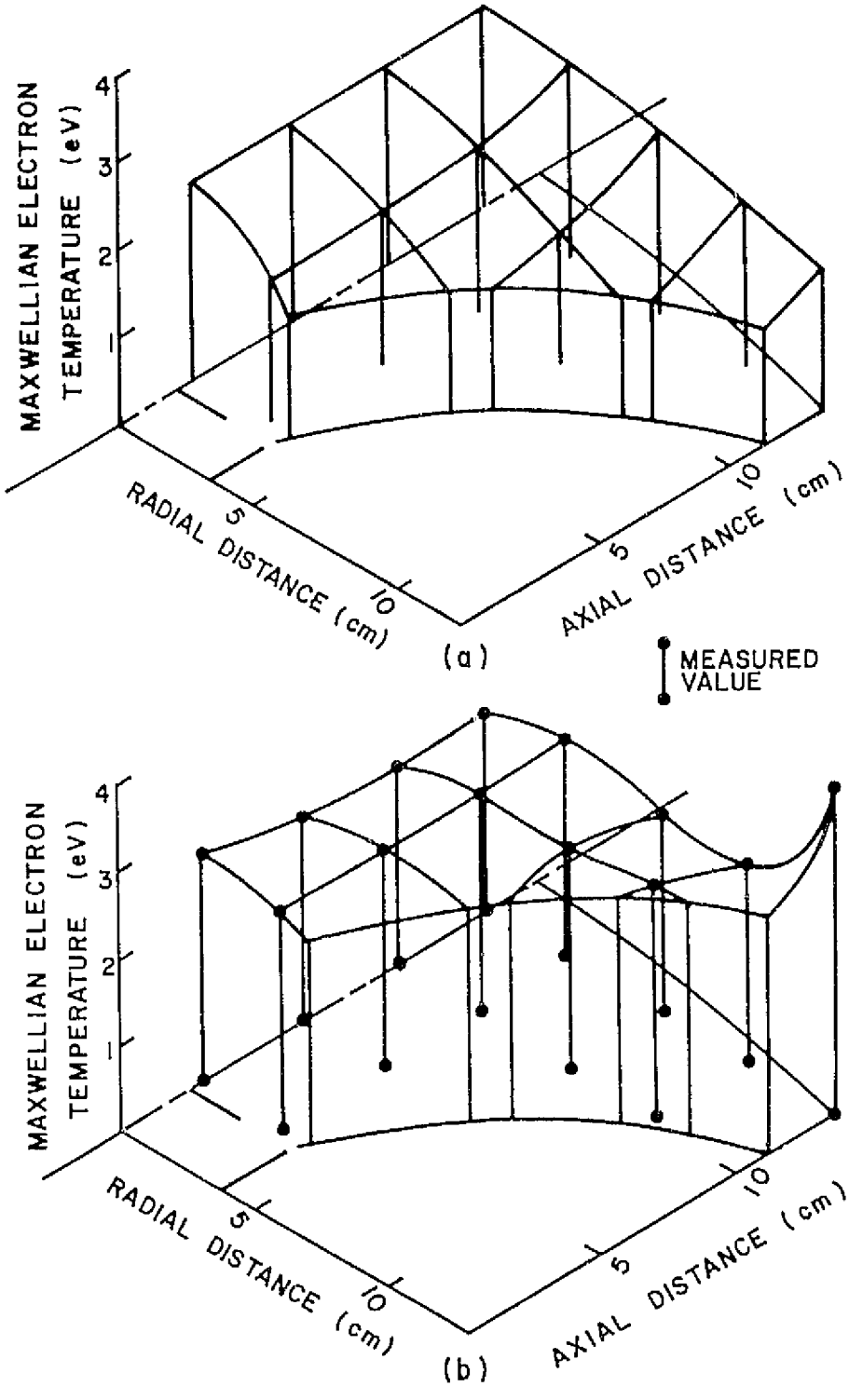

Figure 21. Comparison of (a) calculated with (b) measured Maxwellian electron temperature for the 30 cm thruster operating at 11.7 A, 30 V and 2.30 Aeq propellant mass flow rate.

two density maps of Figure 20). The reason for this discrepancy appears to be related to the degree to which Bohm diffusivity correctly describes the transport of the electrons across the magnetic field. If the diffusivity is greater than the Bohm diffusivity, the actual density profile will be flatter and the total average density lower to give the same flux density at the boundary. As mentioned earlier, it is believed that electric turbulence is related to the diffusivity. This particular thruster is known to have a substantial amount of such turbulence [33], and therefore may be expected to have higher diffusivity. Consideration of Figure 21 suggests that the actual thermal conductivity is greater than the calculated value because there is effectively no transverse gradient of measured temperature. Recalling that the conductivity is directly proportional to the diffusivity, this again suggests that the actual diffusivity is greater than the Bohm value. It is also possible that the divergence of the 30 cm thruster magnetic field is too great to satisfy the mild divergence assumption in the derivation of the equations for the property profiles, or that the input parameters used were in error. The latter is a possibility due to the sketchy nature of the data available on the magnetic field of that thruster.

Figures 17, 19 and 21 all show Maxwellian electron temperatures which are lower than reported values by approximately 20 to 30 per cent. There are several factors which may contribute to this. It is observed from the density maps of Figures 16, 18 and 20, as well as in the normalized density profiles of Figure 14, that the actual plasma density at the upstream end of the ion production region is in every case much less than the calculated value. Because the energy loss rate to the upstream end of the ion production region is directly proportional to the

Maxwellian electron density there, the calculated upstream loss $\dot{E}_b$ will be greater than would actually be expected. Loss of energy to the upstream end typically accounts for less than 15 per cent of the energy. Using the average density n^*_{mx} rather than the average at the upstream end in calculating $\dot{E}_b$ had a negligibly small effect on the calculated Maxwellian electron temperature, however.

Another possibility is that the energy lost to the anode is less than that given by Equation (22) due to anisotropy of the electron velocity distributions near the anode. To investigate the effect of that possibility on the overall result, the energy lost to the anode was reduced by using a scalar multiplier on the $(2\ T_{mx} + V_{s_a})$ term. It was found that while the lower anode loss allowed the temperature to rise slightly, the increased temperature caused the volumetric loss $\dot{E}_{mx_\psi}$ due to inelastic collisions to increase significantly this holding the temperature to near its original level.

One other possibility is that the expression for thermal conductivity, Equation (13), gives values of conductivity that are too high. If the thermal conductivity were lower, the temperature profiles would be steeper and the average temperature would increase. This prospect was examined by dividing the thermal conductivity by integers ranging from 1 to 6. Figure 22 shows the result of that computation. It is seen that while the center line temperature is increased by decreasing the conductivity, the temperature at the virtual anode is diminished such that the volume averaged temperature does not change substantially, although it does increase some.

It is also possible that there is a systematic error in temperature measurements owing perhaps to the limitations of the two group theory.

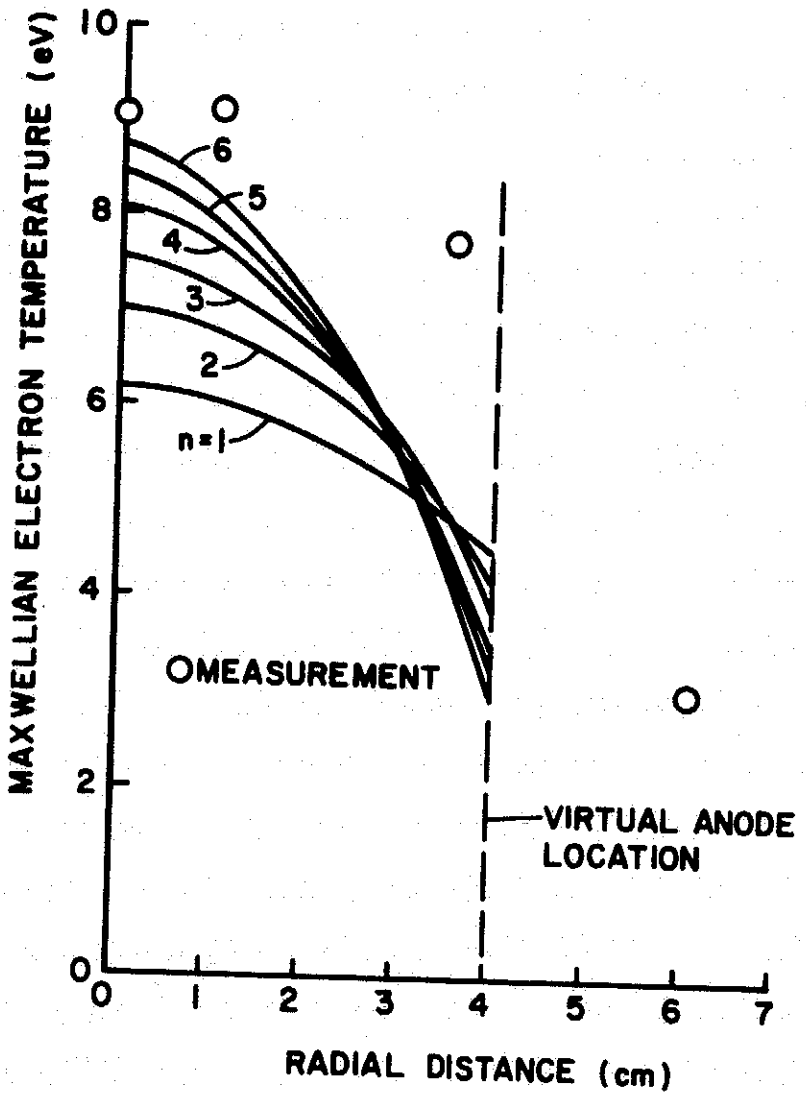

Figure 22. Temperature contours for the SERT-II thruster for thermal conductivities of 1/n times the theoretical value of 4.7 n_{mx} D_B.

It is concluded that the discrepancy is probably due to the simplifying assumptions used to make the problem tractable. If the complicating factors were left in the model, it is possible that a better agreement between the calculated values and the measured values would result. It appears, however, that the entire model would require the additional effort and that the difficulty does not lie with just one or two of the approximations. That additional effort is not justified by the present objective of a first order predictor model.

IX. THRUSTER PERFORMANCE

Having developed the capability to predict to first order the plasma properties in the ion production region for mercury ion thrusters, it is logical to extend the model to predict the performance of these thrusters. Performance is usually measured in terms of the propellant utilization and the discharge loss. Propellant utilization is defined by

$$\eta_u = \frac{I_b}{I_p} \tag{67}$$

where I_b is the beam current and I_p is the propellant mass flow expressed in equivalent amps. It is a measure of the completeness with which the propellant gas atoms are converted to ions and accelerated from the thruster. The discharge loss is a measure of the energy expenditure to produce the ions. It is given in units of eV/ion by the equation

$$\xi = \frac{I_a V_a + I_k V_k}{I_b} \tag{68}$$

where I_a and V_a are the current to the anode and anode voltage, respectively, and I_k and V_k are the current to the keeper and the keeper voltage. Because the keeper current and voltage are generally small compared with the discharge current and voltage, respectively, it is a fair approximation to discard the second term in the numerator of Equation (68). This will be necessary here because the present plasma property model has not been developed to calculate I_k for performance calculations.

The thruster beam current I_b can be estimated, however, from plasma properties as predicted by the present model and the equation

$$I_b = \int_{\text{Screen Grid Area}} (n_+ + 2\sqrt{2}\ n_{++})\ \phi_s\ e\ V_B\ dA_s \qquad (69)$$

where n_+ and n_{++} are the single and double ion densities, ϕ_s is the open area fraction of the screen grid which has area A_s, and V_B is the Bohm velocity as given by Equation (6). The factor $2\sqrt{2}$ in Equation (69) accounts for the fact that the double ions have twice the charge and $\sqrt{2}$ times the Bohm velocity of single ions. To simplify calculations somewhat, it will be assumed that Bohm velocity is constant at the value given using the volume averaged temperature T^*_{mx}. It is also observed that by the quasineutrality assumption, ion densities will be nearly equal to electron densities. Hence, the ratio of ion density at the screen to its volume averaged value will be about the same as the ratio of electron density at the screen to its volume averaged value. Again assuming a constant primary to Maxwellian electron density ratio, Equation (69) may be modified to use volume averaged ion densities as calculated from the production and loss rate equations. Thus, it becomes

$$I_b = (n^*_+ + 2\sqrt{2}\ n^*_{++})\ V^*_B\ \phi_s\ e \left(\frac{1}{n^*_{mx}} \int_{\text{Screen Grid Area}} n_{mx}\ dA_s \right). \qquad (70)$$

The integral may now be evaluated from the calculated Maxwellian electron density spatial distribution given in Equation (66).

Using the computer generated beam current given by Equation (70) with calculated values of the various densities and temperatures, the performance curves of various thrusters may be obtained by exercising the computer model with various combinations of cathode emission current and anode voltage. The resulting plots of ξ against η_u for

several thrusters are shown in Figure 23 together with the performance curves generated from measurements. The calculated performance curves are consistently above and to the left of the actual performance curves indicating a poorer performance calculated than measured. This is because the beam current calculated by the model is consistently lower than the measured beam current for each of the thrusters. The comparison between calculated beam current and measured beam current for different thrusters is shown in Table 3. Several factors may account for the discrepancy. It may be that the actual effective open area of the grids for ion collection is greater than the geometric open area of the screen grid due to plasma sheath contours. Increasing the screen open area of the computer model for each thruster does increase the calculated performance by increasing the beam current. This is accompanied by a decrease in Maxwellian electron density and a slight increase in Maxwellian electron temperature in the calculations. It appears that the density calculation near the grids using the screen grid open area in the model is fairly good. For a comparison, the measured Maxwellian electron density near the screen grid was used with measured temperatures and Equation (70) to calculate the beam current for the same thrusters previously considered in Table 3. The measured parameters and the results of this calculation are also listed in Table 3. It will be seen that the beam current calculated from measured densities and temperatures is also considerably lower than the measured beam current in each of the cases considered.

One other possibility is that the ions may leave at a velocity greater than the Bohm velocity. This, if true, would result in a reduced calculated density and increased calculated temperature of the

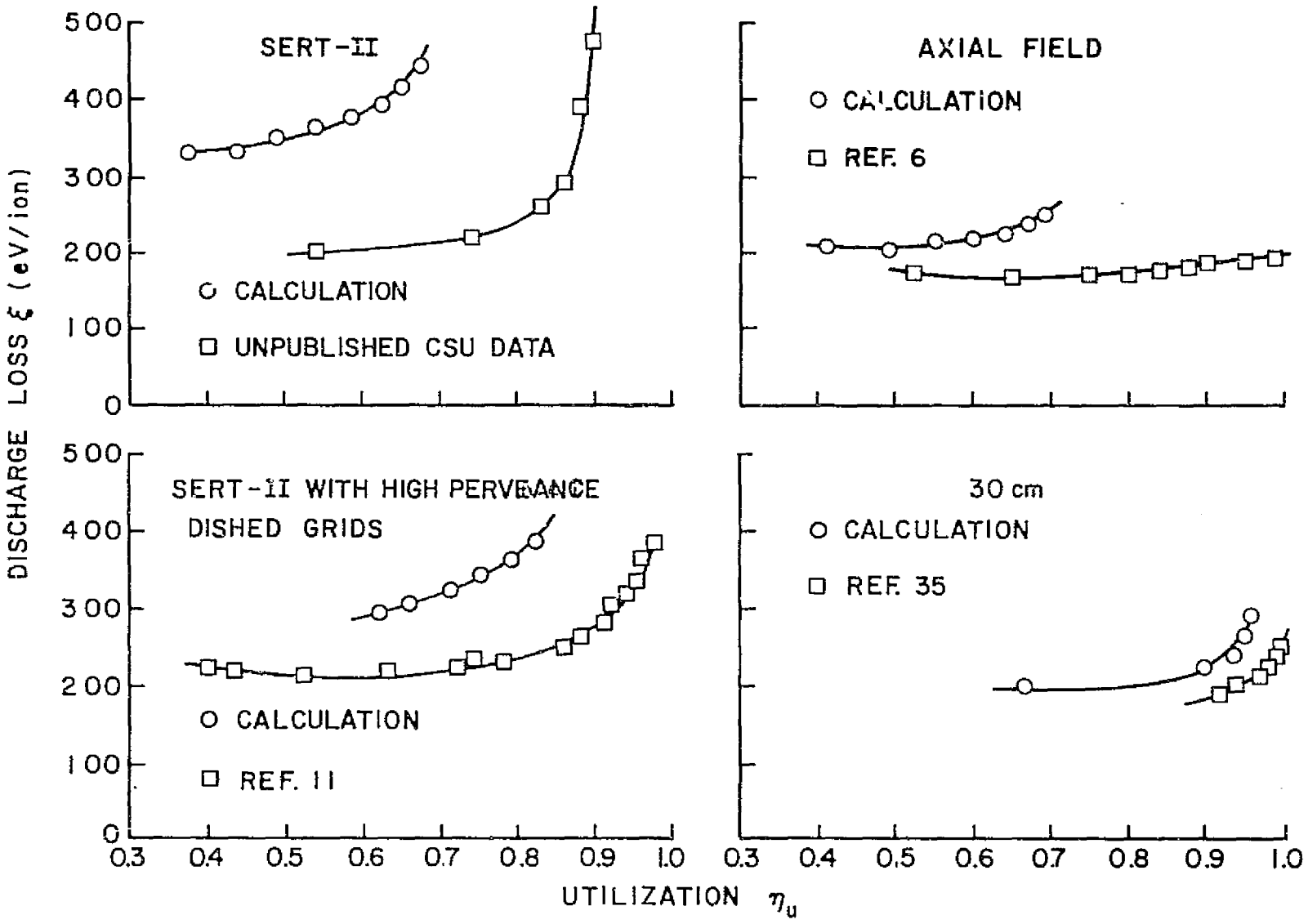

Figure 23. Performance comparison for several thrusters.

Table 3. Comparison of calculated and measured beam currents for several mercury ion thrusters.

Thruster	SERT-II	Axial Field	30 cm	SIT-8
I_b Calculated by Computer (A)	.167	.187	1.90	.05
I_b Measured (A)	.242	.268	2.0	.07
Measurements				
n_{pr}/n_{mx}	.08	.06	.22	.19
n_{mx_s} $(m^{-3}) \times 10^{-16}$	3.6	3.7	10	2.5
T_{mx_s} (eV)	7	5.5	2.3	11.6
ϕ_s	.69	.71	.69	.67
A_s (m^2)	.0154	.0176	.0594	.0061
I_b Calculated from Measurements (A)	.125	.131	.927	.05

Maxwellian electrons in the ion production region. Suffice it to say that the thruster performance as calculated by the computer model is poorer than that expected from an actual thruster, but the calculated performance curves show the same general shape as the measured curves indicating that the model is probably basically correct. It is quite sensitive to geometric parameters, however, and inaccuracies in the input data can lead to further distortions of plasma properties in the calculation.

X. CONCLUSIONS

This investigation has examined the processes ongoing within the ion production region of mercury ion thruster discharge chambers. Those processes have been related to plasma properties, and with the aid of a number of simplifying assumptions a set of equations has been formulated which will give plasma properties to first order from thruster design and operation data only. A computer program has been written which iteratively solves that set of equations to give plasma property maps at any desired operating point for the thruster. Based on the success of that model and the general agreement between calculated and measured values of plasma properties, the following conclusions are drawn:

1. The region of prime importance to ion thruster operation is the ion production region. It is defined as the region of the main discharge chamber bounded by the surface of revolution of the innermost field line to intersect the anode and by the upstream and downstream boundaries which typically include the screen grid at the downstream end and the baffle and cathode pole piece at the upstream end.

2. The innermost magnetic field line to intersect the anode is a virtual anode in the sense that electrons are not collected by the anode until they diffuse across the magnetic field to the virtual anode field line. Then they are collected quickly from a thin layer called the electron collection layer which has a thickness nearly that of the average Larmor radius of the electrons. This description of the electron collection process allows the estimation of average plasma potential from the equations of statistical mechanics.

3. Electrons diffuse across the magnetic field under a density gradient essentially according to the Bohm diffusion model. That

diffusivity may be related to conductive energy transport across the magnetic field.

4. Plasma density in the ion production region is determined by the production and loss rates for ions. Ions are assumed produced from neutral ground state and metastable state atoms. They are assumed lost to the boundaries of the ion production region at the Bohm velocity based on the local Maxwellian electron temperature and at a rate proportional to the local electron density. The potential sheaths at the plasma boundaries adjust themselves to cause the electron fluxes to be such that quasineutrality is obtained in the ion production region.

5. There are three dominant processes which determine Maxwellian electron temperature in the ion production region. The most important is the loss of electron kinetic energy to inelastic collisions with atoms and ions. That accounts for from half to two thirds of the kinetic energy loss. The next most important is the convective loss to the anode of the kinetic energy of the electrons which make up the anode current. That loss is typically one fourth of the total. The remainder is lost to cathode potential boundaries with the high energy electrons in the tail of the Maxwellian distribution which cross the potential sheath at those surfaces. Most of that loss occurs at the upstream end of the ion production region. The calculated temperature which satisfies the energy balance in the ion production region is characteristically lower than the measured value for the thrusters considered here. The reason for that is not apparent.

6. For ion thrusters with reasonably homogeneous magnetic fields, either axial or moderately divergent, the variation in Maxwellian electron density in the direction perpendicular to the magnetic field

may be described by a simple zero order Bessel function. Temperature variation across the magnetic field is a somewhat more complicated expression but is very nearly parabolic. For the divergent field case, the axial variation of Maxwellian electron density appears to follow the rule that the ratio of density to magnetic field strength is constant except near the upstream end. For either axial or divergent magnetic fields, Maxwellian electron temperature is effectively constant along magnetic field lines. These approximations neglect departures from the general behavior at the ends of the ion production region where such things as electric fields and ion inertia appear to have some influence.

7. By varying the input operating parameters of the computer model developed, it is possible to generate thruster performance curves. While these curves have been found to agree in shape with actual measurements for several thrusters, the calculated performance is poorer than measured performance because the beam current calculated is lower than the actual beam current for the same operating conditions. The reason for that discrepancy is not understood.

REFERENCES

1. Kaufman, H. R., and Reader, P. D., American Rocket Society Paper No. 60-1374 (1960).

2. Beattie, J. R., "Numerical Procedure for Analyzing Langmuir Probe Data," AIAA Journal, Vol. 13, No. 7, July 1975, pp. 950-952.

3. Kaufman, H. R., "Technology of Electron Bombardment Ion Thrusters," Advances in Electronics and Electron Physics, Vol. 36, ed. L. Marton, Academic Press, New York, 1974, pp. 265-273.

4. Masek, T. D., "Plasma Properties and Performance of Mercury Ion Thrusters," AIAA Paper No. 69-256 (1969).

5. Longhurst, G. R. and Wilbur, P. J., "Multipole Mercury Ion Thruster," AIAA Paper No. 78-682 (1978).

6. Knauer, W., Poeschel, R. L., King, H. J., and Ward, J. W., "Discharage Chamber Studies for Mercury Bombardment Ion Thrusters," NASA CR-72440, September 1968.

7. Jackson, J. D., Classical Electrodynamics, Wiley, New York, 1962, Chapter 12.

8. Krall, N.A., and Trivelpiece, A. W., Principles of Plasma Physics, McGraw-Hill, New York, 1973, Chapter 6.

9. Longhurst, G. R., "The Diffusion and Collection of Electrons in Ion Thrusters," in "Mercury Ion Thruster Research - 1977," ed. P. J. Wilbur, NASA CR-135317, December 1977.

10. Kaufman, H. R., "Ion Thruster Propellant Utilization," PhD Dissertation, Colorado State University, 1971.

11. Beattie, J. R., "Cusped Magnetic Field Mercury Ion Thruster," NASA CR-135047, July 1976.

12. Kaufman, H. R., "Electron Diffusion in a Turbulent Plasma," NASA TN D-1324, June 1962.

13. Isaacson, G. C., "Multipole Gas Thruster Design," NASA CR-135101, June 1977.

14. Kraal and Trivelpiece, loc. cit., p. 21.

15. Bohm, D., "The Use of Probes for Plasma Exploration in Strong Magnetic Fields," in The Characteristics of Electrical Discharges in Magnetic Fields, eds. A. Guthrie and R. K. Wakerling, McGraw-Hill, New York, 1949, p. 65.

16. Krall and Trivelpiece, loc. cit., Chapters 6, 9 and 10.

17. Cap, F. F., Handbook on Plasma Instabilities, 2 Vols., Academic Press, New York, 1976.

18. Kadomtsev, B. B., Plasma Turbulence, trans. L. C. Ronson, trans. ed. M. G. Rusbridge, Academic Press, New York, 1965.

19. Peters, R. R., "Double Ion Production in Mercury Thrusters," NASA CR-135019, April 1976.

20. Reader, P. D., "Investigation of a 10 Centimeter Diameter Electron Bombardment Ion Rocket," NASA TN D-1163, 1962.

21. Bohm, D., "Minimum Ionic Kinetic Energy for a Stable Sheath," in The Characteristics of Electrical Discharges in Magnetic Fields, eds. A. Guthrie and R. K. Wakerling, McGraw-Hill, New York, 1949, pp. 77-86.

22. Wells, A. A., "Current Flow Across a Plasma 'Double Layer' in a Hollow Cathode Ion Thruster," AIAA Paper No. 72-418, AIAA 9th Electric Propulsion Conference, Bethesda, MD, April 17-19, 1972.

23. Milder, N. A., and Sovie, J. S., "Characteristics of the Optical Radiation from Kaufman Thrusters," NASA TN D-6565, November 1971.

24. Moore, C. E., "Atomic Energy Levels as Obtained from the Analysis of Optical Spectra," Vol, 3, NBS Circ. 467, 1958.

25. von Engel, A., Ionized Gases, Clarendon Press, Oxford, 1965, Appendix 2.

26. Rockwood, S. D., "Elastic and Inelastic Cross Sections for Electron-Hg Scattering from Hg Transport Data," Phys. Rev. A, Vol. 8, No. 5, November 1973, pp. 2348-2358.

27. Penkin, N. P., and Redko, T. P., "Cross Sections for Electron Impact and Mixing of the 6 3P0,1,2 Levels of a Mercury Atom," Opt. Spectrosc., Vol. 36, No. 3, March 1974, pp. 446-452.

28. Phelps, A., Joint Institute for Laboratory Astrophysics, Boulder, CO., private communication, July 13, 1978.

29. Book, D. L., Revised NRL PIasma Formulary, Plasma Physics Division, Naval Research Laboratory, Washington, D. C., p. 14.

30. Wilbur, P. J., "Mercury Ion Thruster Research - 1977," NASA CR-135317, December 1977.

31. Lee, J. F., Sears, F. W., and Turcotte, D. L., Statistical Thermodynamics, 2nd ed., Addison-Wesley, Reading, Mass., 1973, Ch. 4.

32. Hughes Research Laboratories, "High Power and 2.5 kw Advanced Technology Ion Thruster," Contract NAS 3-19703 Monthly Report No. 2, 1 July 75 to 1 Aug. 75, NASA Lewis Research Center, Cleveland, Ohio.

33. Serafini, J. S., and Terdan, F. F., "Plasma Fluctuations in a Kaufman Thruster," Journal of Spacecraft and Rockets, Vol. 11, No. 11, Nov. 1974, pp. 752-758.

34. Rawlin, V. K., "Performance of 30 cm Ion Thrusters with Dished Grids," AIAA Paper 73-1053, AIAA 10th Electric Propulsion Conference, Lake Tahoe, Nevada, 31 Octo. to 2 Nov., 1973.

APPENDIX A

The rate factors for the excitations of metastable and ionized state atoms in a plasma are given by

$$P_a^b(E) = \sigma_a^b(E) \left(\frac{2\, e\, E}{M_e} \right)^{1/2} \tag{A1}$$

and by

$$Q_a^b(T_{mx}) = \int_0^\infty P_a^b(E)\, g(E,T_{mx})\, dE \tag{A2}$$

where σ_a^b is the cross section for the formation of state "b" atoms by electron impact at energy E on state "a" atoms. The parameters e and M_e represent the electron charge and mass, respectively, and $g(E,T_{mx})$ is the Maxwellian energy distribution function. The rate factors for the reactions considered important in mercury ion thruster analysis are given in Figures A1 to A7. When these rate factors are multiplied by the density of state "a" atoms, the result is the rate per incident electron at which state "b" atoms are formed.

Energy rate factors which characterize the rate at which state "a" atoms absorb kinetic energy from impacting electrons due to inelastic collisional processes can be obtained from

$$P_a(E) = \left(\frac{2\, e\, E}{M_e} \right)^{1/2} \sum_j \sigma_a^j(E)\, \Delta E_a^j \tag{A3}$$

and from

$$q_a(T_{mx}) = \int_0^\infty P_a(E)\, g(E,T_{mx})\, dE \tag{A4}$$

where the summation implied in Equation (A3) is over the important inelastic processes involving state a atoms and ΔE_a^j is the characteristic energy associated with each process. Values for the energy rate factors are given in Figures A8 to A10 for the four states of mercury

important to consider in ion thruster analysis. The doubly ionized state 5^1S_0 is assumed not to be involved in inelastic processes for convenience and because Hg III atoms are thought to leave discharge chamber before they will have a significant number of inelastic collisions.

When the energy rate factors are multiplied by the density of target atoms of the appropriate state, the result is the rate per incident electron at which kinetic energy is absorbed.

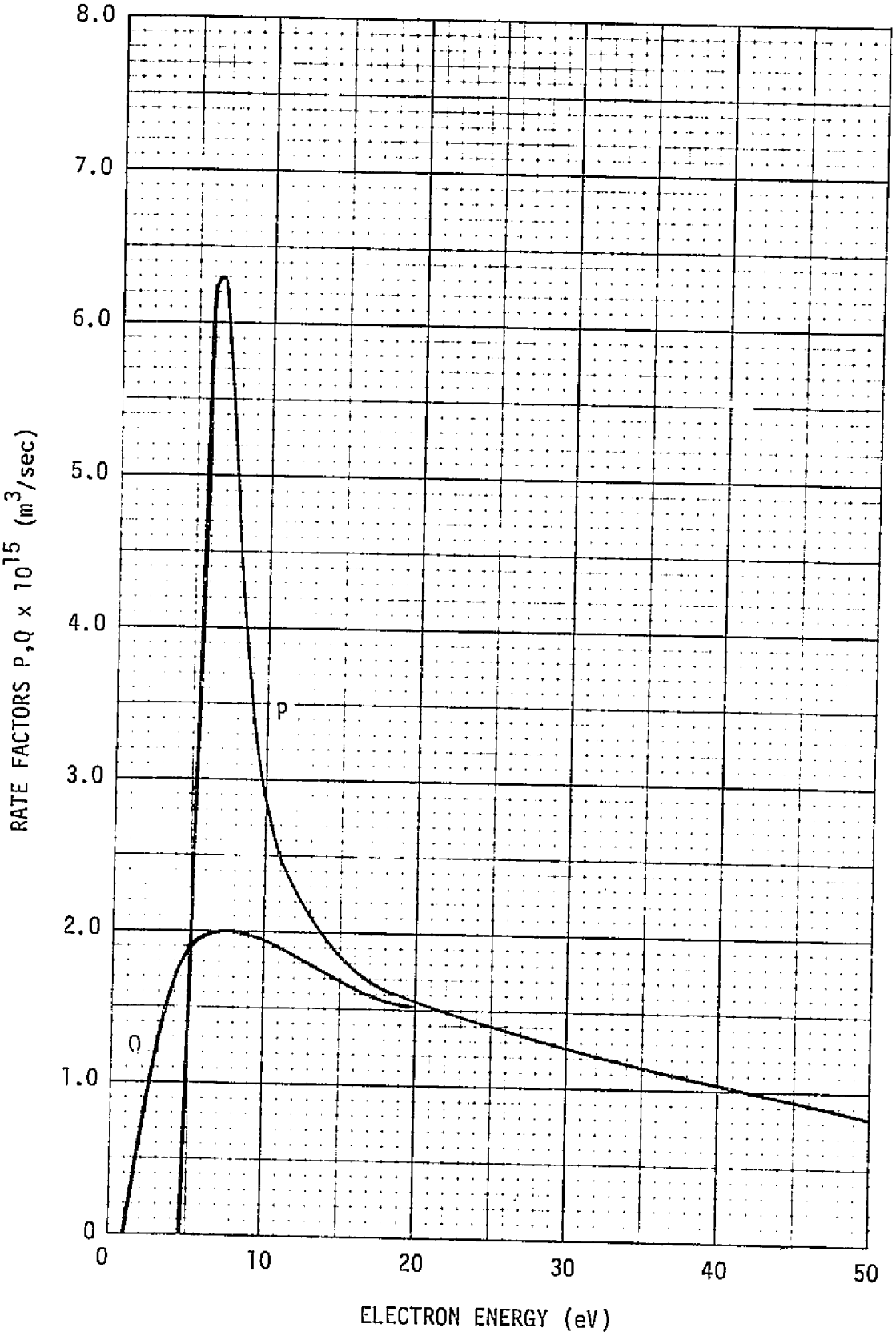

Figure A1. Rate factors for 6^1S_0 to 6^3P_0 reaction.

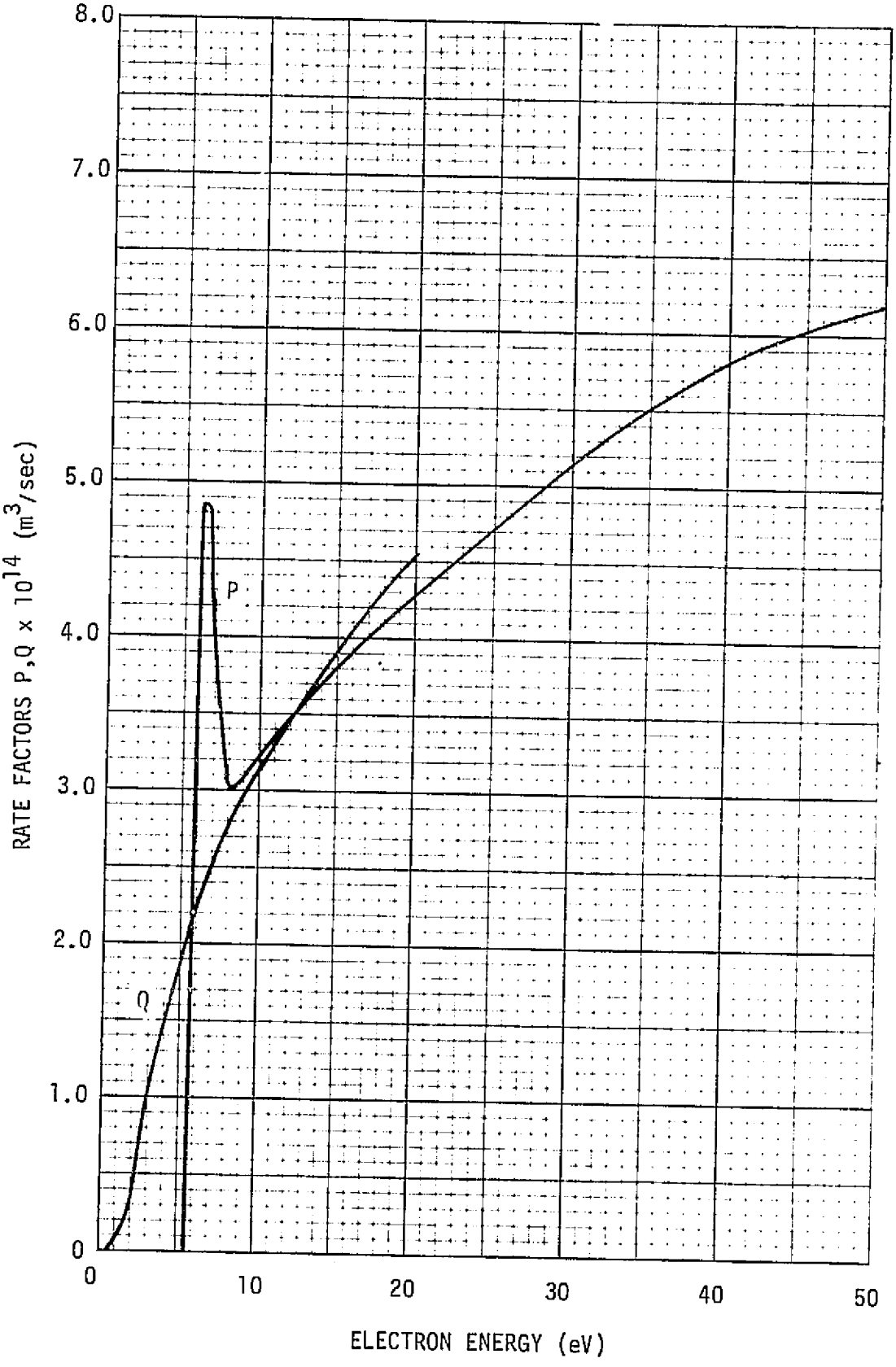

Figure A2. Rate factors for 6^1S_0 to 6^3P_2 reaction.

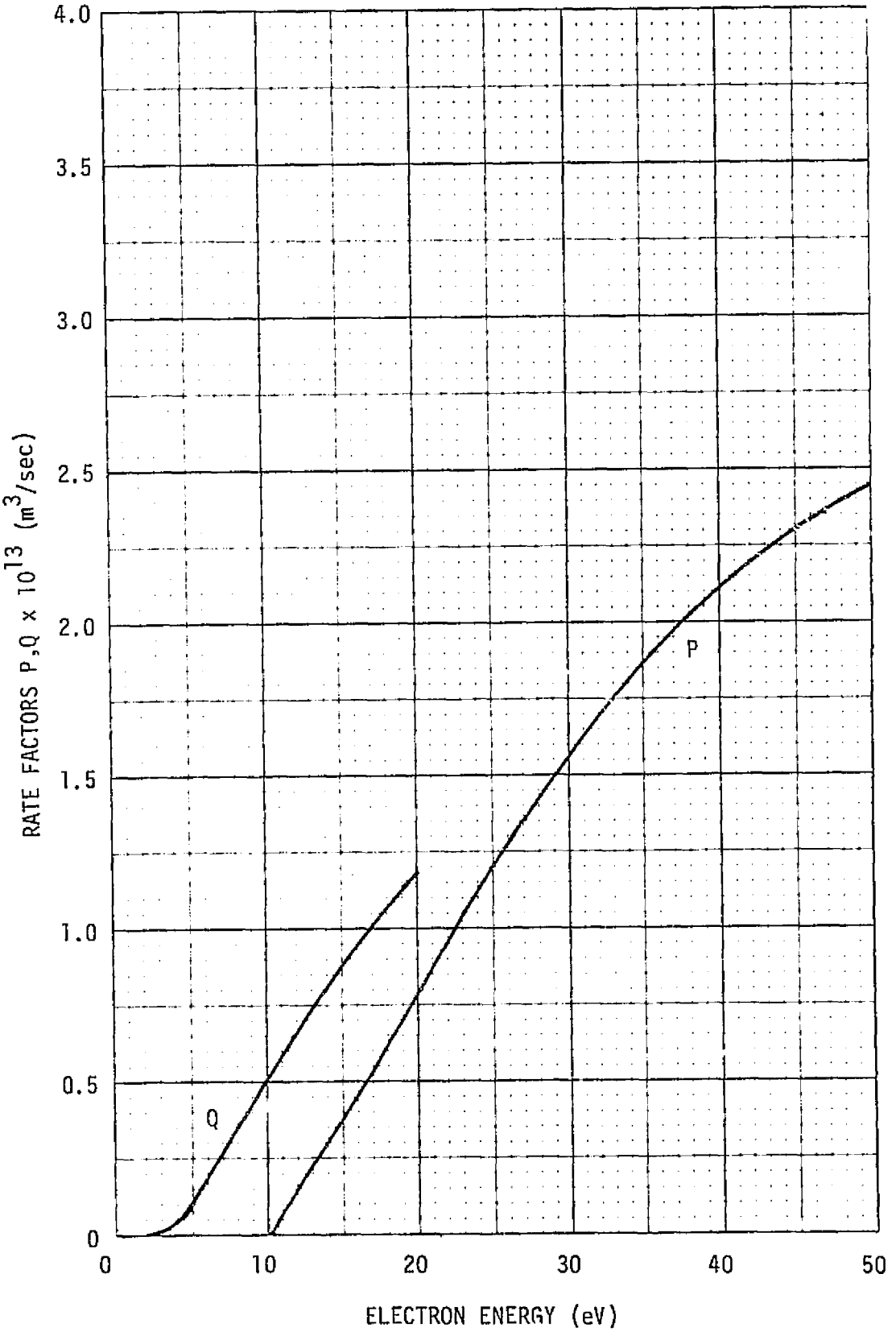

Figure A3. Rate factors for 6^1S_0 to $6^2S_{1/2}$ reaction.

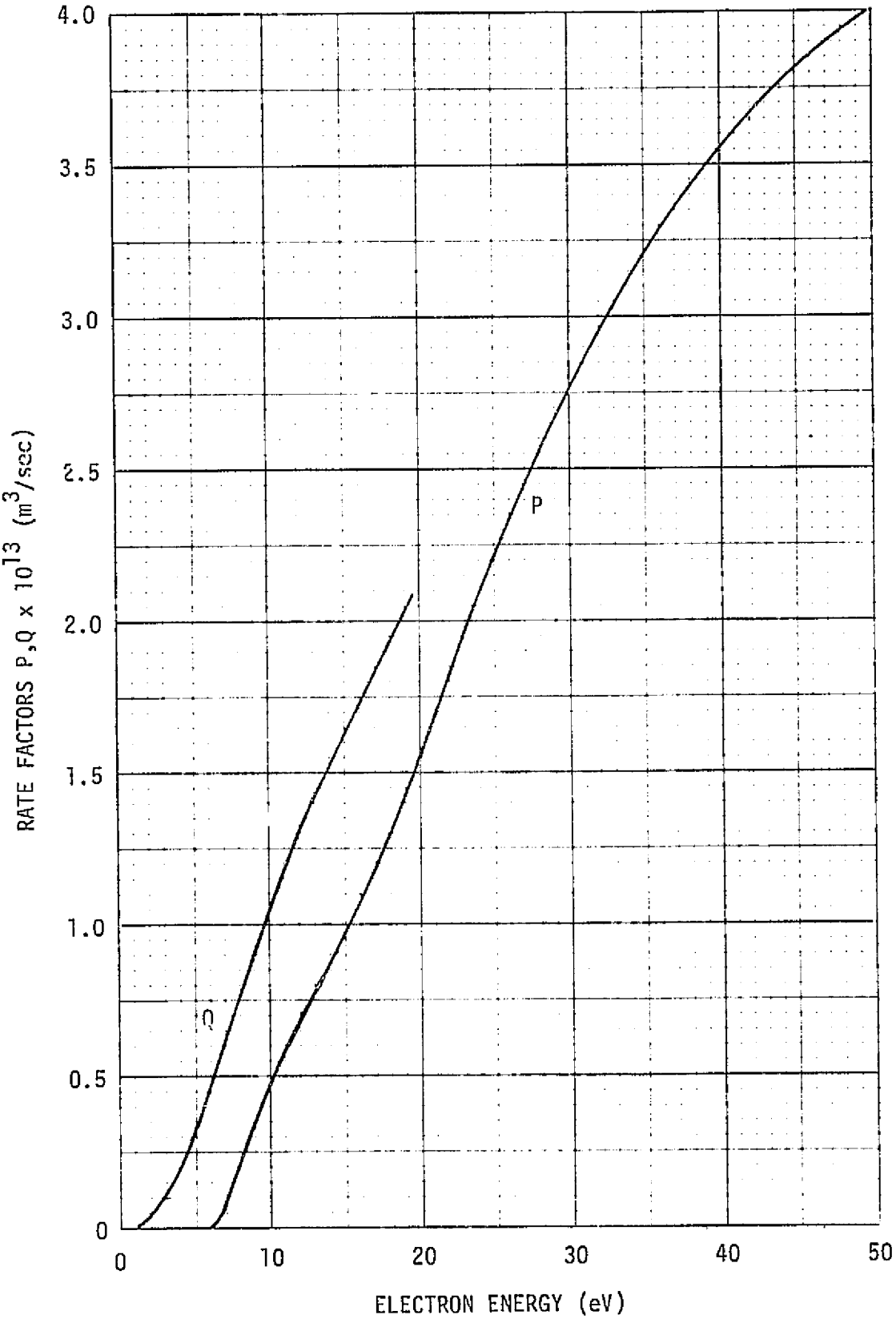

Figure A4. Rate factors for 6^3P_0 to $6^2S_{1/2}$ reaction.

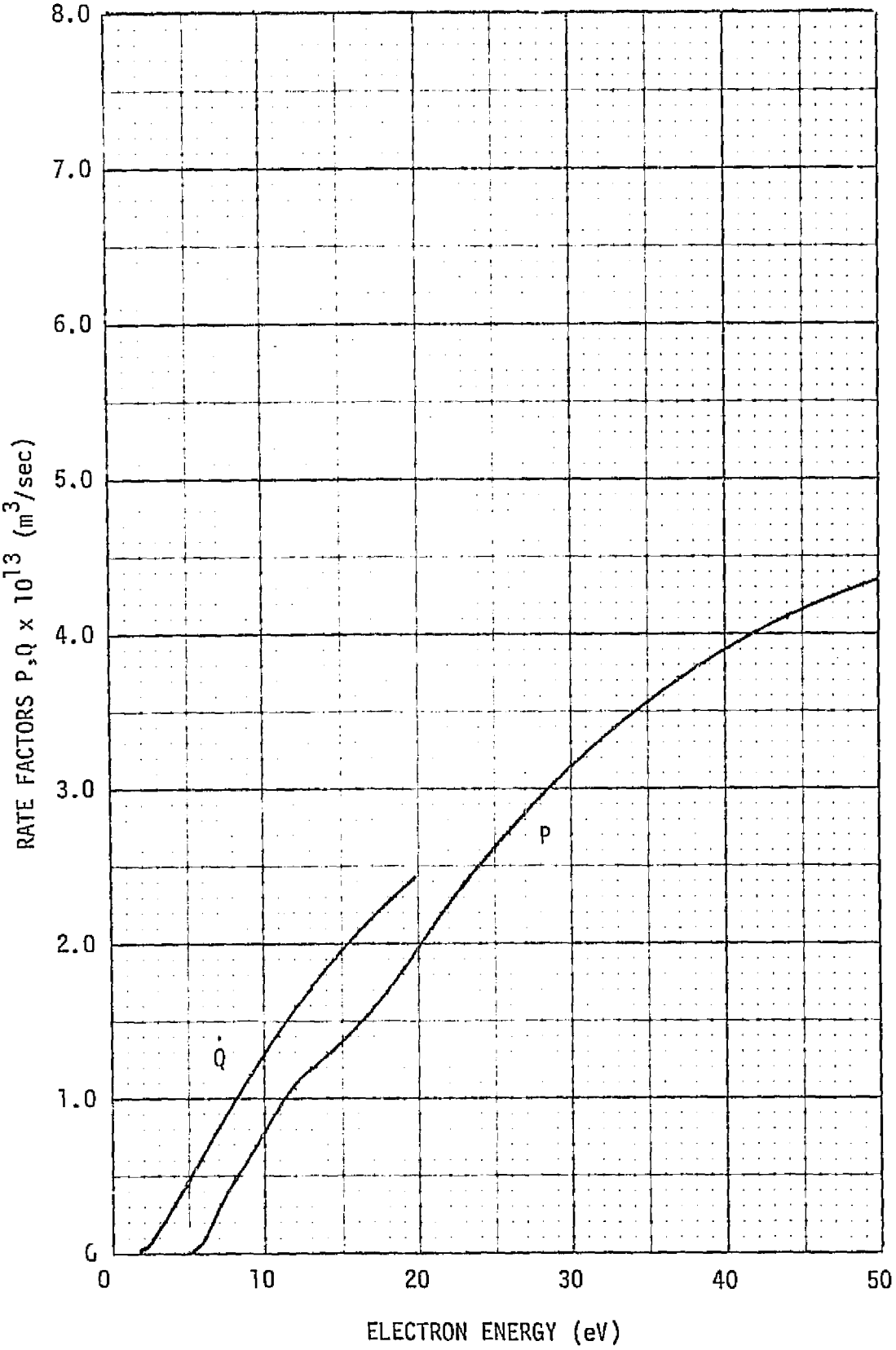

Figure A5. Rate factors for 6^3P_2 to $6^2S_{1/2}$ reaction.

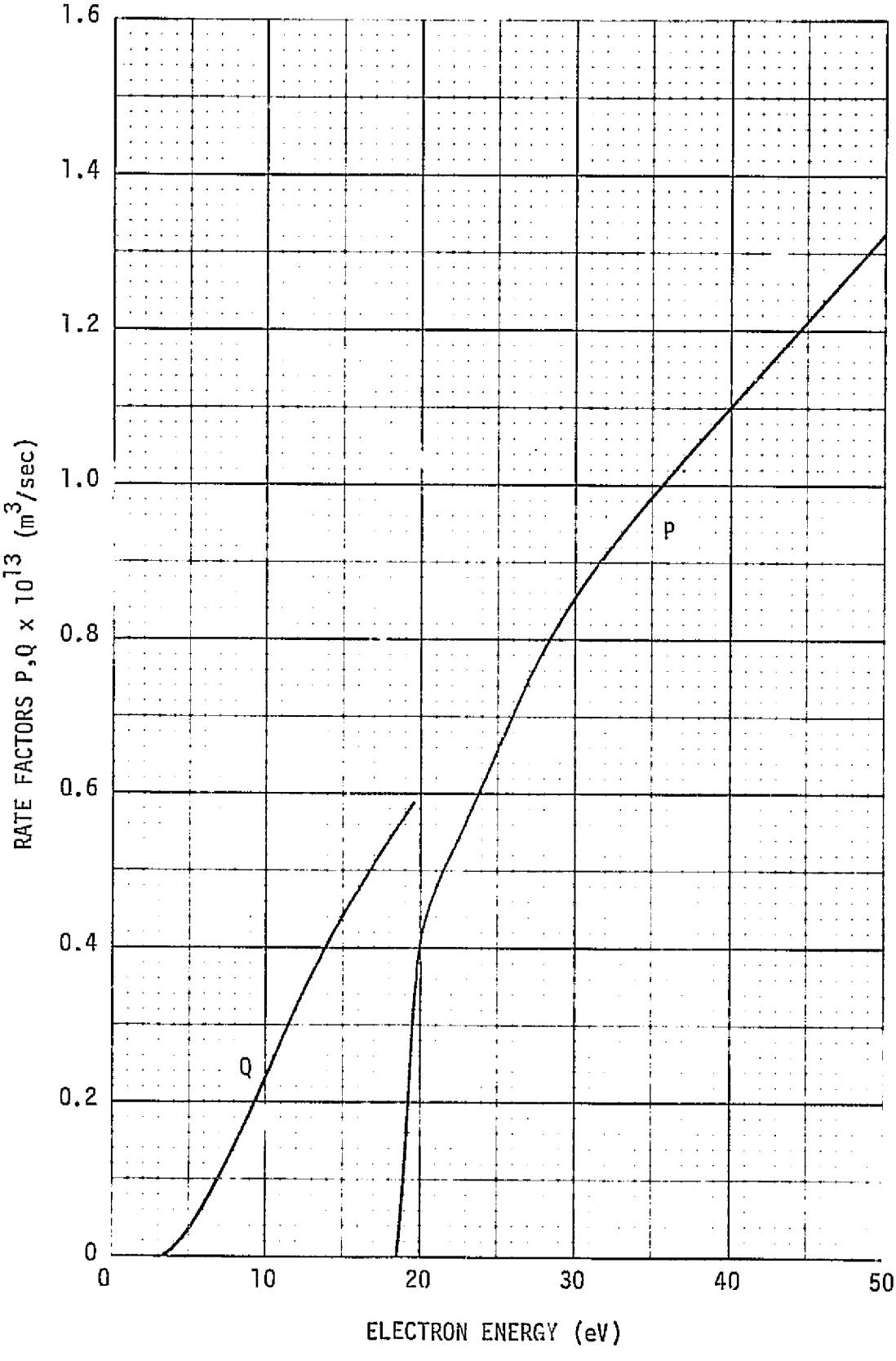

Figure A6. Rate factors for $6^2S_{1/2}$ to 5^1S_0 reactions.

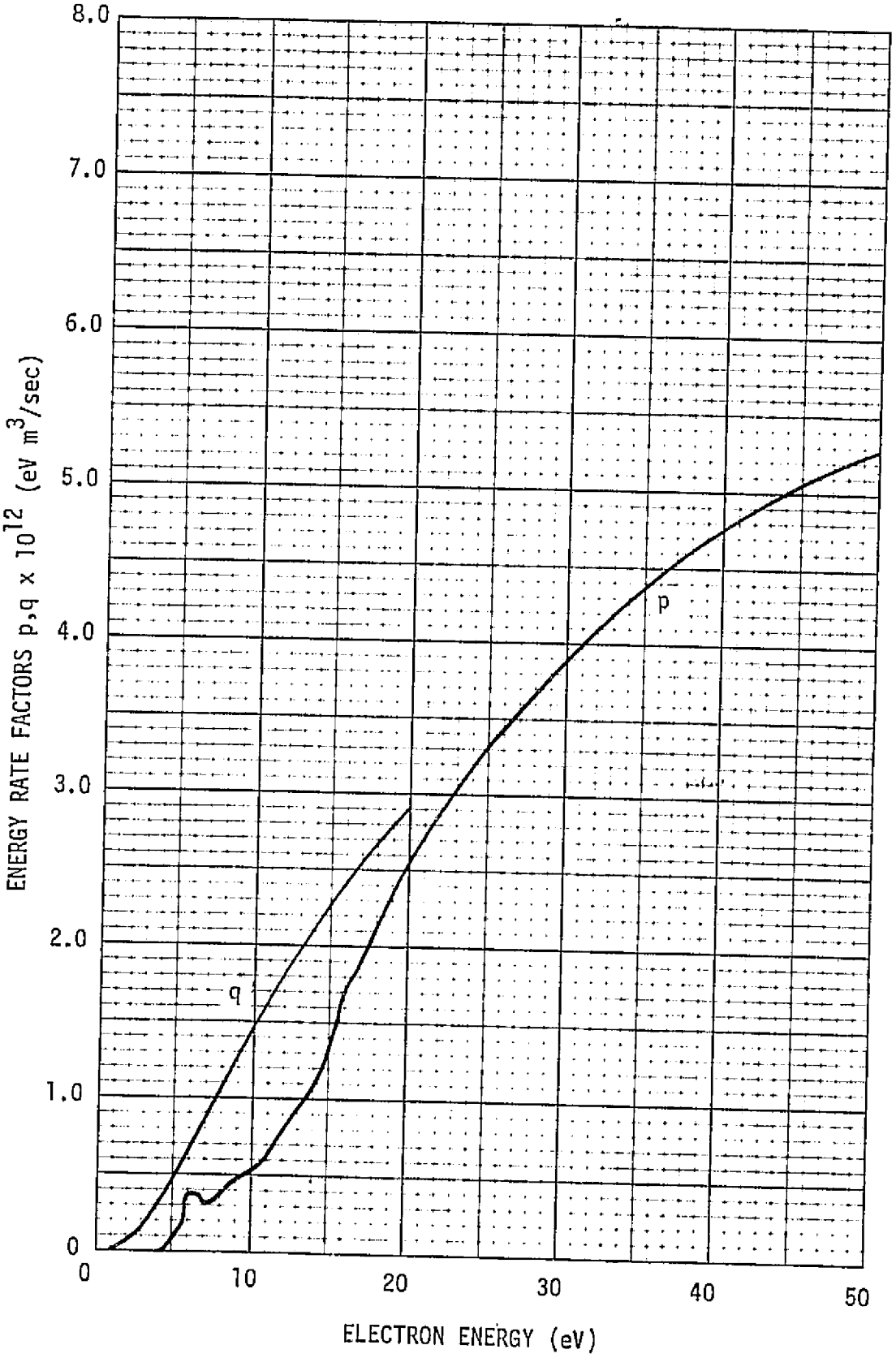

Figure A7. Energy rate factors for 6^1S_0 state atoms.

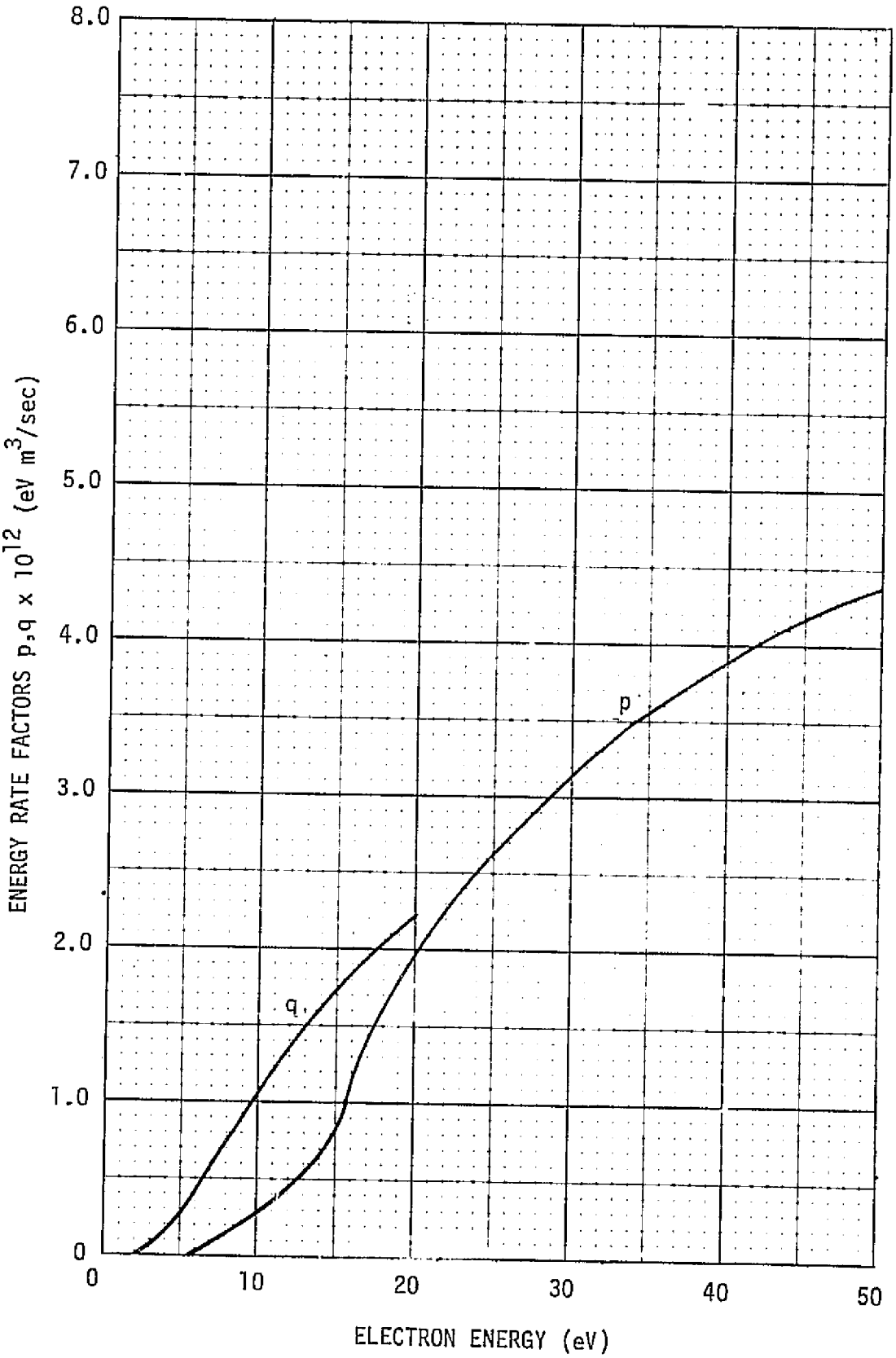

Figure A8. Energy rate factors for 6^3P_0 state atoms.

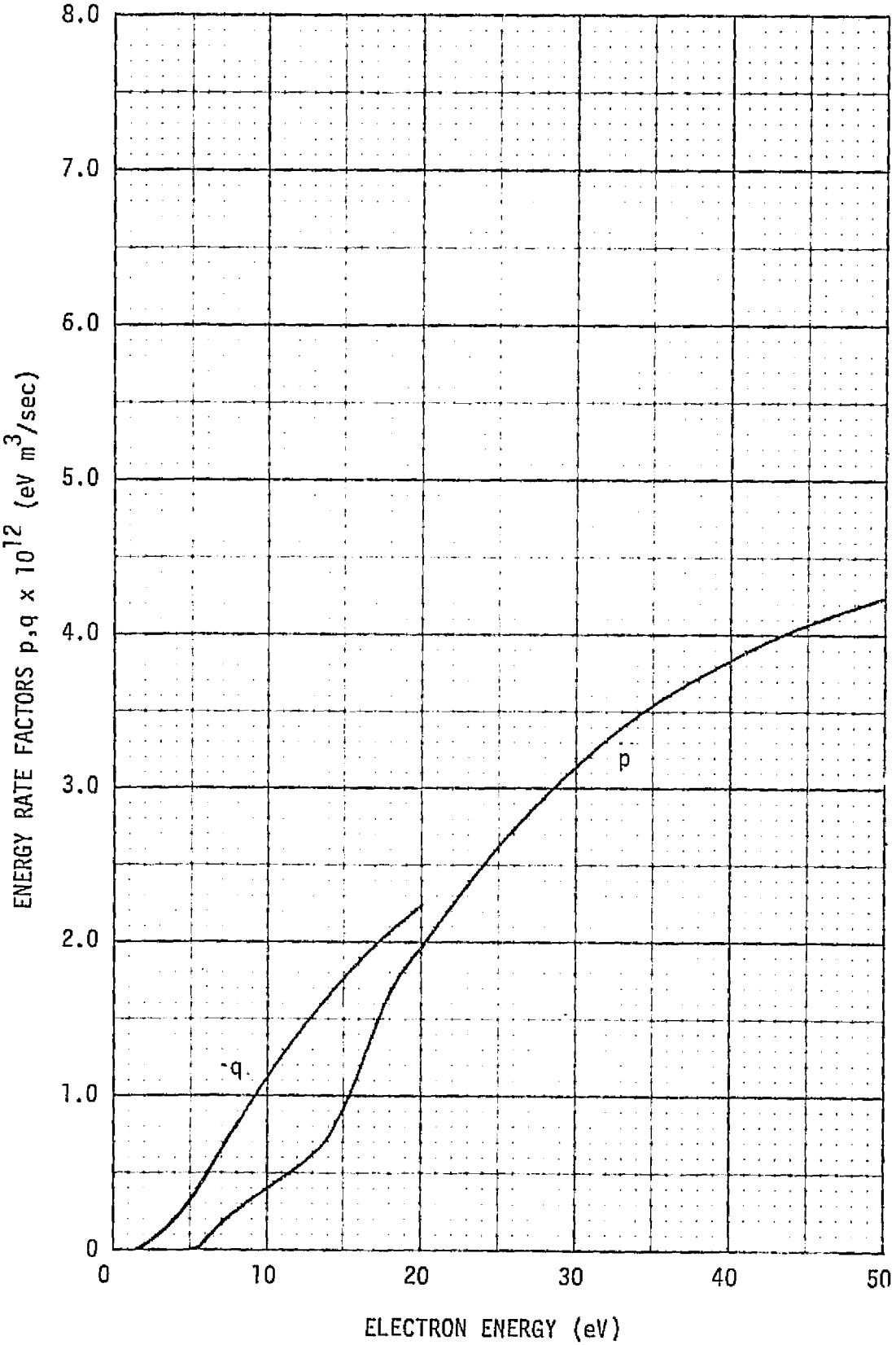

Figure A9. Energy rate factors for 6^3P_2 state atoms.

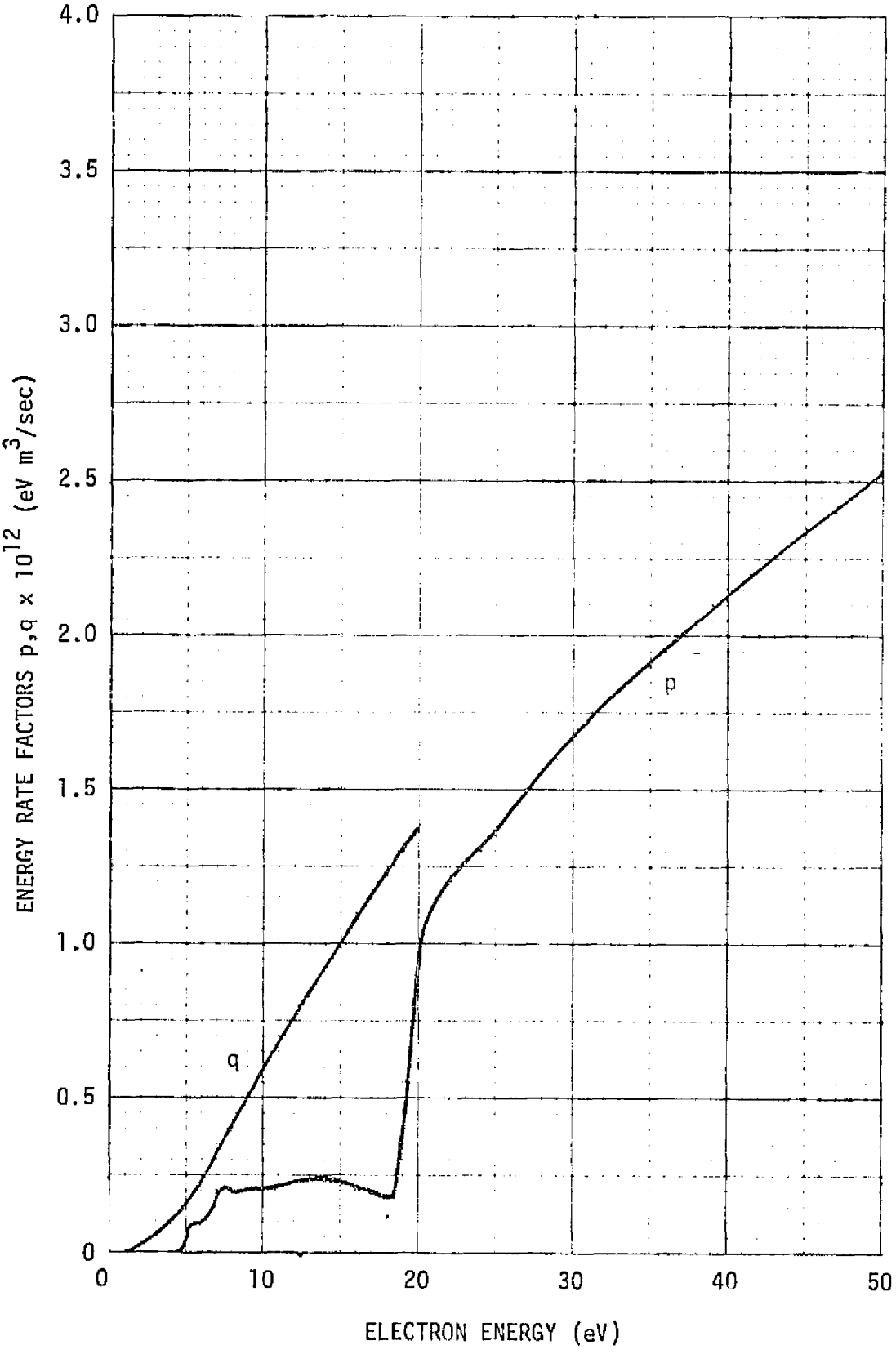

Figure A10. Energy rate factors for $6^2S_{1/2}$ state atoms.

APPENDIX B

As an illustration of the way in which the macroscopic conservation relations may be used in the analysis of ion thrusters, the required cathode emission current I_c to support the plasma properties in the SERT-II thruster as given by Peters [19] and in Figure 7 of the main report will be found. The physical data for this thruster are given in Figure 15 of the main report. From the plasma property maps the following plasma properties are obtained:

Volume Averaged Temperature T^*_{mx}	7.4 eV
Virtual Anode Temperature T_{mx_a}	5 eV
Average Primary Electron Energy E_p	30 eV
Volume Averaged Maxwellian Electron Density n^*_{mx}	8×10^{16} m^{-3}
Upstream Area Averaged Density n_{mx_u}	1.3×10^{17} m^{-3}
Virtual Anode Area Averaged Density n_{mx_a}	4×10^{16} m^{-3}
Screen Grid Area Averaged Density n_{mx_s}	6×10^{16} m^{-3}
Primary to Maxwellian Density Ratio n_{pr}/n_{mx}	0.08
Anode Sheath Potential V_{s_a}	1.5 V

The thruster is operated with the anode (V_a) 37.2 V positive of the cathode and with a propellant mass flow rate of .307 Aeq. The keeper is operated at about 7.7 V positive of the keeper, and the plasma near the keeper is a volt or so positive of that for a total primary electron energy of 30 eV as measured. With this definition of the problem the first task in solving for I_c is to determine the composition of the propellant gas in terms of its atomic states.

In the equations which follow the various atomic states will be indicated by the following index numbers

Index	State	
1	6^1S_0	Ground State Neutral Hg
2	6^3P_0	Metastable Neutral Hg
3	6^3P_2	Metastable Neutral Hg
4	$6^2S_{1/2}$	Ground State singly Ionized Hg
5	5^1S_0	Ground State Doubly Ionized Hg

Using the same symbols as used in the main report, the production and loss rate equations for the various states are as follows:

State 1 (Conservation of 6^1S_0 state atoms)

$$\left\{-\Psi\, n^*_{mx}\left[\sum_{j=2}^{4} Q_1^j(T^*_{mx}) + \frac{n_{pr}}{n_{mx}}\, P_1^j(E_p)\right] - \phi_a\, A_s\, V_{th}\right\} n_1$$
$$+ \left\{V_{th}\,(A_p - \phi_a\, A_s)\right\}(n_2 + n_3) + \left\{\frac{n_{mx_u}}{n^*_{mx}}\, V^*_B\, A_u + \frac{n_{mx_a}}{n^*_{mx}}\, V_{B_v}\, A_v\right.$$
$$\left. + \frac{n_{mx_s}}{n^*_{mx}}\, V^*_B\, A_s\,(1 - \phi_s)\right\}(n_4 + \sqrt{2}\, n_5) = -\frac{I_p}{e}$$

The first term in braces represents the loss rate of ground state neutral atoms by conversion to other states in collisional processes and by escape through the grids. The second term in braces represents the rate at which the metastable state atoms $(n_2 + n_3)$ return to the ground state by going to the thruster walls $(A_p - \phi_a A_s)$ and de-exciting. It has been assumed that many more do that than de-excite by photon emission. The third term in braces describes the rate at which single and double ions go to the thruster walls across the boundaries of the ion production region and recombine to form neutral ground state atoms.

The term on the right of the equation is the number rate at which neutral ground state propellant atoms are introduced into the ion production region from the propellant feed system. Note that the atom thermal drift velocity is given by

$$V_{th} = \left(\frac{k\,T_a}{2\pi M_a}\right)^{\frac{1}{2}} = 62.8 \text{ m/sec for Hg @ } 600^\circ \text{K}$$

and that for constant n_{pr}/n_{mx} the ion densities at the various ion production region surfaces compare with volume averaged values as do the densities of Maxwellian electrons. Note, too, that the factor $\sqrt{2}$ accounts for the increased Bohm velocity of double ions as compared with that of single ions. V_B^* and V_{B_v} are Bohm velocities based on volume averaged Maxwellian electron temperature and the temperature at the virtual anode respectively.

Similarly, the production and loss rates for the other atomic states may be written:

State 2 (Conservation of 6^3P_1 state atoms)

$$\left\{ \Psi\, n_{mx}^* \left[Q_1^2(T_{mx}^*) + \frac{n_{pr}}{n_{mx}} P_1^2(E_p) \right] \right\} n_1$$

$$- \left\{ \Psi\, n_{mx}^* \left[Q_2^4(T_{mx}^*) + \frac{n_{pr}}{n_{mx}} P_2^4(E_p) \right] + A_p\, V_{th} \right\} n_2 = 0$$

State 3 (Conservation of 6^3P state atoms)

$$\left\{ \Psi\, n_{mx}^* \left[Q_1^3(T_{mx}^*) + \frac{n_{pr}}{n_{mx}} P_1^3(E_p) \right] \right\} n_1$$

$$- \left\{ \Psi\, n_{mx}^* \left[Q_3^4(T_{mx}^*) + \frac{n_{pr}}{n_{mx}} P_3^4(E) \right] + A_p\, V_{th} \right\} n_3 = 0$$

State 4 (Conservation of $6^2S_{1/2}$ state ions)

$$\left\{ \Psi\, n^*_{mx} \left[Q_1^4(T^*_{mx}) + \frac{n_{pr}}{n_{mx}} P_1^4(E) \right] \right\} n_1 + \left\{ \Psi\, n^*_{mx} \left[Q_2^4(T^*_{mx}) + \frac{n_{pr}}{n_{mx}} P_2^4(E_p) \right] \right\} n_2$$
$$+ \left\{ \Psi\, n^*_{mx} \left[Q_3^4(T^*_{mx}) + \frac{n_{pr}}{n_{mx}} P_3^4(E_p) \right] \right\} n_3 - \left\{ \Psi\, n^*_{mx} \left[Q_4^5(T^*_{mx}) + \frac{n_{pr}}{n_{mx}} P_4^5(E_p) \right] \right.$$
$$\left. + \frac{n_{mx_u}}{n^*_{mx}} V^*_B\, A_u + \frac{n_{mx_a}}{n^*_{mx}} V_{B_v}\, A_v + \frac{n_{mx_s}}{n^*_{mx}} V^*_B\, A_s \right\} n_4 = 0$$

State 5 (Conservation of 6^1S_0 state double ions)

$$\left\{ \Psi\, n^*_{mx} \left[Q_4^5(T^*_{mx}) + \frac{n_{pr}}{n_{mx}} P_4^5(E_p) \right] \right\} n_4$$
$$- \sqrt{2} \left\{ \frac{n_{mx_u}}{n^*_{mx}} V^*_B\, A_u + \frac{n_{mx_v}}{n^*_{mx}} V_{B_v}\, A_v + \frac{n_{mx_s}}{n^*_{mx}} V^*_B\, A_s \right\} n_5 = 0$$

The following values for the reaction rate factors are obtained from Appendix A:

$Q_1^2(7.4) = 2 \times 10^{-15}$ m^3/sec $P_1^2(30) = 1.26 \times 10^{-15}$ m^3/sec

$Q_1^3(7.4) = 2.6 \times 10^{-14}$ $P_1^3(30) = 5.14 \times 10^{-14}$

$Q_1^4(7.4) = 0.3 \times 10^{-13}$ $P_1^4(30) = 1.56 \times 10^{-13}$

$Q_2^4(7.4) = 0.67 \times 10^{-13}$ $P_2^4(30) = 2.76 \times 10^{-13}$

$Q_3^4(7.4) = 0.86 \times 10^{-13}$ $P_3^4(30) = 3.14 \times 10^{-13}$

$Q_4^5(7.4) = 0.12 \times 10^{-13}$ $P_4^5(30) = 0.85 \times 10^{-13}$

Each term in braces in the previous set of equations represents a matrix element in the matrix of coefficients for solution of the set of linear equations. The following matrix equation is obtained by substituting the appropriate values for the various parameters:

$$\begin{bmatrix} -5.515 & 2.594 & 2.594 & 34.34 & 48.56 \\ 0.1415 & -9.078 & 0 & 0 & 0 \\ 2.028 & 0 & -10.562 & 0 & 0 \\ 2.861 & 6.000 & 7.485 & -51.89 & 0 \\ 0 & 0 & 0 & 1.266 & -71.59 \end{bmatrix} \times \begin{bmatrix} n_1 \\ n_2 \\ n_3 \\ n_4 \\ n_5 \end{bmatrix} = \begin{bmatrix} -1.918 \times 10^{18} \\ 0 \\ 0 \\ 0 \\ 0 \end{bmatrix}$$

This system is easily solved without resorting to matrix methods to give the following volume averaged densities for the various states.

$$n_1(6^1S_0) = 9.6 \times 10^{17}\ m^{-3}$$

$$n_2(6^3P_0) = 1.50 \times 10^{16}$$

$$n_3(6^3P_2) = 1.85 \times 10^{17}$$

$$n_4(6^2S_{1/2}) = 8.124 \times 10^{16}$$

$$n_5(5^1S_0) = 1.43 \times 10^{15}$$

The beam current may now be calculated from

$$I_b = \frac{n_{mx_s}}{n^*_{mx}} V^*_B \phi_s A_s e (n_4 + 2\sqrt{2}\, n_5) = 0.222\ A$$

This is quite close to the measured beam current for this thruster of 0.258 A.

The volumetric energy loss to inelastic processes is given by

$$\dot{E}_{mx_v} = \sum_{j=1}^{4} n_j \left[q_j(T^*_{mx}) + \frac{n_{pr}}{n_{mx}} P_j(E_p) \right]$$

The following values for the energy rate factors were obtained from Appendix A all in units of eV m^3/sec:

$$q_1(7.4) = 0.94 \times 10^{-12} \qquad p_1(30) = 3.89 \times 10^{-12}$$

$$q_2(7.4) = 0.64 \times 10^{-12} \qquad p_2(30) = 3.14 \times 10^{-12}$$

$$q_3(7.4) = 0.73 \times 10^{-12} \qquad p_3(30) = 3.14 \times 10^{-12}$$

$$q_4(7.4) = 0.36 \times 10^{-12} \qquad p_4(30) = 1.67 \times 10^{-12}$$

The volumetric energy loss rate per Maxwellian electron is thus found to be

$$\dot{E}_{mx_v} = 1.435 \times 10^{6} \text{ eV/sec.}$$

The energy lost to the boundary per Maxwellian electron is given by

$$\dot{E}_{mx_b} = \frac{\dot{E}_b + \dot{E}_a}{n^*_{mx} \forall}$$

where

$$\dot{E}_b = n_{mx_u} \left(\frac{e\, T_{mx_u}}{2\pi\, M_e} \right)^{\frac{1}{2}} \exp\left(\frac{-V_p}{T_{mx_u}} \right) (2\, T_{mx_u} + V_p)$$

and

$$\dot{E}_a = \frac{I_c + I_b}{e} (2\, T_{mx_a} + V_{s_a}) \ .$$

The plasma potential V_p is the sum of anode potential V_a and V_{s_a}. Its value is 38.7 V. The upstream average temperature T_{mx_u} is the same as the volume average temperature T^*_{mx} because of the one dimensional variation of temperature. Putting in the appropriate values there is obtained

$$\dot{E}_b = 4.67 \times 10^{19} \text{ eV/sec}$$

and

$$\dot{E}_a = 7.19 \times 10^{19}\, I_c + 1.60 \times 10^{19} \text{ eV/sec} \ .$$

This gives the boundary energy loss per Maxwellian electron as

$$\dot{E}_{mx_b} = 1.066 \times 10^6 \; I_c + 9.30 \times 10^5 \text{ eV/sec.}$$

The energy brought into the ion production region per Maxwellian electron in that region is

$$\dot{E}_{mx_{in}} = \frac{I_c \, E_p}{e \, \forall \, n^*_{mx}} = 2.78 \times 10^6 \; I_c \text{ eV/sec .}$$

Then from the macroscopic energy balance

$$\dot{E}_{mx_{in}} = \dot{E}_{mx_v} + \dot{E}_{mx_b}$$

there is obtained the value for the cathode emission current

$$I_c = 1.38 \text{ A.}$$

The measured value, which is taken as the difference between measured anode current (1.7 A) and measured beam current (0.258 A), is 1.44 A. This is close to the calculated value.